Probabilistic Methods Applied to Fluctuating Systems

By

Lloyd A Corker

In Fulfilment of the degree

Doctor of Philosophy

Department of Physics

UNIVERSITY OF CAPE TOWN

October 2011

Supervisors: Prof. D.T. Britton

Prof. M. Härting

Abstract

Probability Methods Applied to Fluctuating Systems

Lloyd A Corker

PhD Thesis, Department of Physics, University of Cape Town

In this work the hierarchical structure of three diverse stochastic systems is studied by investigating the probability densities of their scale-dependent measures across various scales. In the first system studied, velocity increments are used to investigate the order of complexity and disorder of wind turbulence. The second system investigates the disorders of skeletal muscles and the nervous system by considering the fluctuation of electric potentials of skeletal muscles. The last system studied is a non-physical system where price increments are used to classify the financial markets in terms of predictability of price changes and market efficiency. In all three stochastic systems a Fokker-Planck equation is used to describe how the scale-dependent measure is correlated across nested scales. The drift and diffusion coefficients are given an interpretation which is based on the use of a reciprocal time or spatial interval. The study involves testing three principal assumptions: the variable of interest is a stochastic variable; a binary-scale transition function is sufficient to describe the underlying stochastic process; and the fourth Kramers-Moyal coefficient tends to zero. The successful validation of these assumptions and the reciprocal character of the Fokker-Planck coefficients reveal several new useful applications and interesting theoretical outcomes.

In the study of wind turbulence a linear Boltzmann equation is approximated by a Fokker-Planck equation, which contains the Boltzmann's collision terms in the drift and diffusion coefficients. Hence, this novel approach describes how the velocity increments are related across nested scales for a system which experiences both spontaneous fluctuations and binary interactions between subsystems. The study of skeletal muscle disorders shows that the binary-scale transition function contains both non-Markov and Markov components of the fluctuations which suggests that the Kramers-Moyal expansion, and hence the Fokker-Planck equation, may include expressions on the non-Markov nature of a system.

October 2011

Acknowledgements

This study would not have been possible if it was not for the support of my family, colleagues and dear friends. A special thank you to my supervisors, Prof. D.T. Britton and Prof. M. Härting, for their support and effort. I am also indebted to the National Institute for Theoretical Physics for their financial support.

Thank you Mom and Dad.

Table of Contents

CHAPTER 1

INTRODUCTION

The interest in fluctuations and their description using probabilistic (stochastic) methods, has grown enormously since Andrey Kolmogorov's work on turbulent cascades in 1941 [1,2]. These methods have become so popular and proved to be so versatile, that they have found their way into all fields of science [3-15]. Indeed, some phenomena such as the study of phase transitions and similar critical phenomena [16-19], only become clearer when using probabilistic methods. These systems often consist of a large number and different types of components, for example the different types of molecules when studying a mixture of gases. Each molecule can be characterised by a number of variables which describe its state, such as velocity and position. A fluctuation arises when the system changes its state spontaneously or by means of its constituents interacting with one another. A state change often involves a transfer of energy, momentum, or more abstractly, information [14].

It is possible to describe the fluctuating behaviour of the components of a system with exact laws. The problem is that the huge number of components experiencing changes of state makes it practically impossible to calculate their behaviour exactly. Fortunately it is not the behaviour of a single component, but rather the distribution of states within a system, that is of interest [14]. Moreover, stochastic methods are most suitable when describing the evolution of the distribution of states [14,20]. Even more appealing, is the wide occurrence of a type of stochastic process known as a Markov process [20-25], which simplifies the calculations dramatically when describing how the distribution of states, or probability density function, evolve with time.

The temporal change of a probability distribution, is given in its most basic form, as a master equation [14,20,26]. A master equation is an integro-differential equation for the evolution of the probability distribution, over the microscopic jumps between states. However it is the Fokker-Planck equation [14,20,26-30], which has gained favour over the past decades as a powerful tool for modelling fluctuating subsystems or systems containing noise. Special cases of the Fokker-Planck equation were first used by Lord Rayleigh in 1891 [31,32]; Albert Einstein in 1905 [33,34]; Marian Ritter von Smolan Smoluchowskiin 1906 [35,36] and Adriaan Daniël Fokker in 1913 [37,38]. In 1917 Max Planck then derived the generalised nonlinear Fokker-Planck equation from an arbitrary master equation [39]. Kolmogorov then provided a rigorous mathematical derivation in 1931 in the limit of very small fluctuations [40]. Both Fokker and Planck used the Fokker-Planck equation to describe the

Brownian motion of particles in fluids [26]. Fokker-Planck equations are now widely used in solid-state physics, chemical physics and circuit theory [26]. Recently, probabilistic modelling using the Fokker-Planck equations have been used to study turbulence [41-46]; evaluate financial risk and price changes in the financial markets [47-59]; and in biological systems to study the complex fluctuations of inter-beat heart muscle [60-65].

The Fokker-Planck equation has two appealing features: firstly, it is a differential equation rather than a differentio-integral equation and therefore much easier to calculate than the master equation. The second, and more important feature, is that it does not require knowledge of the entire microscopic transition functions, but merely the first and second Kramers-Moyal coefficients which are the drift and diffusion coefficients [14,20,26]. Therefore a Fokker-Planck equation is particularly useful, in quantifying the deterministic influences and random fluctuations of a stochastic system.

Systems experiencing fluctuations, due to binary collisions with another system or subsystem, are better described by a Boltzmann equation. Boltzmann equations, like Fokker-Planck equations, are transport equations describing the time and spatial variation of the probability density functions. However, although the Boltzmann equation has the structure of a master equation, the transition functions are proportional to the probabilities of the occupation of the states, of both interacting subsystems. Systems experiencing both binary collisions and spontaneous fluctuations can be described by a Fokker-Planck equation, but with the drift and diffusion terms containing the binary collision terms. Such Fokker-Planck equations can be derived by approximating a linear Boltzmann equation, by a Fokker-Planck equation [66-68] and are sometimes referred to as Boltzmann-Fokker-Planck equations [69-72]. The Fokker-Planck approximation to the linear Boltzmann equation, is obtained by applying the Kramers-Moyal expansion [73,74] to the linear Boltzmann equation, and exercising Pawula's theorem [66,67] to terminate at a finite number of terms. Boltzmann integrals are often approximated by a differential operator in studies of relaxation phenomena [72]. These Fokker-Planck equations describing binary collisions can thus be useful in quantifying the deterministic and random influences of a stochastic system, for both spontaneous and induced fluctuations.

In 1997 Friedrich and Peinke had the interesting idea of applying the Fokker-Planck equation to analyse time-series data [43,44]; using the work of Kolmogorov [1,2] it was shown for a turbulent flow that there exists a cascade feature for the energy, from large scale eddies to progressively

smaller scales. The statistics of the scale-dependent measure were shown to obey the Chapman-Kolmogorov equation, which written in differential form, is the Kramers-Moyal expansion from which the Fokker-Planck equation can be derived.

In this work the probabilistic method of analysing time series data, characterised by a degree of stochasticity, is applied to the study of three different systems: wind turbulence; electromyography, (which is a technique for electrical recording of skeletal muscle activity) as a representation of a biological system; and price changes on the financial markets, as a non-physical system. This probabilistic method of analysing time series data is a complex method that is postulated on the successful testing of several assumptions for each data set. Firstly, one has to establish that the variable of interest behaves like a stochastic variable, and that there is a correlation or stochastic dependency between scales.

For the second assumption it has to be shown that this stochastic dependency across many possible nested scales, and involving all possible permutations of the scale-dependent measure, can be reduced to a dependence between one nested time scale and another having a certain probability, a binary transition function. This feature of a stochastic process is commonly considered to be equivalent to the Markov property, a subclass of stochastic processes [21]. Many published works exist on the difficult field of Markov theory [20-25], which is discussed in chapter 2. In the testing of the Markov property many authors [45,46,53-65,75-80] use the Chapman-Kolmogorov equation which is derived from the Markov property; however, even though the Chapman-Kolmogorov equation can be derived from the Markov property, it contains no information about the Markov process [14]. In this work it is shown that the validity of the Chapman-Kolmogorov equation is a necessary but not sufficient condition for the Markov property, and that tests based on the specific conditional moments of the transition function, yield greater insight on the existence of the Markov property. This work also presents evidence for specific cases, which shows that a binary-scale transition function does not only account for the Markov nature of the stochastic process, but also for non-Markov properties. This suggest that the Kramers-Moyal expansion, and hence the Fokker-Planck equation, includes expressions on the non-Markov nature of that system. Therefore, for certain stochastic systems, a binary-scale transition function is sufficient for the use of the Kramers-Moyal expansion.

The third assumption to be tested involves Pawula's theorem, and showing that if an even numbered coefficient in the Kramers-Moyal expansion is zero, then the third and high coefficients are irrelevant.

Chapter 3 discusses the master equation and the derivation of the Fokker-Planck equation for spontaneous fluctuations and systems experiencing fluctuations due to binary collisions. The Boltzmann equation is discussed along with several important and ingenuous assumptions, made by Boltzmann [81,82], which will be used in chapter 4 to consider two interacting fluctuating systems. The second part of chapter 3, discusses systems experiencing fluctuation due to both binary collisions and spontaneous interactions.

Chapter 4 involves the practical application of the mathematical formulism of chapters 2 and 3, to turbulent wind data, from the well-known experiments performed by Kang *et al* [83]. The use of the inverse length scales and how this affects the interpretation of the drift and diffusion coefficients is discussed. In the second part of chapter 4, the novel idea of applying a Fokker-Planck equation to stochastic systems, experiencing both spontaneous and induced fluctuations is introduced. The drift and diffusion coefficients contain the binary collision terms necessary to describe induced fluctuations. Chapter 5 applies probabilistic methods to time series data for electromyography. The aim is to investigate the use of the drift the diffusion coefficients as potential diagnostic tools. In chapter 6 the same probabilistic methods are applied to the study of price fluctuations in the financial markets. Analysis of the drift and diffusion coefficients focuses on obtaining reliable parameters, which may classify the markets in terms of predictability of price changes. The results indicate that the parameters of the drift coefficient are able to classify the financial instruments in terms of anti-persistent behaviour, random behaviour and persistent behaviour.

CHAPTER 2

STOCHASTIC PROCESSES

There are many phenomena in nature in which some quantity varies with time in a very complex manner. For example, the instantaneous sum of the individual forces exerted by the molecules of a gas on a piston varies rapidly and unpredictably, but when integrated over a small time interval, it can be replaced by the pressure which is described by Boyle's law [14]. The calculation of the microscopic parameters over a small time interval can be made easier by replacing an ensemble of functions with a single varying function of time, *i.e.* it is turned into a stochastic process. A stochastic process is the complement to a deterministic process. Instead of having only one possible outcome of how a process might evolve under time, a stochastic process has many possibilities with some paths more probable and others less.

While serious investigation of stochastic processes was underway in the early 20th century one idea was leading in the scientific literature, the Markov property [25]. The Markov property describes a memoryless stochastic process. In other words, the future state of a system having the Markov property depends only on the present and not the past state, intermediate state or any other possible future state. This feature of the Markov property simplifies the calculations of time series analyses dramatically. Markov processes are found in diverse fields such as communication systems, biological systems, DNA analyses, financial markets and diffusion processes in physics [84]. However, the validation of the Markov property given in its most simplest form, as a conditional probability function or binary-scale transition function, is computationally difficult and is often conceptually misused in many disciplines. In van Kampen's words [14], "...the epithet 'Markov' is often used with regrettable looseness. The term has magical appeal, which invites its use in an intuitive sense not covered by the definition". To avoid the computational difficulties in testing for the Markov property many authors [45,46,53-65,75-80] have used the Chapman-Kolmogorov equation. The Chapman-Kolmogorov equation represents an identity that relates the moments of the conditional probability distributions on a stochastic process. Unfortunately even though the Chapman-Kolmogorov equation can be derived from the Markov property it contains no information about the Markov process [14]. In this work it is shown that the Chapman-Kolmogorov equation is a necessary but not sufficient condition for the Markov property. In this chapter, the derivation and definitions of probability density functions, the Markov property and the Chapman-Kolmogorov equation follow closely the work of Gillespie [21].

2.1. Definition of a Random Variable

A random variable X is a quantity that can assume different values in a range or sample space under certain experimental conditions which are physically well defined and fixed [85]. More precisely, a variable X is said to be a random variable if and only if there exists a function P of a variable x such that $P(x)\Delta x$ equals the probability of finding the value of X in the interval, $[x, x + \Delta x)$, *i.e.*

$$P(x)\mathrm{d}x = \mathrm{P}\{X \in [x, x + \mathrm{d}x)\}. \tag{2.1}$$

Equation (2.1) is known as the density of the probability of the random variable X in the range x to $x + \mathrm{d}x$ [21]. To find the probability that a particular value of X will be found inside some finite interval $[a, b)$, divide the interval into a set of non-overlapping vanishingly small subintervals $[x, x + \mathrm{d}x)$. Now the probability of finding a particular value of X, $\mathrm{P}\{X \in [a, b)\}$, is found by summing $\mathrm{P}\{X \in [x, x + \mathrm{d}x)\}$ over all the subintervals [21], *i.e.*

$$\mathrm{P}\{X \in [a, b)\} = \int_a^b P(x)\mathrm{d}x. \tag{2.2}$$

Also, as any sample value of X will be found in the interval $(-\infty, \infty)$, it follows from equation (2.2) that P can be normalised

$$\int_{-\infty}^{\infty} P(x)\mathrm{d}x = 1. \tag{2.3}$$

Furthermore, since $\mathrm{d}x$ in equation (2.1) is conventionally positive and $P(x)\mathrm{d}x$ is a probability [21],

$$P(x) \geq 0 \text{ for all } x. \tag{2.4}$$

A function P which satisfies both conditions described by equations (2.3) and (2.4) is a density function. A diagram of the density function P of a random variable X is given in Fig 2.1. The probability that a sample value of X will fall between x and $\mathrm{d}x$ is equal to $P(x)\mathrm{d}x$. The probability that a sample value of X will be less than x is equal to the area under the curve to the left of the abscissa value x [21]. For individual sampling one cannot be sure of the value of X, but equation

(2.1) infers that, in the limit of infinitely many samplings, a fraction $P(x)\mathrm{d}x$ will produce values in the interval $[x, x+\mathrm{d}x)$. In other words, while individual sampling ensures unpredictability in the behaviour of random variables, for very many samplings the probability density function gives some degree of determinism for the value of X. In August Kronig's words (1856), "The path of each molecule must be so irregular that it will defy all calculations. However, according to the laws of probability theory, one can assume a completely regular motion instead of this completely irregular one" [86].

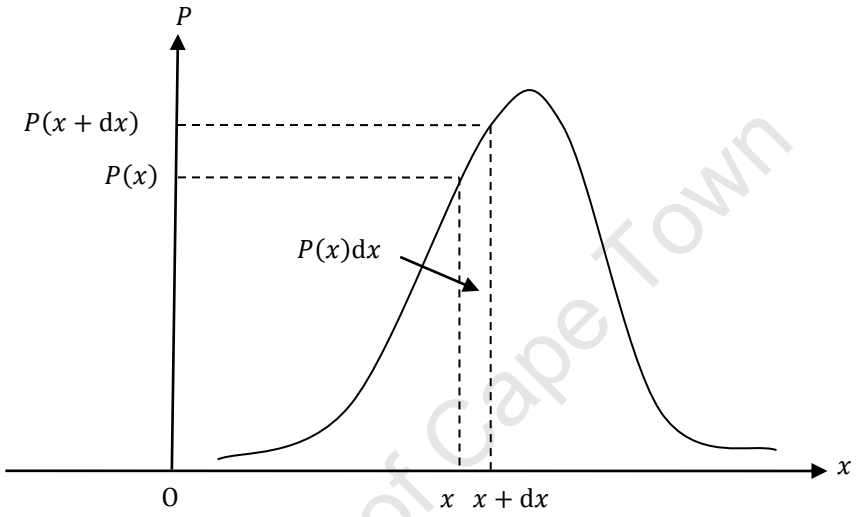

Fig 2.1 The density function P of a random variable X. The probability that a sample value of X will fall between x and $\mathrm{d}x$ is equal to $P(x)\mathrm{d}x$ [21].

At this point it is convenient to define the Dirac Delta function $\delta(x-x_0)$, a special type of density function [21], which will be used later to derive the master equation for a fluctuating system. The Dirac Delta function may be defined by the statements

$$\delta(x-x_0)=0, if\, x\neq x_0 \tag{2.5a}$$

and

$$\int_{-\infty}^{\infty}\delta(x-x_0)\mathrm{d}x=1. \tag{2.5b}$$

These statements satisfy all conditions of equations (2.3) and (2.4) to be a density function. Substituting the delta function in equation (2.2) the random variable X has the property

$$\mathrm{P}\{X \in [a,b)\} = \int_a^b \delta(x - x_0)\mathrm{d}x = \begin{cases} 1, \text{if } x_0 \in [a,b), \\ 0, \text{if } x_0 \notin [a,b). \end{cases} \tag{2.6}$$

This means the probability of finding the value of X inside any given integral is either 1 or 0. This implies that the value of X must be presicely x_0 and implies that X has density function $\delta(x - x_0) \Leftrightarrow X$ is a fixed variable x_0 [21].

2.2. Joint Random Variables

The variables $X_1, X_2, \dots, X_n$ are called a set of joint random variables if and only if all n variables are simultaneously sampled and $P(x_1; x_2; \dots; x_n)\mathrm{d}x_1\mathrm{d}x_2 \dots \mathrm{d}x_n$ equals the probability of finding X_i inside the interval $[x_i; x_i + \mathrm{d}x_i)$, for each $i = 1$ to n [21]. Consider the case of $n = 3$ random variables, X_1, X_2 and X_3 in any simultaneous sampling, the joint density function is

$$P(x_1; x_2; x_3)\mathrm{d}x_1\mathrm{d}x_2\mathrm{d}x_3 = \mathrm{P}\{X_i \in [x_i, x_i + \mathrm{d}x_i)\} \text{ for } i = 1,2 \text{ and } 3. \tag{2.7}$$

Summing $\mathrm{P}\{X \in [x, x + \mathrm{d}x)\}$ over all the subintervals, as in equation (2.2), gives

$$\int_{a_1}^{b_1}\int_{a_2}^{b_2}\int_{a_3}^{b_3} P(x_1; x_2; x_3)\mathrm{d}x_1\mathrm{d}x_2\mathrm{d}x_3 = \mathrm{Prob}\{X_i \in [a_i, b_i)\}, \text{for } i = 1, 2 \text{ and } 3, \tag{2.8}$$

and by equation (2.3), normalisation [21],

$$\int_{-\infty}^{\infty}\int_{-\infty}^{\infty}\int_{-\infty}^{\infty} P(x_1; x_2; x_3)\mathrm{d}x_1\mathrm{d}x_2\mathrm{d}x_3 = 1. \tag{2.9}$$

Also since the vanishingly small intervals $\mathrm{d}x_i$ in equation (2.7) are positive, the function P also satisfies

$$P(x_1; x_2; x_3) \geq 0. \tag{2.10}$$

Any three-variate function P that satisfies both conditions described by equations (2.9) and (2.10) can be regarded as a joint density function, defining the set of random variables, X_1, X_2 and X_3. From the joint density function P there are two classes of sub-ordinate density functions: the first type is the set of marginal density functions, which are defined by

$$P_i(x_i)\mathrm{d}x_i \equiv \mathrm{P}\{X_i \in [x_i, x_i + \mathrm{d}x_i)\}, \qquad \text{regardless of } X_j \text{and } X_k, \tag{2.11}$$

$$P_{i,j}(x_i; x_j)\mathrm{d}x_i\mathrm{d}x_j \equiv \mathrm{P}\{X_i \in [x_i, x_i + \mathrm{d}x_i) \text{ and } X_j \in [x_j, x_j + \mathrm{d}x_j)\}, \text{regardless of } X_k. \tag{2.12}$$

The subscripts (i, j, k) denote any permutation of outcomes (1,2,3) [21]. The second type of sub-ordinate density functions are the set of conditional probabilities defined by

$$P_i^{(j)}(x_i|x_j)\mathrm{d}x_i \equiv \mathrm{P}\{X_i \in [x_i, x_i + \mathrm{d}x_i)\}, \qquad \text{given } X_j = x_j, \text{regardless of } X_k, \tag{2.13}$$

$$P_i^{(j,k)}(x_i|x_j; x_k)\mathrm{d}x_i \equiv \mathrm{P}\{X_i \in [x_i, x_i + \mathrm{d}x_i)\}, \qquad \text{given } X_j = x_j \text{ and } X_k = x_k, \tag{2.14}$$

and

$$P_{i,j}^{(k)}(x_i; x_j|x_k)\mathrm{d}x_i\mathrm{d}x_j \equiv \mathrm{Pb}\{X_i \in [x_i, x_i + \mathrm{d}x_i) \text{ and } X_j \in [x_j, x_j + \mathrm{d}x_j)\}, \text{given } X_k = x_k. \tag{2.15}$$

Now comparing the definitions of equations (2.1) and (2.7) with the definitions of the subordinate density functions above, all the density functions can be normalised as follows:

$$\int_{-\infty}^{\infty} P_i(x_i)\mathrm{d}x_i = \int_{-\infty}^{\infty} P_i^{(j)}(x_i|x_j)\mathrm{d}x_i = \int_{-\infty}^{\infty} P_i^{(j,k)}(x_i|x_j; x_k)\mathrm{d}x_i = 1 \tag{2.16}$$

and

$$\int_{-\infty}^{\infty}\int_{-\infty}^{\infty} P_{i,j}(x_i; x_j)\mathrm{d}x_i\mathrm{d}x_j = \int_{-\infty}^{\infty}\int_{-\infty}^{\infty} P_{i,j}^{(k)}(x_i; x_j|x_k)\mathrm{d}x_i\mathrm{d}x_j = 1. \tag{2.17}$$

The joint, marginal and conditional density functions are all interrelated [21],

$$P_{i,j}(x_i; x_j)\mathrm{d}x_i\mathrm{d}x_j = P_i(x_i)\mathrm{d}x_i \cdot P_j^{(i)}(x_j|x_i)\mathrm{d}x_{j,} \tag{2.18}$$

$$P(x_1; x_2; x_3)\mathrm{d}x_1\mathrm{d}x_2\mathrm{d}x_3 = P_{i,j}(x_i; x_j)\mathrm{d}x_i\mathrm{d}x_j \cdot P_k^{(i,j)}(x_k|x_i; x_j)\mathrm{d}x_k \tag{2.19}$$

and [21]

$$P(x_1; x_2; x_3)\mathrm{d}x_1\mathrm{d}x_2\mathrm{d}x_3 = P_i(x_i)\mathrm{d}x_i \cdot P_{j,k}^{(i)}(x_j; x_k|x_i)\mathrm{d}x_j\mathrm{d}x_k. \tag{2.20}$$

The scripts (i, j, k) refer to any permutation of outcomes (1,2,3).

Eliminating the differentials gives

$$P_{i,j}(x_i; x_j) = P_i(x_i)P_j^{(i)}(x_j|x_i), \tag{2.21}$$

$$P(x_1; x_2; x_3) = P_{i,j}(x_i; x_j)P_k^{(i,j)}(x_k|x_i; x_j) \tag{2.22}$$

and

$$P(x_1; x_2; x_3) = P_i(x_i)P_{j,k}^{(i)}(x_j; x_k|x_i). \tag{2.23}$$

Integrating equation (2.23) over x_j and x_k and substituting equation (2.18) gives

$$P_i(x_i) = \int_{-\infty}^{\infty}\int_{-\infty}^{\infty} P(x_1; x_2; x_3)\mathrm{d}x_j\mathrm{d}x_k \tag{2.24}$$

and integrating equation (2.22) over x_k and substituting equation (2.16) gives [21]

$$P_{ij}(x_i; x_j) = \int_{-\infty}^{\infty} P(x_1; x_2; x_3)\mathrm{d}x_k. \tag{2.25}$$

Dividing equation (2.21) by $P_i(x_i)$and substituting equations (2.24) and (2.25) gives

$$P_j^{(i)}(x_j|x_i) = \frac{\int_{-\infty}^{\infty} P(x_1; x_2; x_3)\mathrm{d}x_k}{\int_{-\infty}^{\infty}\int_{-\infty}^{\infty} P(x_1; x_2; x_3)\mathrm{d}x_j\mathrm{d}x_k}. \tag{2.26}$$

Dividing equation (2.22) by $P_{ij}(x_i; x_j)$ and substituting equation (2.25) gives

$$P_k^{(i,j)}(x_k|x_i; x_j) = \frac{P(x_1; x_2; x_3)}{\int_{-\infty}^{\infty} P(x_1; x_2; x_3)\mathrm{d}x_k}. \tag{2.27}$$

Finally, by dividing equation (2.23) by $P_i(x_i)$ and substituting equation (2.24) gives

$$P_{j,k}^{(i)}(x_j; x_k|x_i) = \frac{P(x_1; x_2; x_3)}{\int_{-\infty}^{\infty}\int_{-\infty}^{\infty} P(x_1; x_2; x_3)\mathrm{d}x_j\mathrm{d}x_k}. \tag{2.28}$$

The two equations (2.24) and (2.25) represent the marginal density functions while equations (2.26) to (2.28) represent the conditional density functions. It follows from equations (2.24) to (2.28) that the joint density function determines all the permutations of the conditional density functions while equations (2.22) and (2.23) show that certain subsets of the conditional density functions uniquely determine the joint density function [21]. By substituting equation (2.21) into equation (2.22), the full conditioning of the joint density function is

$$P(x_1; x_2; x_3) = P_i(x_i)P_j^{(i)}(x_j|x_i)P_k^{(i,j)}(x_k|x_i; x_j), \tag{2.29}$$

which is valid for (i, j, k) and any permutation of outcomes (1,2,3).

2.3. Markov Processes

In this section the Markov property is derived and it is shown why many authors have chosen to test the Markov property using the Chapman-Kolmogorov equation. Consider a time evolving system whose possible states can be represented by points on the real axis, and let $X(t)$ be the state of the system at time t. Assume that at some initial time, $t = t_0$, the value of X is fixed at

$$X(t_0) = x_0, \tag{2.30}$$

but that $X(t_0)$ for any $t > t_0$ is a random variable that can be predicted only probabilistically. Of interest is the state of the system at successive instants $t_1, t_2, \dots, t_n$, where $t_0 < t_1 < t_2 < \cdots < t_n$. For n corresponding random variables $\mathrm{X}(t_1), \mathrm{X}(t_2), \dots, \mathrm{X}(t_n)$, the joint density function $P_n^{(1)}$ is defined as [21]

$$\begin{aligned} P_n^{(1)} &= (x_n, t_n; x_{n-1}, t_{n-1}; \dots; x_1, t_1 | x_0, t_0)\mathrm{d}x_n \mathrm{d}x_{n-1} \cdots \mathrm{d}x_1 \\ &\equiv \mathrm{P}\{\mathrm{X}(t_i) \in [x_i, x_i + \mathrm{d}x_i), \end{aligned} \tag{2.31}$$

for $i = 1,2, \dots, n$, given that $X(t_0) = x_0$, with $t_0 \leq t_1 \leq \dots \leq t_n\}$. If the above conditions holds then $X(t)$ is a stochastic process which has infinitely many joint density functions $P_n^{(1)}$, corresponding to $n = 1,2, \dots$. With each of these functions an abundance of subordinate density functions exists, for example,

$$P_{n-j}^{(j+1)}\big(x_n, t_n; \dots; x_{j+1}, t_{j+1} \big| x_j, t_j; \dots; x_1, t_1; x_0, t_0\big), \tag{2.32}$$

is the joint density function of $n - j$ random variables $\mathrm{X}\big(t_{j+1}\big), \dots, \mathrm{X}(t_n)$ conditional on the $j + 1$ states x_0 to x_j. The function $P_n^{(j)}$ is an n-variate joint density function with j conditioning. For a given $P_n^{(1)}$function it is always possible to calculate the $P_{n+1^{(1)}}$ function by integrating the former over any one of the variables $x_1, \dots, x_n$ however it is not possible to deduce the function $P_{n+1^{(1)}}$ from $P_n^{(1)}$ [14,21]. It is this property and abundance of the subordinate density functions which makes analysis of general stochastic processes very difficult. However, there exists a subclass of stochastic processes, those with the "short-term memory" property, that simplifies the calculations dramatically, *i.e.* for all $j \geq 2$ and $t_{i-1} \leq t_i$,

$$P_1^{(j)}(x_j, t_j | x_{j-1}, t_{j-1}; \dots; x_1, t_1; x_0, t_0) = P_1^{(1)}(x_j, t_j | x_{j-1}, t_{j-1}) \equiv P(x_j, t_j | x_{j-1}, t_{j-1}). \quad (2.33)$$

The left-hand side of equation (2.33) reduces to a binary-scale transition function and is commonly said to describe a Markovian stochastic process [21], in which the future state of the system depends only on the present state, given $X(t') = x'$, our ability to predict $X(t)$ for any $t > t'$ will not be enhanced by a knowledge of any values of the process earlier than t'. For example, consider the triple-scale conditional probability function

$$P(x_3, t_3 | x_2, t_2; x_1, t_1; x_0, t_0) = P(x_3, t_3 | x_2, t_2), \text{for } t_0 < t_1 < t_2 < t_3, \quad (2.34)$$

which expresses the Markov property given in equation (2.33) for $P_1^{(3)}$ [21]. A graphical illustration of equation (2.34) is given in Fig 2.2. The paths shown by the broken lines represent some of the permutations of possible outcomes. The plot shows the probability $P_1^{(3)}(x_3, t_3 | x_2, t_2; x_1, t_1; x_0, t_0)$ of a transition from all possible values of x_0 at fixed time t_0 to all possible values of x_1 at fixed time t_1 to any value of x_2 at fixed time t_2 to a particular value of x_3 at fixed time t_3 is equivalent to the probability $P_1^{(1)}(x_3, t_3 | x_2, t_2)$. The Markov property expresses the path-independence and "short-term memory" of this type of subclass of stochastic process.

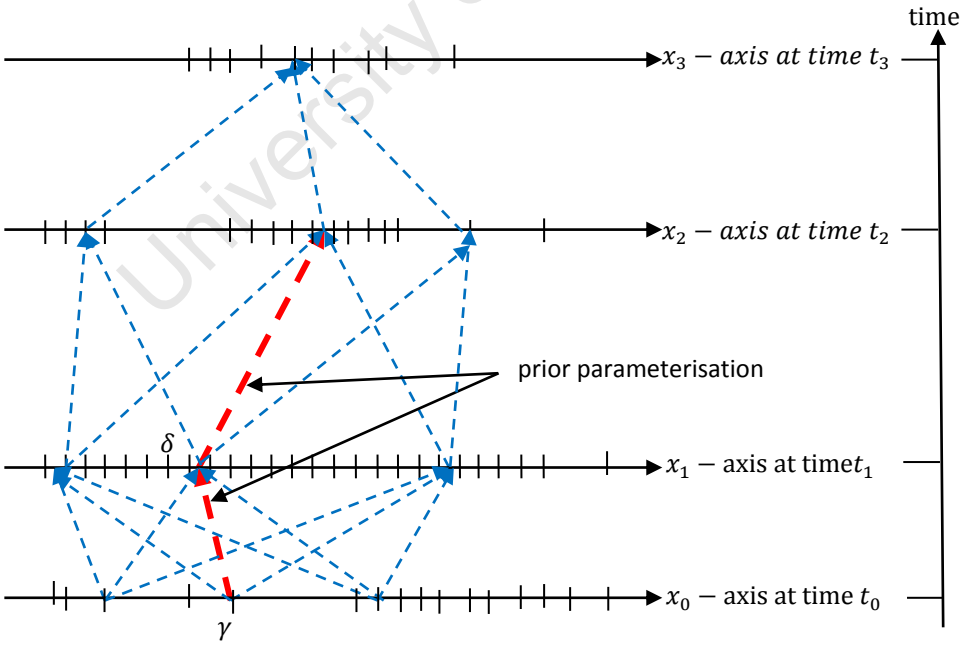

Fig 2.2 Graphical interpretation of the Markov property given by equation (2.34). The broken lines represent only some of the permutations of possible outcomes. The bold line in red represents possible prior parameterisation of the conditional moments for x_0 and x_1.

Confirmation of the Markov property, in this example, centres on the difficult task of calculating all the moments of the joint probability, $P(x_3, t_3; x_2, t_2; x_1, t_1; x_0, t_0)$. Generally, at the very least, one has to calculate all the moments of a 3-dimensional joint probability matrix, *i.e.* for $P_1^{(2)}$. However, one can make some prior parameterisation of the conditional moments for x_0 and x_1 on the left-hand side of equation (2.34), *i.e*. take cross-sections through selected values, say $x_0 = \gamma$ and $x_1 = \delta$, as shown in Fig 2.2. The joint probability $P(x_3, t_3; x_2, t_2; x_1, t_1; x_0, t_0)$ then reduces to a manageable 2-dimensional matrix $P(x_3, t_3; x_2, t_2; x_1 = \delta, t_1; x_0 = \gamma, t_0)$. This method of testing the Markov property by making prior parameterisation of the conditional moments, using the condition probability function (2.34) is illustrated graphically by the bold line in red, in Fig 2.2.

2.4. The Chapman-Kolmogorov Equation

Consider the conditional probability function $P(x_2, t_2|x_1, t_1)$ with respect to its argument x_2 satisfying the conditions of equations (2.3) and (2.4), *i.e.*

$$\int_{-\infty}^{\infty} P(x_2, t_2|x_1, t_1)\mathrm{d}x_2 = 1, \tag{2.35}$$

and

$$P(x_2, t_2|x_1, t_1) \geq 0 \text{ for all } x. \tag{2.36}$$

If t_2 equal its minimum value t_1 then the condition $X(t_1) = x_1$ implies that $X(t_2) = x_1$ or that $X(t)$ is a fixed variable x_1 [21]. Therefore by equation (2.6)

$$P(x_2, t_2 = t_1|x_1, t_1) = \delta(x_2 - x_1). \tag{2.37}$$

For any three times $t_1 \leq t_2 \leq t_3$

$$P_1^{(1)}(x_3, t_3|x_1, t_1) = \int_{-\infty}^{\infty} P_2^{(1)}(x_3, t_3; x_2, t_2|x_1, t_1)\mathrm{d}x_2 \tag{2.38}$$

$$= \int_{-\infty}^{\infty} P_1^{(1)}(x_2, t_2|x_1, t_1)\, P_1^{(2)}(x_3, t_3|x_2, t_2; x_1, t_1)\mathrm{d}x_2. \tag{2.39}$$

By equation (2.33) [21]

$$= \int_{-\infty}^{\infty} P_1^{(1)}(x_2, t_2|x_1, t_1)\, P_1^{(1)}(x_3, t_3|x_2, t_2)\mathrm{d}x_2. \tag{2.40}$$

Interchanging the two factors in equation (2.40) and using $P_n^{(1)} \equiv P$ gives the well-known Chapman-Kolmogorov equation [21]

$$P(x_3, t_3|x_1, t_1) = \int_{-\infty}^{\infty} P(x_3, t_3|x_2, t_2)P(x_2, t_2|x_1, t_1)\,\mathrm{d}x_2, \qquad \text{for } (t_1 \le t_2 \le t_3), \tag{2.41}$$

which states state that knowledge of the distribution at a single instance t, *i.e.*, $t = t_1$ allows one to predict the distributions at all later times. The Chapman-Kolmogorov equation is a necessary condition for the existence of the Markov property [14]. A graphical interpretation of this equation is given in Fig 2.3. The probability of a path from x_1 at time t_1 to the interval $[x_3, x_3 + \mathrm{d}x_3)$ at time t_3 is $P(x_3, t_3|x_1, t_1)\mathrm{d}x_3$, which can be written as the sum of the probabilities of this occurring via all possible intervals $[x_2, x_2 + \mathrm{d}x_2)$ at any fixed intermediate time t_2.

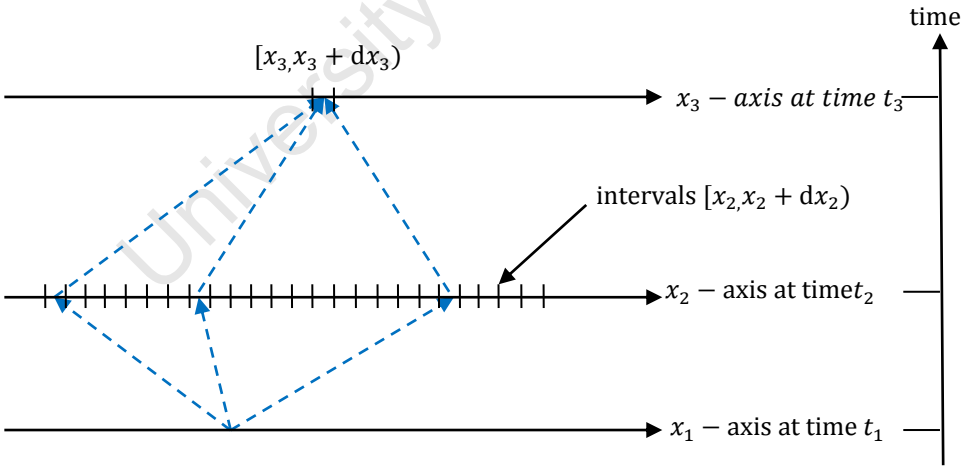

Fig 2.3 Graphical interpretation of the Chapman-Kolmogorov equation (2.41) [21].

The Chapman-Kolmogorov equation is derived from the Markov property, but contains no specific information about any Markov process [14]. Despite this it has been argued [87] that the use of the Chapman-Kolmogorov equation over tests based on the specific conditional moments brings about several advantages. Firstly, no prior parameterisations of the conditional moments are required for

the transition density, *i.e.* the joint probability function is reduced to a manageable 2-dimensional matrix. Secondly, the whole transition density is evaluated when using the Chapman-Kolmogorov equation, unlike tests which are based on specific conditional moments. Lastly, the Chapman-Kolmogorov transition density remains well defined even within a multiple variable description [87].

CHAPTER 3

EVOLVING PROBABILITY DISTRIBUTIONS

A simple and convenient way of describing the evolution of any system, mathematically, is with differential equations. However, differential equations are deterministic in nature and will always evolve in the same way regardless of the system's initial state. For example, in principle, the time evolution of a system consisting of many parts such as a mole of gas, which contains 6×10^{23}gas molecules, can be entirely predicted. The actual microscopic properties are not random and are described by Newton's Laws. In practice, it is however impossible to make such exact predictions for a fluctuating system using these exact laws. Here the full set of initial conditions, $6 \times 6 \times 10^{23}$ for all generalised coordinates (positions and momenta), as well as the full trajectories of all the molecules need to be specified. Fortunately, it is not the behaviour of the constituents of the system that is of interest, but rather the macroscopic behaviour, which can be described by a suitable average and which is given by the distribution of states within a system. [14]. These macroscopic variables are governed by approximate deterministic equations. The approximate nature of these differential equations is due to their fluctuating terms. The macroscopic variables are thus stochastic functions of time whose description is called mesoscopic. In a mesoscopic model, the fluctuations are caused by the discrete nature of that system. For example the density of a gas fluctuates because gases consist of molecules and radio-active decay fluctuates because of the individuality of the nuclei [14]. In the mesoscopic model each transition occurs with a certain probability yielding a stochastic process.

The idea that the macroscopic behaviour can be governed by its own equations of motion regardless of the microscopic motion is based on the assumption of randomness. The microscopic variables vary much more rapidly than the few macroscopic variables and reach their equilibrium distribution effectively instantaneously. These equilibrium distributions correspond to the values of the macroscopic variables that behave as if they are fixed [14]. This randomness assumption is the general form of the molecular chaos assumption made by Boltzmann in his study of dilute gases [14,81,82]. One of its effects is the Markov property given by equation (2.33).

The physical process of changes in state, in terms of the probability of a certain state to occur, is given in its most basic form as a master equation. The master equation uses the assumption of randomness to govern the transitions back and forth between the microscopic states, to produce

macroscopic equations (deterministic and approximate) from the microscopic equations (deterministic and exact) [88], as shown in Fig 3.1.

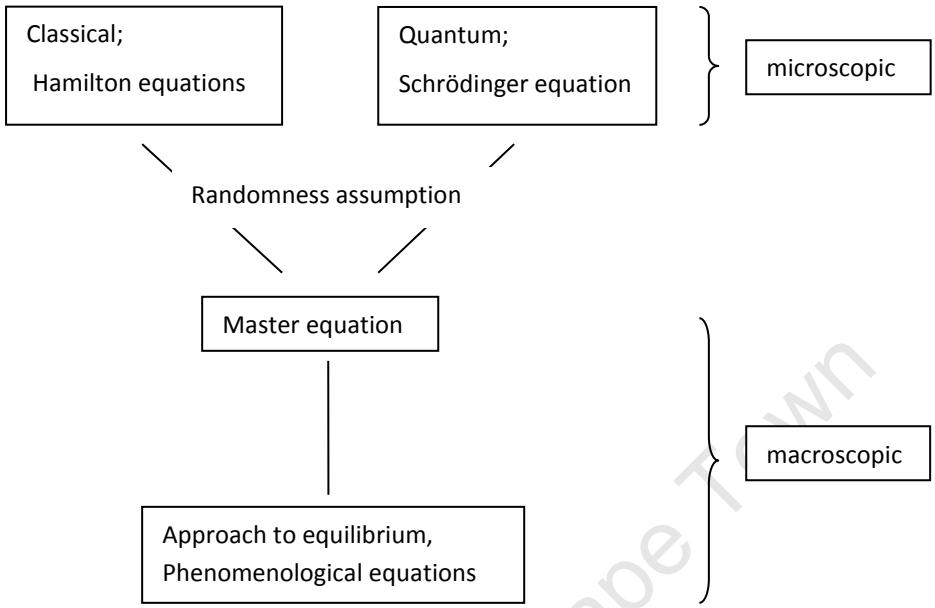

Fig 3.1 Relationship of the master equation to microscopic and macroscopic behaviour, based on the randomness assumption [88].

In this chapter master equations are formulated for systems undergoing changes in state, due to spontaneous fluctuations and binary collisions with another subsystem. As it is only in rare cases that the master equation can be solved, a suitable approximation is often needed [14]. In the case of systems undergoing changes in state due to spontaneous fluctuations, the master equation is approximated by a Fokker-Planck equation, a differential equation, which gives the probability density for such systems with different system's states over time. Systems experiencing fluctuations due to binary collisions are described by a Boltzmann equation, a particular class of master equation. For systems experiencing both binary collisions and spontaneous fluctuations a Boltzmann equation is approximated by a Fokker-Planck equation containing the binary collision terms in the drift and diffusion coefficients [69-72].

The drift term describes the evolution of the probability distribution in terms of the rate of change of the mean and describes the systematic bias in the random variable of the fluctuating system. The diffusion term describes the change of the variance of the probability density. The drift and diffusion coefficients of the derived Fokker-Planck equations are used later in this thesis, to quantify the

deterministic and random influences of a stochastic system, for both spontaneous and induced fluctuations for various fluctuating systems.

3.1. The Master Equation

Consider a random process $x(t)$ which can take on a range of continuous values as a function of time t. For example $x(t)$ may represent, position, speed or energy of a gas particle. Let $P(x,t)$ be the probability density function of the random variable $x(t)$ at time t. If the conditional probability density function of $x(t)$ at time t is $P(x,t|x_0,t_0)$, given that $x(t)=x_0$ at time $t=t_0$, then $P(x,t)$ satisfies the linearised Boltzmann equation [66]

$$\frac{\partial P(x,t)}{\partial t}=\lim_{\Delta t\to 0}\frac{1}{\Delta t}\int_{-\infty}^{\infty}[P(x,t+\Delta t|x',t)P(x',t)-P(x',t+\Delta t|x,t)P(x,t)]\,\mathrm{d}x'. \tag{3.1}$$

This is a gain-loss equation for the probabilities of the separate states. The first term on the right is the gain of state x due to transitions from other states x', and the second term is the loss due to transitions from x into other states [14]. The flow out of state x' into state x is proportional to the probability $P(x',t)$ of state x' to occur and to the transition probability density function $P(x,t+\Delta t|x',t)$. If the transition rate $W(x|x')$ denotes the transition probability $P(x,t+\Delta t|x',t)\geq 0$ from state x' to state x per unit time Δt, then [14,72]

$$W(x|x')=\lim_{\Delta t\to 0}\frac{1}{\Delta t}P(x,t+\Delta t|x',t)\geq 0,\quad (x\neq x'). \tag{3.2}$$

Substituting equation (3.2) into the Boltzmann equation (3.1) gives the more familiar form of the master equation

$$\frac{\partial P(x,t)}{\partial t}=\int[W(x|x')P(x',t)-W(x'|x)P(x,t)]\,\mathrm{d}x'. \tag{3.3}$$

The master equation was first so called in a 1940 paper by Nordsieck *et al* [89], in which it was introduced as a general form from which other special cases were derived. It is a more convenient differential form than the Chapman-Kolmogorov equation and much closer to the physical concepts. It considers the transformation probabilities as given by the specific system and is a linear equation for the probabilities which determine the mesoscopic state of that system. Depending on the reason

for the uncertainty concerning the system, the correct derivation of the corresponding master equation varies.

To consider systems undergoing changes in state due to binary collisions with another system or subsystem, two types of systems denoted by an index α and β are defined. For example in the study of wind turbulence (chapter 4), α may be the velocity component of wind generated in wind tunnels in the streamwise direction colliding with wind travelling in the cross-stream direction, denoted by an index β. Thus for a system of type α the master equation (3.3) becomes

$$\frac{\partial P_\alpha(x,t)}{\partial t} = \int [W(x|x')P_\alpha(x',t) - W(x'|x)P_\alpha(x,t)]\,\mathrm{d}x'. \tag{3.4}$$

If one only considers spontaneous transitions of system α and transitions due to binary collisions of particles from system β colliding with particles from system α, then the transition function $W(x'|x)$ in equation (3.4), can be decomposed into [71,72]

$$W(x'|x) = W_\alpha(x'|x) + \int\int W_{\alpha\beta}(x',y'|x,y)P_\beta(y,t)\mathrm{d}y\mathrm{d}y'. \tag{3.5}$$

Here $W_\alpha(x'|x)$ describes the rate of spontaneous transitions from state x to state x' for systems of type α. $W_{\alpha\beta}(x',y'|x,y)$ is the transition rate for the two systems of types α and β to change their states from x and y to x' and y'. Inserting equation (3.5) into equation (3.4) gives a Boltzmann-like equation [71]

$$\begin{aligned}\frac{\mathrm{d}P_\alpha(x,t)}{\mathrm{d}t} = &\int [W_\alpha(x|x')P_\alpha(x',t) - W_\alpha(x'|x)P_\alpha(x,t)]\mathrm{d}x' \\ &+ \int\int\int W_{\alpha\beta}(x,y'|x',y)P_\beta(y,t)P_\alpha(x',t)\,\mathrm{d}x'\mathrm{d}y\mathrm{d}y' \\ &- \int\int\int W_{\alpha\beta}(x',y'|x,y')P_\beta(y,t)\,P_\alpha(x,t)\,\mathrm{d}x'\mathrm{d}y\mathrm{d}y'.\end{aligned} \tag{3.6}$$

If the spontaneous transitions due to internal fluctuations are set to zero, *i*.e. $W_\alpha(x'|x) = 0$, equation (3.6) agrees with the Boltzmann equation, which was originally developed for the description of kinetic gases [81,82].

3.2. The Fokker-Planck Equation – Spontaneous Fluctuations

The Fokker-Planck equation, like a Boltzmann equation, is a transport equation which gives the equation of motion for the probability distribution function. The general Fokker-Planck equation, in one dimension and independent of time is

$$\frac{\partial P(x,t)}{\partial t} = -\frac{\partial}{\partial x}[D_1(x)P(x,t)] + \frac{1}{2}\frac{\partial^2}{\partial x^2}[D_2(x)P(x,t)], \tag{3.7}$$

where $D_1(x)$ is the drift or convection term and $D_2(x)$ the diffusion term or fluctuating term. To derive the Fokker-Planck equation, the master equation (3.3) is rewritten by expressing the transition probability W as a function of the size r of a jump, and of the starting point for the first term $r = x - x'$ and $r = x' - x$ for the second term, giving

$$\frac{dP(x,t)}{dt} = \int [W(x|x-r)P(x-r,t) - W(x+r|x)P(x,t)]\mathrm{d}x'. \tag{3.8}$$

The basic assumption is that only small jumps occur, *ie*. $W(x|x-r)$ is a sharply peaked function of r but varies slowly with x. More precisely, there exists a $\delta > 0$ such that

$$W(x|x-r) \approx 0 \qquad \text{for } |r| > \delta \tag{3.9}$$

and

$$W(x+\Delta x|x-r) \approx W(x|x-r) \qquad \text{for } |\Delta x| > \delta\,. \tag{3.10}$$

But as $W(x|r) = W(x+r|x)$ equation (3.8) can be rewritten as

$$\frac{dP(x,t)}{dt} = \int [W(x-r|x)P(x-r,t) - W(x|r)P(x,t)]\,\mathrm{d}x'. \tag{3.11}$$

The Fokker-Planck equation is obtained by applying the Kramers-Moyal expansion to equation (3.11) and terminating after the second term. The general expansion methods [20], of passing from an integral operator to a differential operator, require several assumptions [14]. One has to assume the convergence properties of certain series, the existence of certain partial derivatives and the

interchange of certain limits [14,74,66]. A second reasonable assumption is that the solution $P(x,t)$ varies slowly with x, as in (3.11). The Kramers-Moyal expansion is given by [73,74]

$$\frac{\partial P(x,t)}{\partial t} = \sum_{k=1}^{\infty} \frac{(-1)^k}{k!} \frac{\partial^k}{\partial x^2} [D_k(x,t)P(x,t)] \tag{3.12}$$

where

$$D_k(x,t) = \frac{1}{k!} \lim_{\Delta t \to 0} \frac{1}{\Delta t} \int_{-\infty}^{\infty} (x' - x)^k P(x', t + \Delta t | x, t) \mathrm{d}x'. \tag{3.13}$$

Pawula's theorem [66,67] states that if D_k exist for all k, and if $D_k = 0$ for some even k, then $D_k = 0$ for all $k \geq 3$. Exercising the Kramers-Moyal expansion and Pawula's theorem to equation (3.11) gives the Fokker-Planck equation

$$\frac{\partial P(x,t)}{\partial t} = -\frac{\partial}{\partial x}[D_1(x)P(x,t)] + \frac{1}{2}\frac{\partial^2}{\partial x^2}[D_2(x)P(x,t)], \tag{3.14}$$

where the drift term $D_1(x)$ is

$$D_1(x) = \int (x' - x) W(x'|x) \mathrm{d}x' \tag{3.15}$$

and the diffusion term $D_2(x)$ is

$$D_2(x) = \frac{1}{2} \int (x' - x)^2 W(x'|x) \mathrm{d}x'. \tag{3.16}$$

Substituting the transition function of equation (3.2) into the drift and diffusion terms gives

$$\begin{aligned} D_1(x,t) &= \int (x' - x) \lim_{\Delta t \to 0} \frac{1}{\Delta t} P(x', t + \Delta t | x, t) \mathrm{d}x' \\ &= \lim_{\Delta t \to 0} \frac{1}{\Delta t} \int (x' - x) P(x', t + \Delta t | x, t) \, \mathrm{d}x' \end{aligned} \tag{3.17}$$

and

$$D_2(x,t) = \frac{1}{2}\int (x'-x)^2 \lim_{\Delta t\to 0}\frac{1}{\Delta t}P(x',t+\Delta t|x,t)\mathrm{d}x' \qquad (3.18)$$
$$= \frac{1}{2}\lim_{\Delta t\to 0}\frac{1}{\Delta t}\int (x'-x)^2 P(x',t+\Delta t|x,t)\mathrm{d}x'.$$

Equations (3.17) and (3.18) give the first two expansion terms of the Kramers-Moyal expansion for systems experiencing spontaneous fluctuations.

To obtain an understanding of how the drift and diffusion coefficients affect the evolution of the probability density function $P(x,t)$ with time, the general Fokker-Planck equation (3.7) is solved for arbitrary values of the drift and diffusion coefficients and for suitably chosen Dirichlet boundary and Gaussian initial conditions. The solution profile of equation (3.7) is plotted in Fig 3.2 for a fixed diffusion coefficient at $D_2(x) = 3$ and for three positive values of $D_1(x) = 0.5, 1$ and 2.

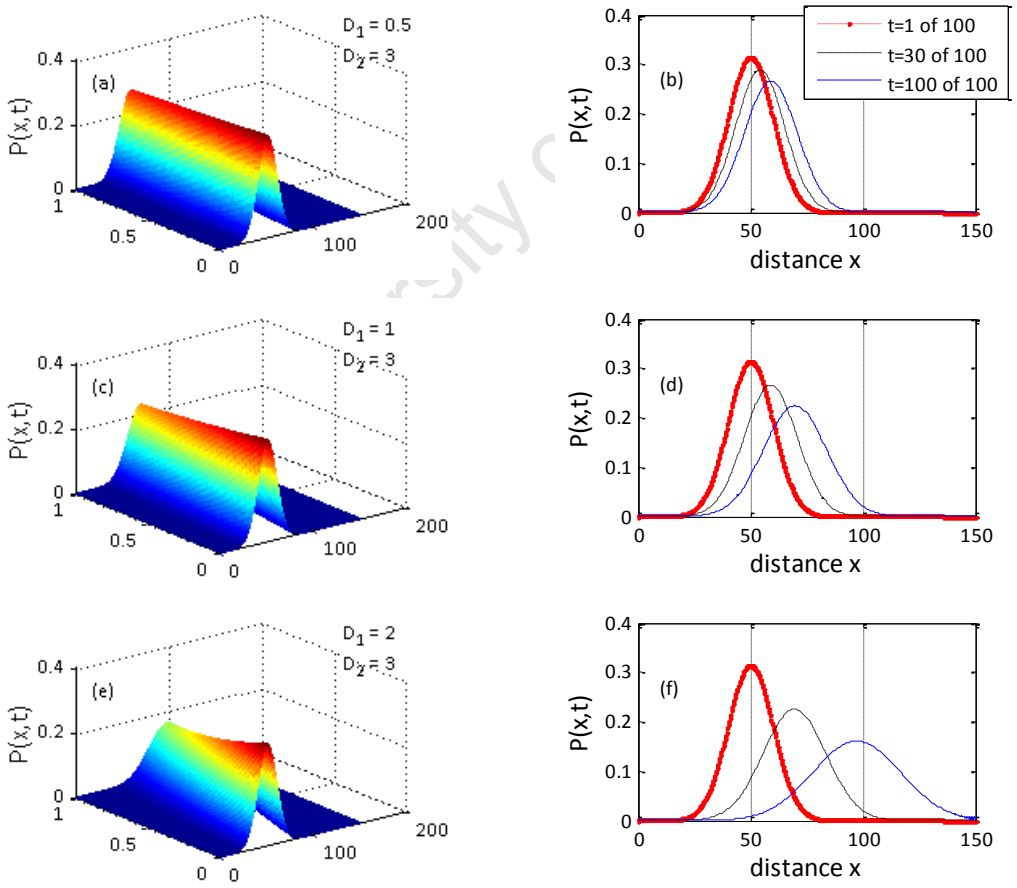

Fig 3.2 Solution profile of the general Fokker-Planck equation (3.7) for a fixed value of $D_2(x) = 3$ and for three positive values of $D_1(x) = 0.5, 1$ and 2.

The positive drift coefficient causes the mean of $P(x,t)$ to shift towards larger values of x. The drift coefficient describes the speed and direction of the mean of the distribution. As a result of the normalised property described in section 2.2, equation (2.3), the shift towards greater values of x is interpreted as an increase in larger fluctuations of x. A negative drift coefficient causes the mean of $P(x,t)$ to shift towards smaller values of x. By the normalised property equation (2.3), the shift towards smaller values of x is interpreted as an increase in smaller fluctuations of x. Thus the drift coefficient describes the drift of the probability distribution corresponding to a systematic bias and also gives the rate of change of the mean, which is just equation (3.15). To consider the effect of the diffusion coefficient the drift term is held constant for three arbitrary values of the diffusion term. The solution profile is plotted in Fig 3.3 for $D_1(x) = 0.3$ and for values of $D_2(x) = 0.5, 1.5$ and 2.5.

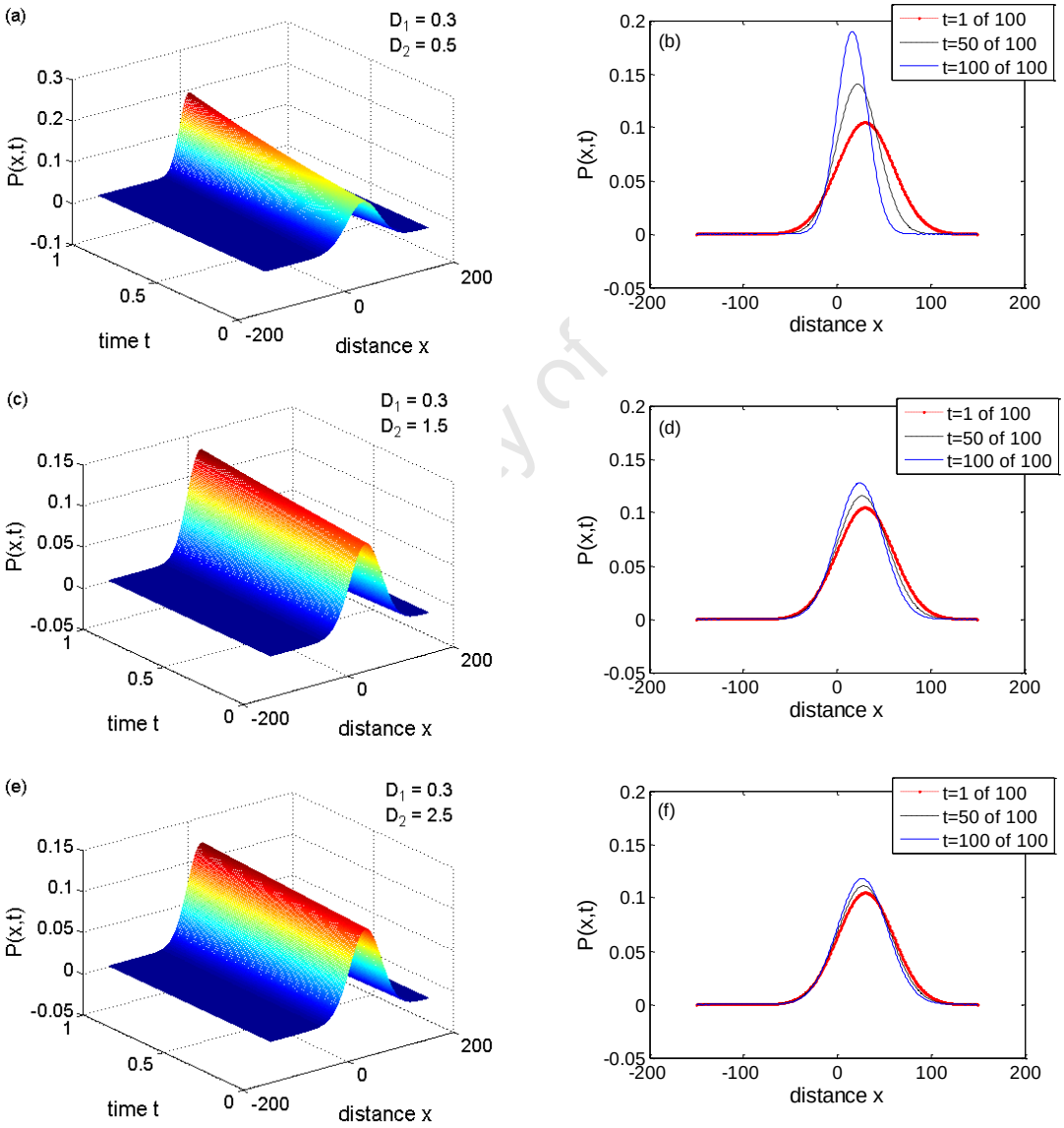

Fig 3.3 Solution profile of equation (3.7) for fixed values of $D_1(x) = 0.3$ and for three values of $D_2(x) = 0.5, 1.5$ and 2.5.

The diffusion term causes the distribution to spread out around the mean of the distribution, as can be seen in Fig 3.2 as well. The diffusion term describes the change of the variance of the probability density, which is equation (3.16).

3.3. Boltzmann's Molecular Chaos Assumption

To apply a Fokker-Planck equation to systems undergoing changes in state due to binary collisions with another system an important assumption is used. The molecular chaos assumption, also called the randomness assumption, was formulated by Boltzmann and referred to as the Stosszahl Ansatz [14]. With his kinetic theory of gases Boltzmann attempted to explain the properties of dilute gases by analysing the basic collision processes between pairs of molecules. The Boltzmann equation describes the evolution of the probability distribution of position and momentum of a single particle in an ideal gas. In a very general way the Boltzmann equation is given by [81]

$$\frac{\partial P}{\partial t} + v_1 \frac{\partial P}{\partial x_1} = G - L, \tag{3.19}$$

where P represents the distribution function of the position and velocity of a single particle at a given time. $L\mathrm{d}x_1\mathrm{d}v_1dt$ gives the expected number of particles with position between x_1 and $x_1 + \mathrm{d}x_1$ and velocity between v_1 and $v_1 + \mathrm{d}v_1$ that is loss from these ranges of values should it encounter a collision in the time interval between t_1 and $t_1 + \mathrm{d}t_1$. $G\mathrm{d}x_1\mathrm{d}v_1\mathrm{d}t$ gives the analogous number of particles gained in the same range in the same time interval [81]. The first term on the left-hand side of Boltzmann equation (3.19) describes how the distribution function of the particles varies with respect to time while the second term describes how the distribution function varies with respect to space. The right-hand side of the Boltzmann equation describes how these two terms are related in terms of the effect of collisions between the particles.

Consider a box whose volume is 1 cm^3 at room temperature and atmospheric pressure. In a rarefied gas N is a very large number of particles, say $N \cong 10^{21}$ and δ is very small, $\delta = 10^8$ cm, then $(N-1)\delta^2 \cong N\delta^2 = 10^4\mathrm{cm}^2 = 1\ \mathrm{m}^2$ is a sizable quantity, while the difference between x_1 and $x_1 + \delta n$ can be neglected. Since the volume occupied by the particles is about $N\delta^3 \cong 10^{-4}\ \mathrm{cm}^3$, it is reasonable to assume that collisions between two marked particles are a rare event [14,81]. On this basis it is assumed that two particles that happen to collide are considered to be two randomly chosen particles whose position and velocity prior to collision are independent of one another. Then

the probability of finding the first particle at x_1 with velocity v_1 and the second at x_2 with velocity v_2 is equal to product of the probability of finding the first particle at x_1 with velocity v_1 times the probability of finding the second particle at x_2 with velocity v_2, *i.e.* [81]

$$P(x_1, v_1; x_2, v_2, t) = P(x_1, v_1, t)P(x_2, v_2, t). \tag{3.20}$$

Equation (3.20) characterises Boltzmann's molecular chaos assumption. The factorisation of equation (3.20) into its factors clearly shows independence and a property of randomness. The chaos property, if initially present, is almost immediately destroyed after the collision [14, 81]. The molecular chaos property is required only for particles that are about to collide [14].

3.4. The Fokker-Planck Equation – Induced Fluctuations

There are two ways of deriving a Fokker-Planck equation which contains collision terms [71,72]. One could exercise the Kramers-Moyal expansion and Pawula's theorem on equation (3.6) or expand the drift and diffusion functions in the Fokker-Planck equation (3.14) to include the collision terms. These methods both require the molecular chaos assumption to factorise the joint probability (3.20) into

$$P(x_\alpha, t_\alpha; x_\beta, t_\beta) = P(x_\alpha, t_\alpha)P(x_\beta, t_\beta). \tag{3.21}$$

Using the latter method, the decomposed transition function $W(x'|x)$, equation (3.5), is substituted into the drift and diffusion coefficients, equations (3.15) and (3.16), respectively, to give

$$D_1(x,t) = \int (x' - x) W_\alpha(x'|x)\mathrm{d}x' + \int\int\int (x' - x)\, W_{\alpha\beta}(x'y'|x,y)P_\beta(y,t)\mathrm{d}y'\mathrm{d}y\mathrm{d}x' \tag{3.22}$$

and

$$D_2(x,t) = \int (x' - x)^2 W_\alpha(x'|x)\mathrm{d}x' + \int\int\int (x' - x)^2\, W_{\alpha\beta}(x'y'|x,y)P_\beta(y,t)\mathrm{d}y'\mathrm{d}y\mathrm{d}x'. \tag{3.23}$$

The first terms of equations (3.22) and (3.23) describe internal transitions from state x to x' while the second terms contains the collision terms which describe the interaction of system y on x. Now substituting equation (3.2), the transition rate $W(x|x')$, into equations (3.22) and (3.23) gives

$$D_1(x,t) = \lim_{\Delta t \to 0} \frac{1}{\Delta t}\Big[\int (x' - x) P_\alpha(x', t+\Delta t|x,t)\mathrm{d}x' + \int\int\int (x' - x)\, P_{\alpha\beta}(x', y', t+\Delta t|x,y,t) P_\beta(y,t)\, \mathrm{d}y'\mathrm{d}y\mathrm{d}x'\Big] \tag{3.24}$$

and

$$D_2(x,t) = \lim_{\Delta t \to 0} \frac{1}{\Delta t}\Big[\int (x' - x)^2 P_\alpha(x', t+\Delta t|x,t)\mathrm{d}x' + \int\int\int (x' - x)^2\, P_{\alpha\beta}(x', y', t+\Delta t|x,y,t) P_\beta(y,t)\, \mathrm{d}y'\mathrm{d}y\mathrm{d}x'\Big]. \tag{3.25}$$

Equations (3.14), (3.24) and (3.25) together form the Fokker-Planck equation which describes the evolution of the probability density function of a fluctuating system α due to spontaneous fluctuations and induced fluctuations of system β by means of binary collisions of their particles. It is emphasized in [66] that when a Boltzmann integral is approximated by a differential operator, such as in the Kramers-Moyal expansion, one has to assume the convergence properties of certain series and the existence of certain partial derivatives. Another assumption is that the expansion parameter must be the mass ratio of a light to a heavy particle in the binary collision process [66].

CHAPTER 4
WIND TURBULENCE

Turbulence is often observed in physical systems as a chaotic and irregular flow of a gas or liquid, for example, in the motion of the clouds and ocean currents, smoke from a chimney, atmosphere of the Sun and the flow of electric current in a conductor. More recently, turbulence has been used in the study of biological systems [60-65,90,91], like the flow of blood in arteries, and in non-physical systems to describe the flow of information on the financial markets [47-59]. It seems that turbulence is the usual state while smooth laminar flow, is the exception.

4.1. Turbulent Flow

In laminar flow the local velocity of a fluid is a continuous function of time and position. If additional kinetic energy is introduced into the flow, the velocity distribution develops many random spikes, corresponding to rapidly varying velocity fluctuations with respect to space or time. This is turbulent flow. As an example, these rapidly varying velocity fluctuations can be observed in Fig 4.1, for an arbitrary sample of 12 000 wind velocity measurements taken from the well-known experiments performed by Kang *et al* [83,92]. At shorter spatial intervals more local maxima and minima over smaller length scales are observed.

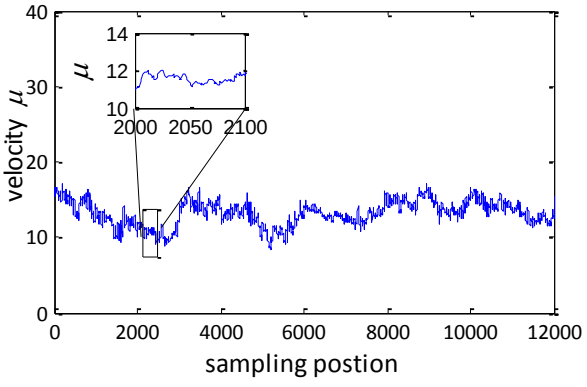

Fig 4.1 An example of rapidly varying wind velocity measurements showing the self-similar structure of the velocity measurements.

Turbulence is best described using the concepts of eddies and vortices. An eddy can be thought of as a body of gas or liquid in which some of the microscopic elements, composing the eddy, behave as a

unit while others undergo a short reversal in the flow around a void. The backward flow fills this void causing a swirling motion. A vortex has similar backward flow around an area of low pressure, causing a spiralling motion [93].

Eddies of different sizes and behaviour can also be grouped together to form a larger eddy. Fully turbulent flow means eddies of all shapes and sizes exist. Larger eddies are formed by drawing on the kinetic energy from the mean flow in fully turbulent flow [93]. They are also inherently unstable and continually break down into smaller eddies, which break down further into smaller ones, successively until the energy is dissipated. This feature of a turbulent flow is called an energy cascade and describes a transfer of kinetic energy from large scale eddies to progressively smaller scales [93]. Kolmogorov proposed that the cascade is essentially one-directional, self-similar and uniformly distributed over the turbulent flow [93]. An example of the self-similar appearance of these eddies at different length scales can be observed in Fig 4.2 [94]. It shows a turbulent cascade of a large eddy of scale L with a cascade of smaller eddies. The image shows the concentration of jet fluid directed downward into water [94].

Fig 4.2 A jet of water directed downward into water showing the different scales of eddy motion and self-similar appearance at different length scales [94].

One of the important outcomes of Kolmogorov's work [1,2] on turbulent cascades, was that the statistical properties of turbulence depend only on the rate at which energy produced at the largest scale, cascades down to smaller scale eddies [95]. Kolmogorov found this to be true for systems with large Reynolds numbers and above the viscous dissipation scale. Reynolds numbers are related to the length of the cascade, which is defined as the ratio of the largest to smallest scales [93]. Also, at high Reynolds numbers, and if the energy scale is long, the information carried by the larger scales

may be lost at the smaller scales [46]. In addition, should there be a distinct separation of scales between the large and small eddies, *i.e*. at high Reynolds, a range of scales exist which is independent of the largest and smallest scales, and therefore viscosity. Such a range is called the inertial subrange, which is illustrated in the energy spectrum of turbulence in Fig 4.3 [96], which shows a typical energy spectrum of a turbulent flow. The energy spectrum is a function of the wave number or inverse wavelength, L^{-1}. Kinetic energy is absorbed from the mean flow to produce the large eddies with low wave numbers. Smaller eddies are then progressively formed with an increase in wave number and energy flows down the energy spectrum to where it is dissipated into heat at the smallest eddies.

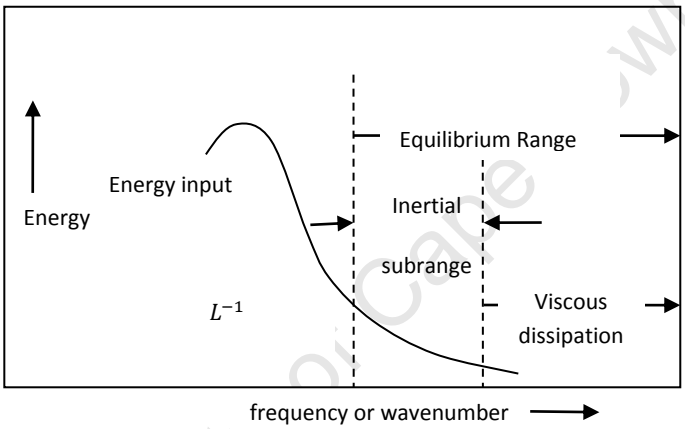

Fig 4.3 Schematic representation of the energy spectrum of turbulence. [96]

Experimental studies [97] of general stochastic systems have shown that the order of complexity and disorder depends on the scale at which they are observed. Therefore, stochastic analysis of those systems uses scale-dependent quantities for their description. Typical analyses of the scale-dependent measures focus on increments for a given length separation. For a turbulent flow the main focus is the velocity increment, $v(r)$ between two spatial locations x which are a distance kd apart,

$$v(r) \equiv \Delta u(x) = u(x + kd) - u(x), \tag{4.1}$$

where $u(x)$ is the velocity fluctuation, k an integer number of the dispersion d of the time series. The dispersion or resolution of the time series is the temporal or spatial distance between recordings of successive observations, *i.e.* the period. Other examples [98] for scale-dependent

measures of complexity are the autocorrelation function [99,100] $R(r) = \langle y(x)y(x+r)\rangle$, the root-mean-square [101] $w_r(x) = \langle [y(x) - y]^2 \rangle^{\frac{1}{2}}$, and wavelet functions [102,103] which are used in chapter 6. Typical scale-dependent analysis of stochastic data uses structure functions $\langle \big(v(r)\big)^n \rangle$ given by the probability density functions $P(v(r))$. One can extend such analyses by focusing on the probability density functions of these increments [95,104]. This involves describing the joint statistics of the chosen measure on many different scales r_i [105] by the knowledge of the joint probability density functions

$$P\big(v(r_1); v(r_0)\big) \tag{4.2}$$

and the conditional probability density functions

$$P\big(v(r_1)\big|v(r_0)\big) = \frac{P\big(v(r_1); v(r_0)\big)}{P\big(v(r_0)\big)}. \tag{4.3}$$

Using these probability density functions the correlations between scales are evaluated, showing how the complexity is linked across scales [105]. If the statistics of the scale-dependent measure can be captured by a binary-scale transition function, as is commonly presented as the Markov property (equation (2.33)) then knowledge of the binary-scale conditional probability density function (binary-scale transition function) is sufficient for a complete description of a multi-scale joint probability density function [83]. The Fokker-Planck equation is obtained by applying the Kramers-Moyal expansion to equation (3.11) and terminating after the second term [66-68,71,72]. The Fokker-Planck equation can therefore be postulated to govern the joint probability density functions of the correlations between scales.

4.2. Methodology

To investigate the description of turbulence by means of the Fokker-Planck equations, data from the well-known experiments performed by Kang *et al* [83] are used. The data was generated using return-type Corrsin wind tunnels [106,107] of normal laboratory size with an active grid. A schematic of the experimental wind-tunnel used by Kang *et al* is shown in Fig 4.4.

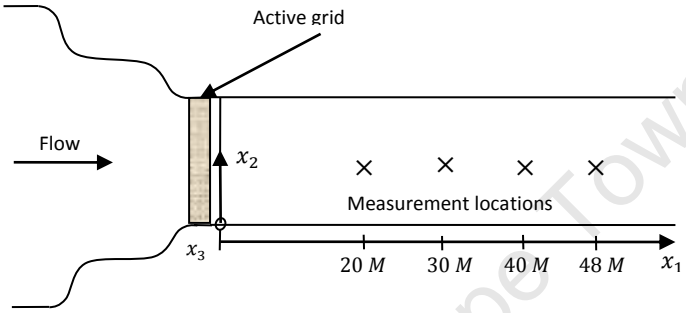

Fig 4.4 A schematic of the experimental wind-tunnel used by Kang *et al* [83,46] to generate the data used in this work.

The active grid is located at the beginning of the test section. The measurement locations in the streamwise direction (x_1) were at $x_1/M = 20,\ 30,\ 40 \text{ and } 48$, where x is the downstream distance and *M* is the mesh size of the grid.

To measure the wind velocities, Kang *et al* used an X-wire probe array [83] to record two velocity components, in the (x_1, x_2)-plane and (x_1, x_3)-plane. Here x_2 and x_3 are the cross-stream (transverse), *i.e.* vertical and perpendicular to x_1 and spanwise, *i.e*. horizontal and perpendicular to x_1 directions, respectively. Four different filter scales: Δ1 = 10 mm, Δ2 = 20 mm, Δ3 = 40 mm, and Δ4 = 80 mm were considered. The data and full details of the experimental setup can be downloaded from the JHU Turbulence Database Cluster [92]. Only data passing through filter scale $\Delta 1 = 10 \text{ mm}$ measured at the $x_1/M = 20$ downstream position, in the streamwise direction and cross-stream direction were used in this work. The data consist of 1.2×10^6 observations for each wind direction and filter. See Appendix A for more details about the data. An arbitrary chosen sample of 1.2×10^5 observations measured at the $x_1/M = 20$ downstream position is plotted in Fig 4.5.

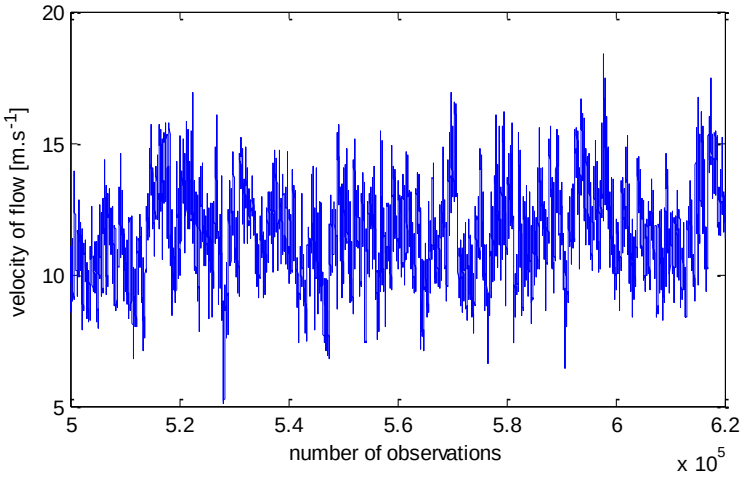

Fig 4.5 A plot of a random sample of 120 000 data points sampled from the dataset 'm20h1-01.dat'.

Field experiments usually measure variables that evolve with time, whereas laboratory experiments and numerical simulations calculate statistics as a function of space. The two frameworks are related by Taylor's hypothesis of frozen turbulence. According to this hypothesis, the conversion from time to space coordinates is obtained by considering the relation

$$\frac{r}{d} = \frac{t}{\Delta t}, \tag{4.4}$$

where d is the spatial resolution, t the time variable and Δt is the sampling interval. From the data $d = \langle u \rangle \times \Delta t = 0.3\ \text{mm}$, where $\langle u \rangle = 12\ \text{m.s}^{-1}$ is the average velocity of the series x_1/M and $\Delta t = 1/40000$ seconds.

The use of probability methods to investigate complex fluctuating systems, such as turbulence, requires the construction of different sizes of nested scales r_i, to produce a hierarchical system defined on the scales $r_n < r_{n-1} < \cdots < r_0$. A Fokker-Planck equation describes the change in the stochastic dependency across these different scales. This method requires the testing of several assumptions.

The first assumption to be tested is whether there is a correlation between velocity increments $v(r_i)$ across different length scales r_i. Assuming that $v(r)$ is a random variable, for individual sampling one cannot be sure of its value, but equation (2.1) implies that, in the limit of infinitely many samplings, a fraction $P\big(v(r)\big)\mathrm{d}v$ will yield values in the interval $[v, v + \mathrm{d}v)$. Suppose the value of

$v(r)$ at some initial position (scale) r_0 is fixed and that $v(r_i)$ for any $r_i < r_0$ can be predicted only probabilistically, then a stochastic system is defined by the investigation of the state of the system at successive instants $r_n < r_{n-1} < \cdots < r_0$. The joint density function for n random variables $v(r_n), v(r_{n-1}), \ldots,$ and $v(r_0)$ is then defined as

$$P\big(v(r_n); v(r_{n-1}); \ldots; v(r_1); v(r_0)\big) = P\big(v(r_0)\big)P\big(v(r_n); v(r_{n-1}); \ldots; v(r_1)\big|v(r_0)\big). \tag{4.5}$$

Equation (4.5) describes a dependency of $v(r_i)$ for any $r_i < r_0$. If the velocity increments are independent across scales then equation (4.5) factorises into

$$P\big(v(r_n); v(r_{n-1}); \ldots; v(r_1); v(r_0)\big) = P\big(v(r_0)\big)P\big(v(r_{n-1})\big)P\big(v(r_n)\big) \ldots P\big(v(r_1)\big), \tag{4.6}$$

a random process.

The second assumption that should be tested is whether the stochastic process described by equation (4.5) can be reduced to a binary-scale transition function, as represented by the right-hand side of equation (4.7) below

$$P_1^{(n)}\big(v(r_n)\big|v(r_{n-1}); \ldots; v(r_1); v(r_0)\big) = P_1^{(n)}\big(v(r_n)\big|v(r_{n-1})\big) \equiv P\big(v(r_n)\big|v(r_{n-1})\big), \tag{4.7}$$

for all $n \geq 2$ and $r_{n-1} \leq r_n$.

This feature of a stochastic process is commonly considered to be equivalent to the Markov property. The existence of the Markov property provides a convenient computational tool in that it is no longer necessary to deduce all possible permutations of the velocity increments, $v(r_i)$ for all possible scales r_i. A common test for the Markov property is to use the Chapman-Kolmogorov equation, given by

$$P\big(v(r_1)\big|v(r_0)\big) = \int_{-\infty}^{\infty} P\big(v(r_1)\big|v(r_i)\big)P\big(v(r_i)\big|v(r_0)\big)\,\mathrm{d}x_i, \qquad \text{for } (r_1 \leq r_i \leq r_0). \tag{4.8}$$

The Chapman-Kolmogorov equation describes the stochastic dependency, given by the probability density functions $P\big(v(r_1); v(r_0)\big)$ and $P\big(v(r_1)\big|v(r_0)\big)$, across length scales r. In this work the Chapman-Kolmogorov equation and the conditional probability function, equation (4.7), are used to evaluate the Markov property. The results of these two methods are compared and discussed.

It is convenient to consider a logarithmic length scale $\rho = \ln(r_0/r_1)$, as $r_1 < r_0$, then the limiting case as $r \to 0$ corresponds to $\rho \to \infty$. The Fokker-Planck equation now describes how the velocity increments are correlated across scales ρ, *i.e.*

$$\frac{\partial P(v(r),\rho)}{\partial \rho} = -\frac{\partial}{\partial x}[D_1(v(r),\rho)P(v(r),\rho)] + \frac{1}{2}\frac{\partial^2}{\partial x^2}[D_2(v(r),\rho)P(v(r),\rho)]. \tag{4.9}$$

The third assumption to be tested is whether any even Kramers-Moyal coefficient greater than the second order equals zero. If $D_k(v(r),\rho) = 0$, where k is an even number, then Pawula's theorem [66,67] applies and the Kramers-Moyal expansion may be truncated at the second order. The drift and diffusion coefficients of the Fokker-Planck equation are then the first and second Kramers-Moyal moments. The Kramers-Moyal moments are calculated directly from the time series as the limiting moments M_k of the transition probability distributions [2, 12]

$$\begin{aligned} D_k(v(r_i),\rho_i) &= \frac{1}{k!}\lim_{\rho\to\rho_i} M_k(v(r_i),\rho_i) \\ &= \frac{1}{k!}\lim_{\rho\to\rho_i}\frac{1}{\rho-\rho_i}\int (v(r)-v(r_i))^k P(v(r),\rho|v(r_i),\rho_i)\mathrm{d}v. \end{aligned} \tag{4.10}$$

The Fokker-Planck equation quantifies the deterministic influences and random fluctuations of a stochastic system. For systems experiencing both binary collisions and spontaneous fluctuations a Fokker-Planck equation, containing the collision terms, is used, as described in chapter 3. The idea of a binary collision used in this work, is equivalent to Boltzmann's idea of a binary collision between two uncorrelated gas molecules in his theory of dilute gases [81,82]. In this work the collision is between two systems, denoted by α and β, referring to wind velocities propagated in the streamwise and cross-stream direction, respectively.

The transitions of system α are due to both spontaneous fluctuations $W_\alpha(x'|x)$ and induced transitions $W_\beta(y'|y)$ of system β changing its state from y to y'. $u_\alpha(x)$ is the velocity component passing through filter scale $\Delta 1 = 10$ mm in the streamwise direction while $u_\beta(x)$ is the velocity component of the wind passing through the $\Delta 1 = 10$mm filter in the cross-stream direction. Using equations (3.24) and (3.25) the drift and diffusion coefficients are estimated. No such method to analyse time series data has yet been reported. This novel method considers the correlation of the probability density function $P(v(r), \rho)$ of system α due to binary interactions of system β with system α. This use of the Fokker-Planck equation allows the further quantification of the deterministic and random influences due to the internal (spontaneous) and external (induced) fluctuations.

To use the Fokker-Planck equation, in this situation, it is necessary to test the molecular chaos assumption, given by equation (3.21). The joint probability density function $P\big(u_\alpha(x); u_\beta(x)\big)$ is defined as the probability of the streamwise velocity component having a value of $u_\alpha(x)$ at position x and the cross-stream velocity component having a value of $u_\beta(x)$ at the same position x, for all x. To successfully conclude the molecular chaos assumption the joint probability density function must factorise into its two components,

$$P\big(u_\alpha(x); u_\beta(x)\big) = P(u_\alpha(x))P\big(u_\beta(x)\big). \tag{4.11}$$

Equation (4.11) is the last assumption to be tested and if valid permits the construction of a Fokker-Planck equation

$$\frac{\partial P_\alpha(v_\alpha(r), \rho)}{\partial \rho} = -\frac{\partial}{\partial x}[D_1(v_\alpha(r), \rho)P_\alpha(v_\alpha(r), \rho)] + \frac{1}{2}\frac{\partial^2}{\partial x^2}[D_2(v_\alpha(r), \rho)P_\alpha(v_\alpha(r), \rho)]. \tag{4.12}$$

The drift coefficient is given by

$$D_1(v_\alpha(r), \rho) = \lim_{\Delta\rho \to 0} \frac{1}{\Delta\rho}\Big[\int (v'_\alpha - v_\alpha)P_\alpha(v'_\alpha, \rho + \Delta\rho | v_\alpha, \rho)\mathrm{d}v'_\alpha + \int\int\int (v'_\alpha - v_\alpha)\, P_{\alpha\beta}\big(v'_\alpha; v'_\beta, \rho + \Delta\rho \big| v_\alpha; v_\beta, \rho\big)P_\beta\, \mathrm{d}v'_\beta \mathrm{d}v_\beta \mathrm{d}v'_\alpha\Big], \tag{4.13}$$

and the diffusion term is given by

$$D_2(v_\alpha(r),\rho) = \lim_{\Delta\rho\to 0}\frac{1}{\Delta\rho}\Big[\int (v'_\alpha - v_\alpha)^2 P_\alpha(v'_\alpha,\rho+\Delta\rho|v_\alpha,\rho)\mathrm{d}v'_\alpha + \int\int\int (v'_\alpha - v_\alpha)^2\, P_{\alpha\beta}\big(v'_\alpha;v'_\beta,\rho+\Delta\rho\big|v_\alpha;v_\beta,\rho\big)P_\beta\,\mathrm{d}v'_\beta\mathrm{d}v_\beta\mathrm{d}v'_\alpha\Big]. \quad (4.14)$$

The first terms of equations (4.13) and (4.14) describe the internal transitions of system α from state x to x', while the second terms include the collision terms, describing the transitions from states x and y to $x'$and y' due to the binary collision of system β on system α.

4.3. Testing of the Assumptions

The first assumption to be tested for the particular data is whether velocity increments $v(r)$ are a stochastic process in some length scale r. Consider the joint probability density functions $P\big(v(r_0);v(r_1)\big)$ for two carefully chosen length scales $r_1 = 100d$ and $r_0 = 300d$, where $d = 0.3\text{mm}$. If increments $v(r)$ are found to be a stochastic process in r for the above scales then it will be true also for scales $r_1 < r_i$, where $r_1 < r_i < r_0$. It is for this reason that r_0 is carefully chosen such that r_0 is greater than the length scales one is interested in. A contour plot of the the joint probability density functions $P\big(v(r_0);v(r_1)\big)$ is plotted in Fig 4.6.

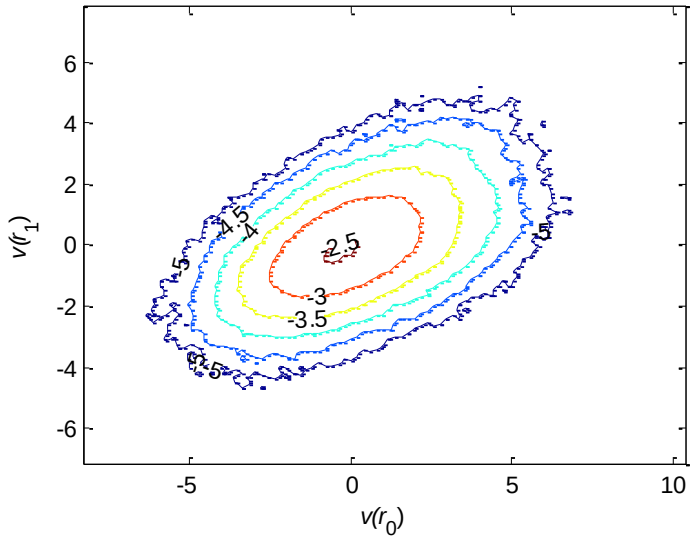

Fig 4.6 Contour plot of the joint probability density functions$P\big(v(r_1);v(r_0)\big)$ for the simultaneous occurrence of velocity increment $v(r_1 = 100d)$ and $v(r_0 = 300d)$ for all x in r.

The contour lines correspond to $\log_{10}P\big(v(r_1);v(r_0)\big) = -2.5,-3,-3.5,4,-4.5,-5$. For example if $P\big(v(r_1);v(r_0)\big) = 0.001$, then $\log_{10}(0.001) = -3$. Contour lines of -5.5 and -6 have been deleted

for presentation purposes. This plot was generated using the Matlab program Kramers_Moyal_Turb.m, (see Appendix B for all Matlab programs used in this work). The contour lines are aligned at a 45 degree angle to the axis of the plots which is evidence of a correlation across these two length scales [41], which implies that

$$P\big(v(r_1); v(r_0)\big) = P\big(v(r_0)\big)P\big(v(r_1)\big|v(r_0)\big) \tag{4.15}$$

and that the velocity increments $v(r)$ are a stochastic process for length scales $r_1 < r_i < r_0$.

In cases where $r_1 \ll r_0$, the correlation breaks down as shown in Fig 4.7. Plots (a), (c) and (e) are contour plots of the joint probability density functions $P\big(v(r_0); v(r_1)\big)$ of length scales $r_0/r_1 = 200d/100d, 500d/100d$ and $1000d/100d$ and plots (b), (d) and (f) are of length scales $r_0/r_1 = 6d/3d, 15d/3d$ and $30d/3d$, respectively. The contour lines show a progression from the tilted to circular form for increasing values of r_0, while holding r_1 constant. This corresponds to a loss in correlation between scales r_0 and r_1 leading to a factorisation into

$$P\big(v(r_1); v(r_0)\big) = P\big(v(r_1)\big)P\big(v(r_0)\big). \tag{4.16}$$

Equation (4.16) describes the velocity increment as a random variable across scales.

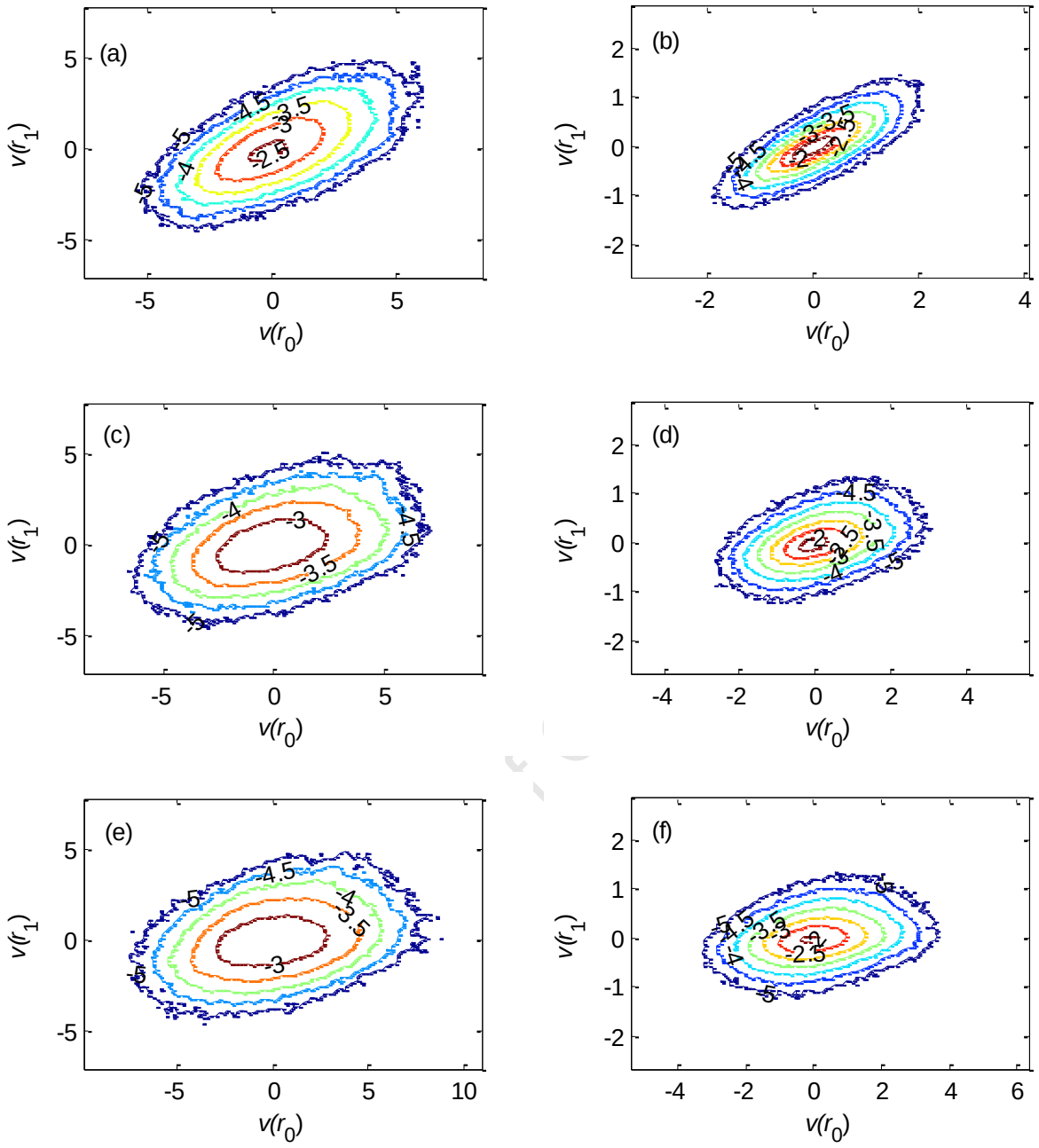

Fig 4.7 Contour plot of the joint probability density functions$P\big(v(r_1); v(r_0)\big)$. For plots (a), (c) and (e) $r_1 = 100d$ and $r_0 = 200d, 500d\ and\ 1000d$, and for plots (b), (d) and (f) $r_1 = 3d$ and $r_0 = 6d, 15d$ and $30d$, respectively.

Two features are worth noting in Fig 4.7. Firstly, for smaller length scales, *i.e.* plots (b), (d) and (f), there is a greater measure of certainty of the increment v having a value of $v(r_1)$ on r_1 given it had a value of $v(r_0)$ on r_0 when compared to plots (a), (c) and (d) of larger scales. The contour lines are closer together with smaller velocity fluctuations around a mean of zero. Thus if one is interested in smaller fluctuations one would consider smaller length scales. However, the certainty of the

conditional (or joint) probability for the velocity increment having a certain value declines faster than for larger scales. The closer the contour lines the steeper the gradient. For larger scales, plots (a), (b) and (c) the certainty of $P\big(v(r_1);v(r_0)\big)$ is less than for smaller scales but this certainty decreases slower for changes in the velocity increment. Secondly, the larger the value of r the slower the dependency decreases across scales. Thus provided equation (4.15) holds the increment v is a stochastic variable in r for carefully chosen values of r. The loss of dependence across scales, equation (4.16), can be seen as being analogous to the molecular chaos assumption given by Boltzmann in equation (3.20).

A plot of the conditional probability density functions, equation (4.3), is given in Fig 4.8. Here the contour lines are aligned at the same 45 degree angle to the axis of the plots as in Fig 4.6.

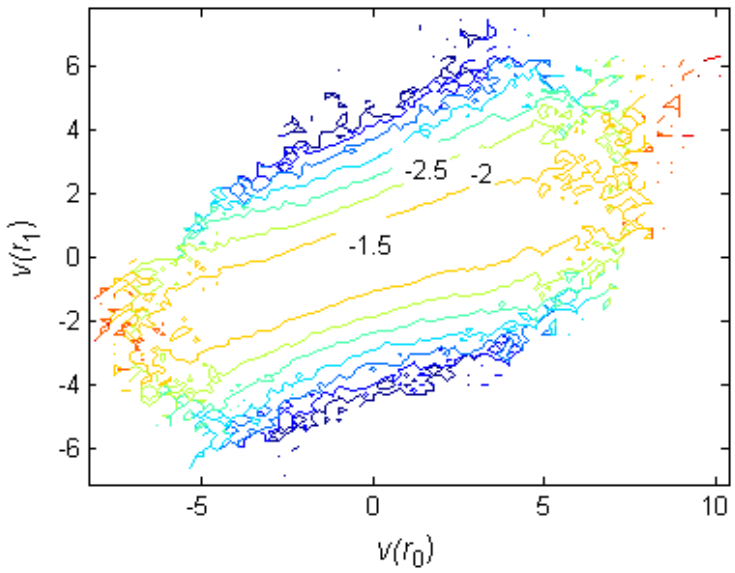

Fig 4.8 Contour plot of the conditional probability density function

$P(v(r_1)\,|\,v(r_0)) = P(v(r_1);v(r_0))/P(v(r_0))$. Here $r_1 = 100d$ and $r_0 = 300d$.

When binning the data the original observation, in this case the velocity increment $v(r)$, is replaced by the mean (median) of the data values which fall in a given small interval, the bin. In Fig 4.9 (a) the joint probability density function is plotted using a bin value of 30. This means that each velocity increment for $v(r_1)$ and $v(r_0)$ were each binned into one of 30 bins and the velocity increment $v(r)$ is then represented by the mean of $v(r)$ for that bin, in r. In Fig 4.9 (b) a bin of 60 was used. The effect of increasing the number of bins reduces the statistics on smaller fluctuations. The smallest contour line is -2.5 while for Fig 4.9 (a) it is -1.5. The choice of the number of bins depends on what

resolution in the statistics is desired. For example, the fourth Kramers-Moyal coefficient is shown in Fig 4.10, calculated using bin numbers of 100 and 25. A bin number of 100 produced 98 points while a bin number of just 25 produced 24 points. In this instance, both bin sizes produce sufficient points to obtain equal and reliable statistics. Thus for carefully chosen length scales, where contour lines of the joint and conditional probabilities functions are aligned at a 45 degree angle to the axis of the plots, the velocity increments $v(r_i)$ are a stochastic process in r.

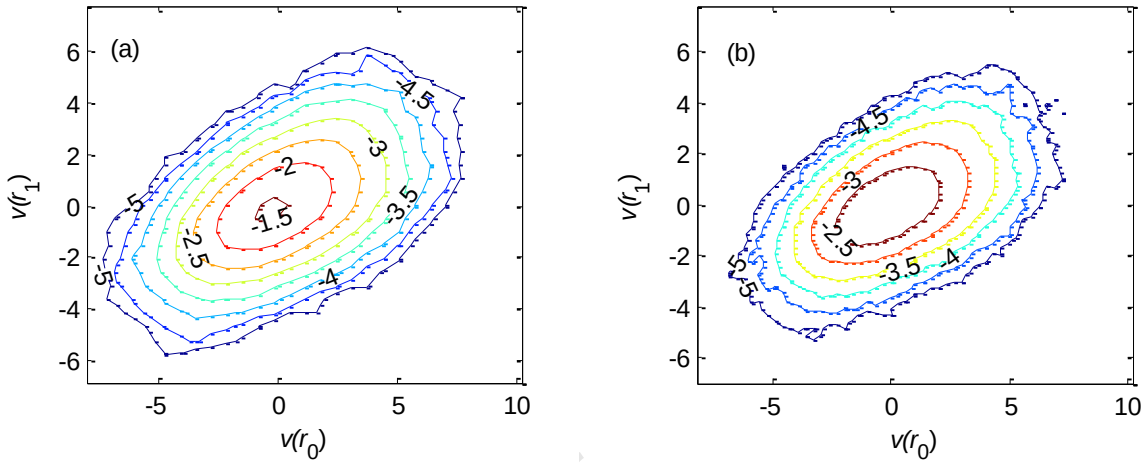

Fig 4.9 (a) Contour plot using number of bins = 30; (b) number of bins equal = 60.

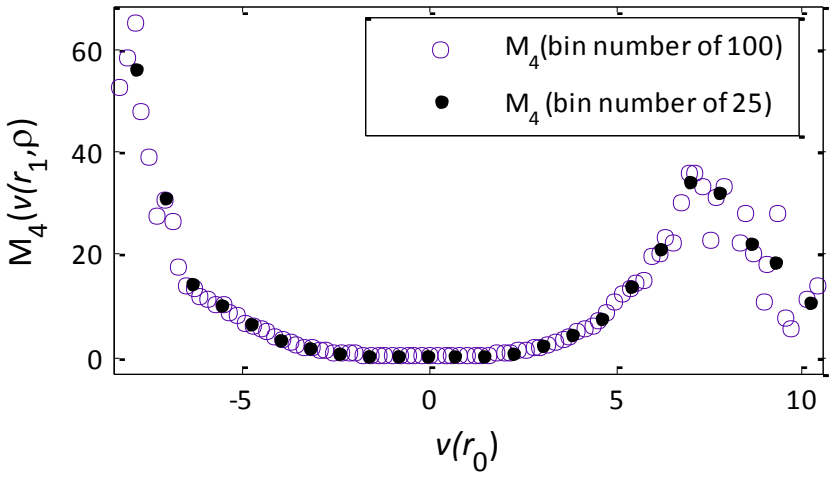

Fig 4.10 Plot of the moment $M_4(v(r), \rho)$ for $r_1 = 100d$, and $r_0 = 300d$.

To test the second assumption most authors have taken the validity of the Chapman-Kolmogorov equation (4.8) [45,46,53-65,75-80]. Using this equation it is necessary to show that for values of r_1, $r_0$and for various r_i, the left-hand side of the Chapman-Kolmogorov equation is equal to the integral

on the right-hand side, for $(r_1 \leq r_i \leq r_0)$. More precisely, rewriting Chapman-Kolmogorov equation (4.8) in the form

$$CK = P\big(v(r_1)\big|v(r_0)\big) - \int_{-\infty}^{\infty} P\big(v(r_1)\big|v(r_i)\big)P\big(v(r_i)\big|v(r_0)\big)\,\mathrm{d}x_i, \qquad \text{for } (r_1 \leq r_i \leq r_0), \tag{4.17}$$

necessary conditions exist for the Markov property, for $CK = 0$. A mesh plot of equation (4.17) for the triplet $(r_1 \leq r_i \leq r_0)$, where $r_1 = 100d$, $r_i = 200d$ and $r_0 = 300d$ is given in Fig. 4.11 and Fig. 4.12.

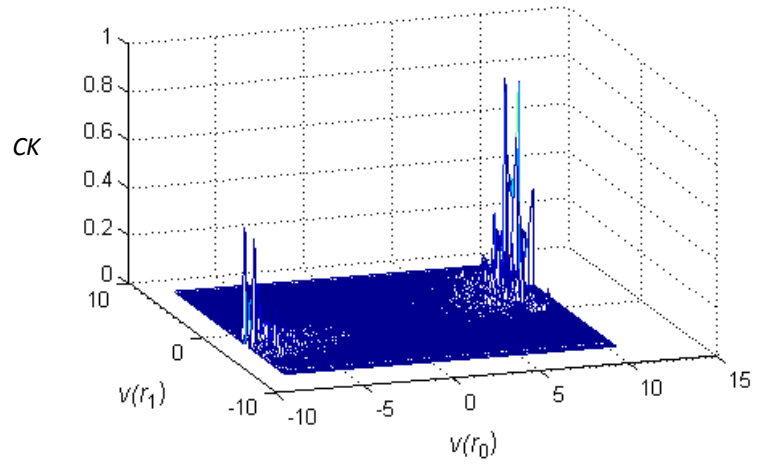

Fig 4.11 A mesh plot of equation (4.17).

Equation (4.17) is plotted as a mesh plot in Fig 4.11 and has minimum values approximately between $v(r_0) = -5\ \mathrm{m.s^{-1}}$ and $5\ \mathrm{m.s^{-1}}$. To obtain more precise values the sum of all $v(r_1)$ for each $v(r_0)$ is taken, *i.e*. sum the columns of the two dimensional matrix, plotted in Fig 4.11, for both the first and second terms of equation (4.17), and then differencing the two terms. From the plot in Fig 4.12 a minimum is obtained near zero for approximately $v(r_0) = -2.5\ \mathrm{m.s^{-1}}$ and $3\ \mathrm{m.s^{-1}}$. This is referred to as the as the *CK*–interval for which the Chapman-Kolmogorov equation is valid.

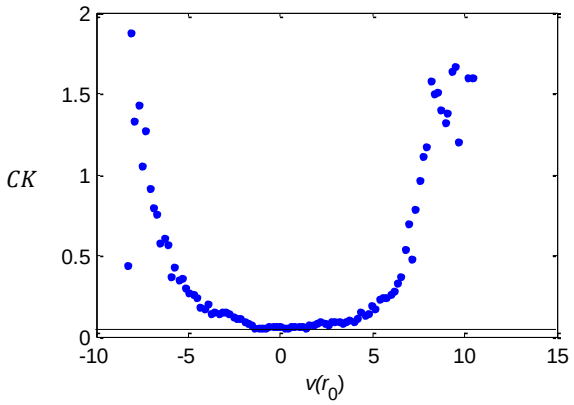

Fig 4.12 A plot of the sum for all $v(r_1)$ for each $v(r_0)$ of equation (4.17).

The Chapman-Kolmogorov equation (4.8) is now evaluated for $r_1 = 100d$, $r_i = 200d$ and $r_0 = 300d$ and is plotted as a contour plot in Fig 4.13(a). The integral on the right-hand side of equation (4.8) is plotted as a broken line while the solid line represents the left-hand side of equation (4.8). Three cross-sections are made in plot (a), at $v(r_0) = -2.5\ \mathrm{m.s^{-1}}$ to produce plot (b), $v(r_0) = 0$ to produce plot (c) and $v(r_0) = 3\ \mathrm{m.s^{-1}}$ to produce plot (d). The solid circles represent the integral on the right-hand side. A Kolmogorov-Smirnov goodness-of-fit test [108] is used to compare the distributions produced by the cross-sections in Fig 4.13. This test is included in MATLAB's Statistics Toolbox and is referred to as the two-sample Kolmogorov-Smirnov test. This test compares the distributions of values in the two vectors X and Y representing the two distributions in the MATLAB function, H_0 = kstest2(X,Y). The null hypothesis states that X and Y are randomly sampled from the same continuous distribution. The alternative hypothesis is that they are sampled from different continuous distributions. If H_0 produces a result of 1 the null hypothesis is rejected and the distributions are the same. If the result is 0 then the distributions are significantly different at a 5% level of significance. It was found that the two-sample Kolmogorov-Smirnov test validates the Chapman-Kolmogorov equation (4.8) for $r_1 = 100d$, $r_i = 200d$ and $r_0 = 300d$, and for velocity increments between -2.5 m.s^{-1} and 3 m.s^{-1}. For values laying outside the CK-interval the Chapman-Kolmogorov equation is approximately valid.

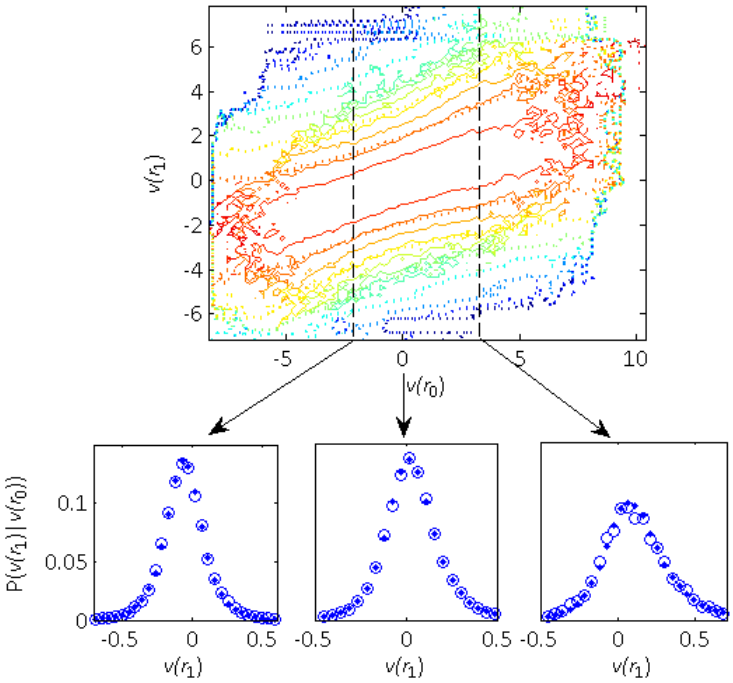

Fig 4.13. (a) A contour plot of the of Chapman-Kolmogorov equation (4.8). The integral on the right-hand side is plotted as a broken line while the solid line represents the left-hand side of equation (4.8). Three cross-sections are made in plot (a) at $v(r_0) = -2.5\ \mathrm{m.s^{-1}}$ to give plot (b), $v(r_0) = 0$ to produce plot (c) and $v(r_0) = 3\ \mathrm{m.s^{-1}}$ to produce plot (c). The solid circles represent the integral on the right-hand side of equation (4.8) while the crosses represent the left-hand side. The open circles are drawn larger for clarity.

The test using the Chapman-Kolmogorov equation of evaluating the Markov property is now compared using the conditional probability density function, for the triplet-scale, given by

$$P\big(v(r_2)\big|v(r_1)\big) = P\big(v(r_2)\big|v(r_1); v(r_0)\big) \tag{4.18}$$

where $r_2 < r_1 < r_0$ for $r_2 = 100d$, $r_2 = 200d$ and $r_0 = 300d$. A contour plot of equation (4.18) is produced in Fig 4.14(a). The right-hand side of equation (4.18) is plotted as broken lines while the solid line represents the left-hand side of equation (4.18). The right-hand side of the equation is in three dimensions. To reduce this to two dimensions a cross-section is made through $v(r_0) = 0$, the mean of the fluctuations on this scale.

Three cross-sections are made in plot (a), at $v(r_1) = -0.997\ \mathrm{m.s^{-1}}$ to give plot (b), $v(r_1) = 0.118\ \mathrm{m.s^{-1}}$ to produce plot (c) and $v(r_1) = 1.0721\ \mathrm{m.s^{-1}}$ to produce plot (d). The open circles represent the right-hand side of equation (4.18). In Fig 4.14 the Markov property is seen to be approximately satisfied for $r_1 = 100d$, $r_i = 200d$ and $r_0 = 300d$. The two-sample Kolmogorov-Smirnov test confirms this result.

Curiously the Chapman-Kolmogorov equation (4.17) was strongly satisfied for most scales, great and small, but this necessary condition for the Markov property broke down for larger scales when using equation (4.18).

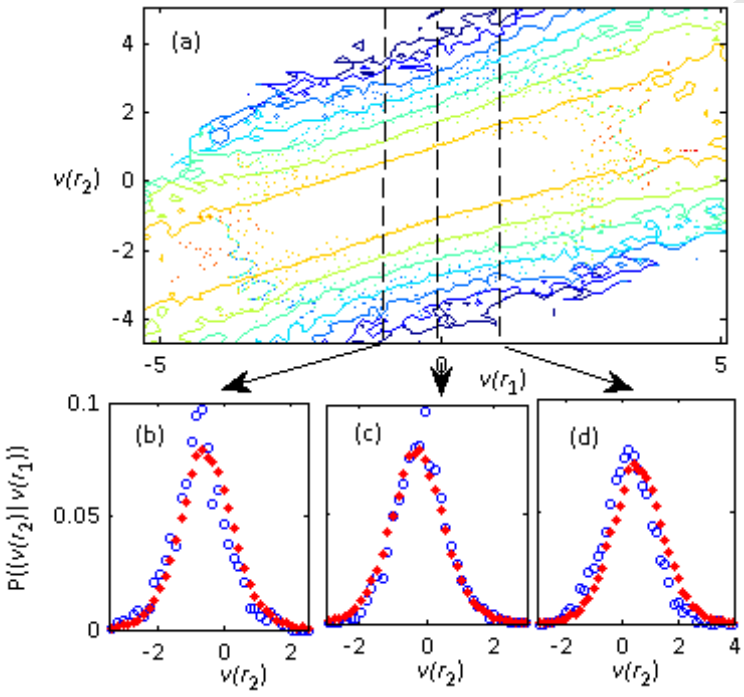

Fig 4.14 (a) A contour plot of the of the conditional probability density function, equation (4.18). The right-hand side is plotted as broken lines while the solid line represents the left-hand side. Three cross-sections are made in plot (a) at $v(r_1) = -0.997\ \mathrm{m.s^{-1}}$ to give plot (b), $v(r_1) = 0.118\ \mathrm{m.s^{-1}}$ to produce plot (c) and $v(r_1) = 1.072\ \mathrm{m.s^{-1}}$ to produce plot (c). The solid circles represent the integral on the right-hand side of equation (4.18) while the crosses represent the left-hand side. The open circles are drawn larger for clarity.

To further the investigation of the relationship between the Chapman-Kolmogorov equation and the Markov property, the Chapman-Kolmogorov equation, given by equation (4.17), is compared to the conditional probability density function equation (4.18) which is minimised to

$$MP = P\big(v(r_2)\big|v(r_1)\big) - P\big(v(r_2)\big|v(r_1); v(r_0)\big). \tag{4.19}$$

The method involves taking cross-sections at $v(r_0) \cong 0$ for Chapman-Kolmogorov case and at $v(r_1) \cong 0$ for the conditional probability density function. Increments are calculated for length intervals $r_2 = 50d$ and for $r_1 = (80 + 20n)d$ and $r_0 = (90 + 60n)d$ for $n = 1$ to 100. The results of exercising equations (4.17) and (4.19) to the above cross-sections are plotted in Fig 4.15.

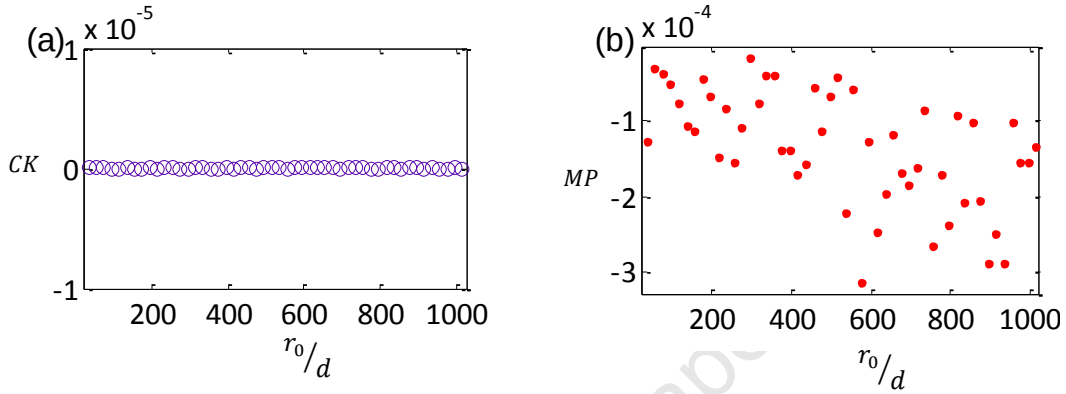

Fig 4.15 (a) Plot of the Chapman-Kolmogorov equation (4.17) for a cross-section $v(r_0) \cong 0$. (b) Plot of the conditional probability density function equation (4.19) for a cross-section $v(r_1) \cong 0$.

Fig 4.15 shows the values of CK are zero confirming the validity of the Chapman-Kolmogorov equation for these scales. However, the values of MP in Fig 4.15 (b) show a spreading out of the points from zero for increasing scales. The Chapman-Kolmogorov equation is consistently valid for all scales while this condition weakens when considering the conditional probability density functions, for increasing scales. This result confirms the Chapman–Kolmogorov equation as a necessary but not sufficient condition for Markov processes. More discussion on the discrepancy between the Chapman–Kolmogorov equation and prior parametisation of the conditional probability density function when testing for the Markov property is discussed in chapters 5 and 6.

The third assumption to test is Pawula's theorem, see section 3.2 [66,67]. The fourth coefficient $D_4(v(r), \rho)$ is chosen to be tested and $M_4(v(r), \rho)$ is plotted in Fig 4.16. The quadratic form with $M_4(v(r), \rho) = 0$ is visible for velocity increments of between -3 m.s^{-1} and 3 m.s^{-1}.

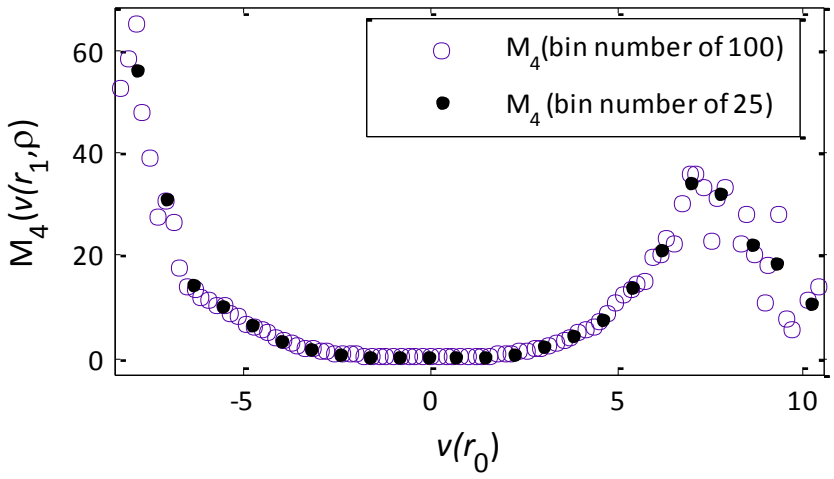

Fig 4.16 Plot of the moment $M_4(v(r),\rho)$ for $r_1 = 100d$, and $r_0 = 300d$.

The Kramers-Moyal expansion can thus be truncated at the second moment to produce the Fokker-Planck equation (4.10). The Kramers-Moyal first and second terms are the drift and diffusion coefficients, $D_1(v(r),\rho)$ and $D_2(v(r),\rho)$ respectively and are given as

$$D_1(v(r),\rho) = \lim_{\Delta\rho\to 0}\frac{1}{\Delta\rho}\int (v'-v)P(v',\rho+\Delta\rho|v,\rho)\mathrm{d}v' \tag{4.20}$$

and

$$D_2(v(r),\rho) = \frac{1}{2}\lim_{\Delta\rho\to 0}\frac{1}{\Delta\rho}\int (v'-v)^2P(v',\rho+\Delta\rho|v,\rho)\mathrm{d}v'. \tag{4.21}$$

The drift and diffusion coefficients are estimated using the same length scale and bin sizes and are plotted in Figs. 4.17 and 4.18, respectively. The plot of the drift term indicates a linear relationship between the velocity fluctuation $v(r)$ and $D_1(v(r),\rho)$. The drift coefficient is calculated as a linear function of $v(r_0)$

$$D_1(v(r),\rho) = a_1 + a_2 v, \tag{4.22}$$

in the *CK*-interval with numerical values

$$D_1(v(r),\rho) = 0.00365 - 0.5831v. \tag{4.23}$$

95% confidence bounds coefficients on the coefficients are

$$a_1 = (-0.00286, 0.0102) \qquad (4.24)$$
$$a_2 = (-0.5871, -0.579).$$

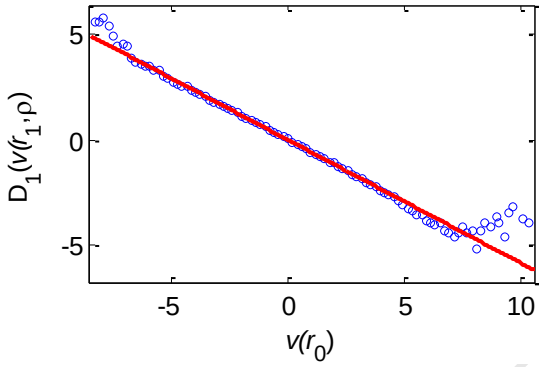

Fig 4.17 The drift coefficient $D_1(v(r), \rho)$ as a function of $v(r_0)$ in the CK-interval. The solid line is a linear fit to the data.

The diffusion coefficient is a quadratic function of $v(r_0)$ in the CK-interval, see Fig. 4.18,

$$D_2(v(r), \rho) = b_1 + b_2 v + b_3 v^2. \qquad (4.25)$$

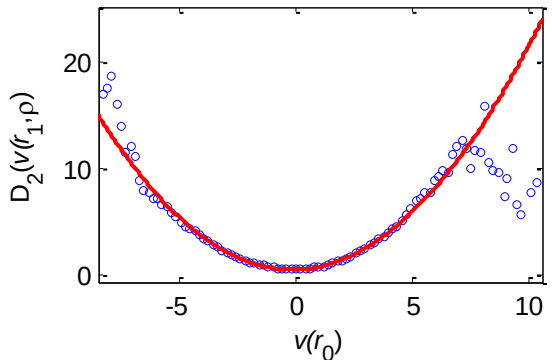

Fig 4.18 The diffusion coefficient $D_2(v(r), \rho)$ as a function of $v(r_0)$ in the CK-interval. The solid line is a quadratic fit to the data.

The analyses of the data yields the following approximants

$$D_2(v(r),\rho) = 0.4526 + 0.04514v + 0.206v^2, \tag{4.26}$$

and 95% confidence bounds coefficients on the coefficients

$$\begin{aligned} b_1 &= (0.441, 0.464) \\ b_2 &= (0.040, 0.050) \\ b_3 &= (0.203, 0.209). \end{aligned} \tag{4.27}$$

4.4. Interpretation of the Kramers-Moyal Coefficients

Few authors have discussed the significance of the Kramers-Moyal coefficients in describing the dynamics of a fluctuating system. When this has been done, the discussion is usually in terms of a distribution function evolving over increasing linear time intervals [109, 110]. Huang *et al* [106] have examined the drift coefficient for stock exchange returns, assuming a Langevin force, to find the equilibrium configuration, and investigate the properties of the restoring force. On the other hand, Mizuno *et al* [110] focused on the influence of the diffusion coefficient, without the drift, finding that instability is described by a large positive diffusion coefficient. The discussion in section 3.2 shows that for an evolutionary stochastic system a positive drift coefficient causes the mean of $P(x,t)$ to shift towards larger values of x, and that the drift coefficient describes the speed and direction of the mean of the distribution. To interpret the Kramers-Moyal coefficients in terms of wind turbulence the continuous time variable t, in $P(x,t)$, has to be replaced by the reciprocal of a discrete length scale ρ, contained in the probability density of the velocity increment $P(v(r),\rho)$. This reciprocal reasoning of the drift and diffusion coefficients is simpler to understand when rewriting the Fokker-Planck equation (4.10) in the form

$$-t\frac{\partial P(x,t)}{\partial t} = -\frac{\partial}{\partial x}[D_1(x)P(x,t)] + \frac{1}{2}\frac{\partial^2}{\partial x^2}[D_2(x)P(x,t)], \tag{4.28}$$

where $-t$ on the left-hand side of equation (4.28) has the same effect as the inverse length scale and also indicates a flow from long to the shorter nested scales, describing a hierarchical system. Thus, using the reciprocal of the change in length scales, one has to interpret the coefficients in an inverse

way. A negative value of D_1 as seen in Fig 4.17 causes the mean of $P(v(r),\rho)$ to shift towards a greater number of larger wind velocity fluctuations rather than acting as a restoring force to the equilibrium situation [109]. In other words, a negative drift coefficient would describe an upward pressure on the velocity increments, and a positive value describes a downward pressure. A negative slope for the drift coefficient can be interpreted as driving the system towards a greater number of larger velocity fluctuations and thus greater wind turbulence. The greater the diffusion term the greater the fluctuations around the mean.

4.5. Induced Fluctuations by means of Binary Collisions

Filtered velocities for two velocity components were measured by Kang *et al* [83], one in the x_1, x_3 (streamwise) and one in the x_2, x_3 (cross-stream) planes, see Fig 4.4. So far only internal fluctuations of the velocity $u(x)$ passing through filter scale $\Delta 1 = 10\ \mathrm{mm}$, in the streamwise direction, have been considered. In this section, transitions $W_\alpha(x'|x)$ of system α due to external transitions $W_\beta(y'|y)$, of system β, from state y to y' are considered. System α is taken to be the velocity component $u_\alpha(x)$ passing through filter scale $\Delta 1 = 10\ \mathrm{mm}$ in the streamwise direction while system β is the velocity component $u_\beta(x)$ of the wind passing through the $\Delta 1 = 10\ \mathrm{mm}$ filter in the cross-stream direction. It is assumed that the two systems interact through binary collisions.

To apply the Fokker-Planck equation containing the collision terms, given by equations (4.12) to (4.14), the test of Boltzmann's molecular chaos assumption, equation (4.11), is required. The joint probability density function $P\big(u_\alpha(x); u_\beta(x)\big)$ is defined as the probability of the streamwise velocity component having a value of $u_\alpha(x)$ at position x and the cross-stream velocity component having a value of $u_\beta(x)$ at the same position x and for all x. The molecular chaos assumption is valid if

$$P\big(u_\alpha(x); u_\beta(x)\big) = P(u_\alpha(x))P\big(u_\beta(x)\big). \tag{4.29}$$

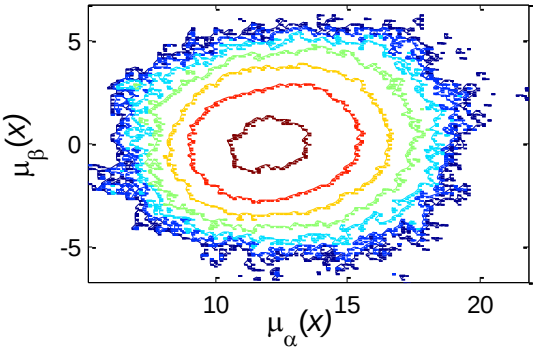

Fig 4.19 Contour plot of the joint probability density function $P(u_\alpha(x); u_\beta(x))$ as the probability of the streamwise velocity component having a value of $u_\alpha(x)$ at position x and the cross-stream velocity component having a value of $u_\beta(x)$.

A contour plot of equation (4.29) for the data of Kang *et al* is given in Fig 4.19. The plot has a circular form to the contour lines and is evidence of the independence between the streamwise and cross-stream velocity components. The molecular chaos assumption is thus valid in this instance.

The first Kramers-Moyal term, equation (4.13) is plotted in Fig 4.20 for both internal fluctuations and external interactions. Internal fluctuations M_1(FP) are plotted with points, fluctuations due to external interactions M_1(B) are plotted with open circles and the fluctuations due to the sum of the two terms M_1(BFP) are plotted as crosses. It can be seen that the cross-stream and streamwise velocity components are equal for velocity fluctuations approximately between $v(r_0) = -4$ m.s^{-1} and 2 m.s^{-1} but diverge for greater fluctuations. The effect of the external interactions is to increase the absolute value of the drift term. Using the inverse length scale interpretation the cross-stream velocity component collides with the streamwise velocity component and enhances the shifting of the mean of the distribution towards a greater number of velocity fluctuations. In other words the cross-stream velocity component acts as though it injects energy into the streamwise velocity component leading to greater turbulence.

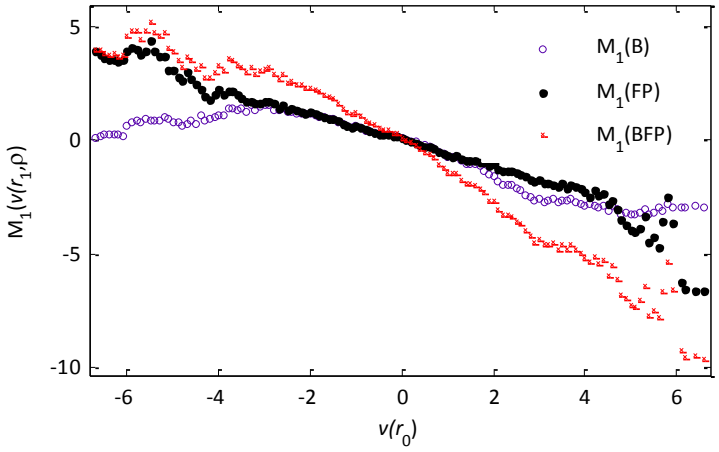

Fig 4.20 A plot of the first Kramers-Moyal term, equation (4.13) for both internal fluctuations and external interactions. Internal fluctuations $M_1(FP)$ are plotted with points, fluctuations due to external interaction $M_1(B)$ are plotted with open circles and the sum of the two terms $M_1(BFP)$ are plotted as crosses.

The second Kramers-Moyal term, equation (4.14) is plotted in Fig 4.21.

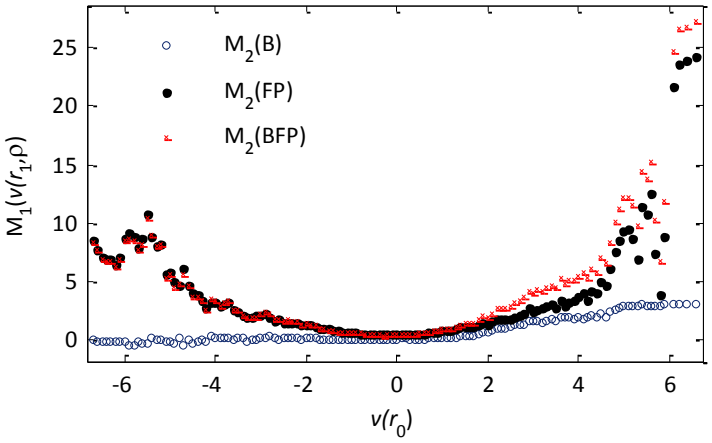

Fig 4.21 The same notation is used as in Fig 4.20. It can be seen that $M_2(B) = 0$ for approximately $v(r_0) < 2$ m.s^{-1} and that the cross-stream velocity component for approximately $v(r_0) \geq 2$ m.s^{-1} contributes to $M_2(BFP)$. The effect is to increase the diffusion coefficient for $v(r_0) \geq 2$ m.s^{-1}.

The same notation is used as in Fig 4.20. It can be seen that $M_2(B) = 0$ for approximately $v(r_0) < 2$ m.s^{-1} and that the cross-stream velocity component for approximately $v(r_0) \geq 2$ m.s^{-1} contributes to $M_2(BFP)$. The effect is to increase the diffusion coefficient for $v(r_0) \geq 2$ m.s^{-1}.

4.6. Summary and Conclusions

In this present work it was necessary to test several assumptions before arriving at the Fokker-Planck equation. Firstly, it had to be shown that the velocity increments $v(r)$ are stochastic in r. This was found to be true for suitably chosen scales. For large scales the correlation across scales breaks down. The second assumption concerns the fact that it is not possible, to deduce all possible paths or permutations of velocity increments between all possible nested length scales, as shown in section 2.3. It is therefore convenient to use the binary-scale transition function which expresses the path independence and short-term memory of a subclass of stochastic processes. It was found that the Chapman-Kolmogorov equation is valid for most large and small scales, while for the same large scales the Markov property breaks down when evaluated using the conditional probability density function, equation (4.18). In addition to this discrepancy it was shown that the Chapman-Kolmogorov equation is not valid for all velocity increments, but only for velocity increments contained in a certain interval, around the equilibrium position referred to in this work as the CK-interval.

The last assumption to be tested was Pawula's theorem and it was found that $D_4(v(r), \rho) \approx 0$ for velocity increments of between -3 $m.s^{-1}$ and 3 $m.s^{-1}$. The Kramers-Moyal expansion was then truncated at the second moment to produce the Fokker-Planck equation. The drift term was found to be a linear function of the velocity increments. Using the reciprocal of the change in length scales, one has to interpret the coefficients in an inverse way. A negative value of D_1 as seen in Fig 4.17 causes the mean of $P(v(r), \rho)$ to shift towards a greater number of larger wind velocity fluctuations rather than acting as a restoring force to the equilibrium situation. In other words, a negative drift coefficient would describe an upward pressure on the velocity increments; and a positive value describes a downward pressure. A negative slope for the drift coefficient can be interpreted as driving the system towards a greater number of larger velocity fluctuations and thus greater wind turbulence. The diffusion term was found to be a quadratic function of the velocity increments. The greater the diffusion term, the greater the fluctuations around the mean.

In the last section a new idea was introduced of using a Fokker-Planck equation to describe the correlation of the probability density of the velocity increments of one system (streamwise velocity component) interacting with another system (cross-stream velocity component). This type of Fokker-Planck equation allowed the further quantification of the deterministic and random influences due to the internal fluctuations, and by means of the collision terms in the drift and

diffusion coefficients, the external fluctuations. It was assumed that the two systems interacted through binary interactions. The application of this method required the Boltzmann molecular chaos condition to be valid. The spontaneous and externally induced velocity fluctuations were found to have similar velocity fluctuations between $v(r_0) = -4$ m.s^{-1} and 2 m.s^{-1} but diverge for greater fluctuations. The effect of the external interactions was to increase the absolute value of the drift term. Using the inverse length scale interpretation it was concluded that the cross-stream velocity component collided with the streamwise velocity component and enhanced the velocity of the mean of the distribution towards a greater number of velocity fluctuations. In other words the cross-stream velocity component acts as though it injects energy into the streamwise velocity component leading to greater turbulence. For the diffusion coefficient it was found that $M_2(B) = 0$ for approximately $v(r_0)2$ m.s^{-1} and that the cross-stream velocity component for approximately $v(r_0) \geq 2$ m.s^{-1} contributes to M_2(BFP). The effect is to increase the diffusion coefficient for $v(r_0) \geq 2$ m.s$^{-1.}$

CHAPTER 5
A DIAGNOSTIC TOOL FOR ELECTROMYOGRAPHY

In the previous chapter it was found that the Fokker-Planck equation governs the statistics of a scale-dependant measure, the velocity increment $v(r)$, across nested length scales r. Other recent studies using length scale-dependent measures, to investigate orders of complexity in fluctuating systems, are studies on surface roughness of materials [111,112] and turbulence [41-46]. However most studies into phenomena that are characterised by a degree of stochasticity require time scales. For example, prices on the financial markets, internet traffic, neutrally stratified cirrus clouds, seismic recordings and inter-beat heart fluctuations [113-117], are all examples of stochastic systems in which the stochastic nature refers to the correlation, of the time scale-dependent variable, between one nested time scale and another, having a certain probability.

Recent studies on interbeat heart fluctuations [60-65,90,91] found that electrical signals due to muscle activity fluctuate in a complex manner. Such studies, using similar probability methods to those applied to turbulence in chapter 4, found that the Fokker-Planck coefficients could be used to distinguish between normal and unhealthy heart rhythms. Studies investigating neuromuscular disease [118,119] require electromyography (EMG). EMG is the recording and analysis of the electric potential fluctuations in skeletal muscle. The analysis of EMG data can assist the clinician in determining whether symptoms are due to muscle disease or a neurological disorder. Fig 5.1 shows three different types of EMG data [120]; a) a 44 year old man without history of neuromuscular disease; b) a 57 year old man with myopathy; and c) a 62 year old man with neuropathy. Myopathies are skeletal muscle diseases where the primary symptom is muscle weakness due to the dysfunction of the muscle fibre. Neuropathy describes disorders to the nervous system. Common symptoms are temporary numbness, tingling, pricking sensations, sensitivity to touch, or muscle weakness. More extreme symptoms, include muscle wasting or paralysis.

In this chapter probability methods are applied to EMG data to develop a diagnostic tool for the different medical conditions, illustrated by the time series data in Fig 5.1. The method, similar in concept to chapter 4, involves estimating the Fokker-Planck coefficients directly from the data and comparing their behaviour across arbitrary chosen time scales.

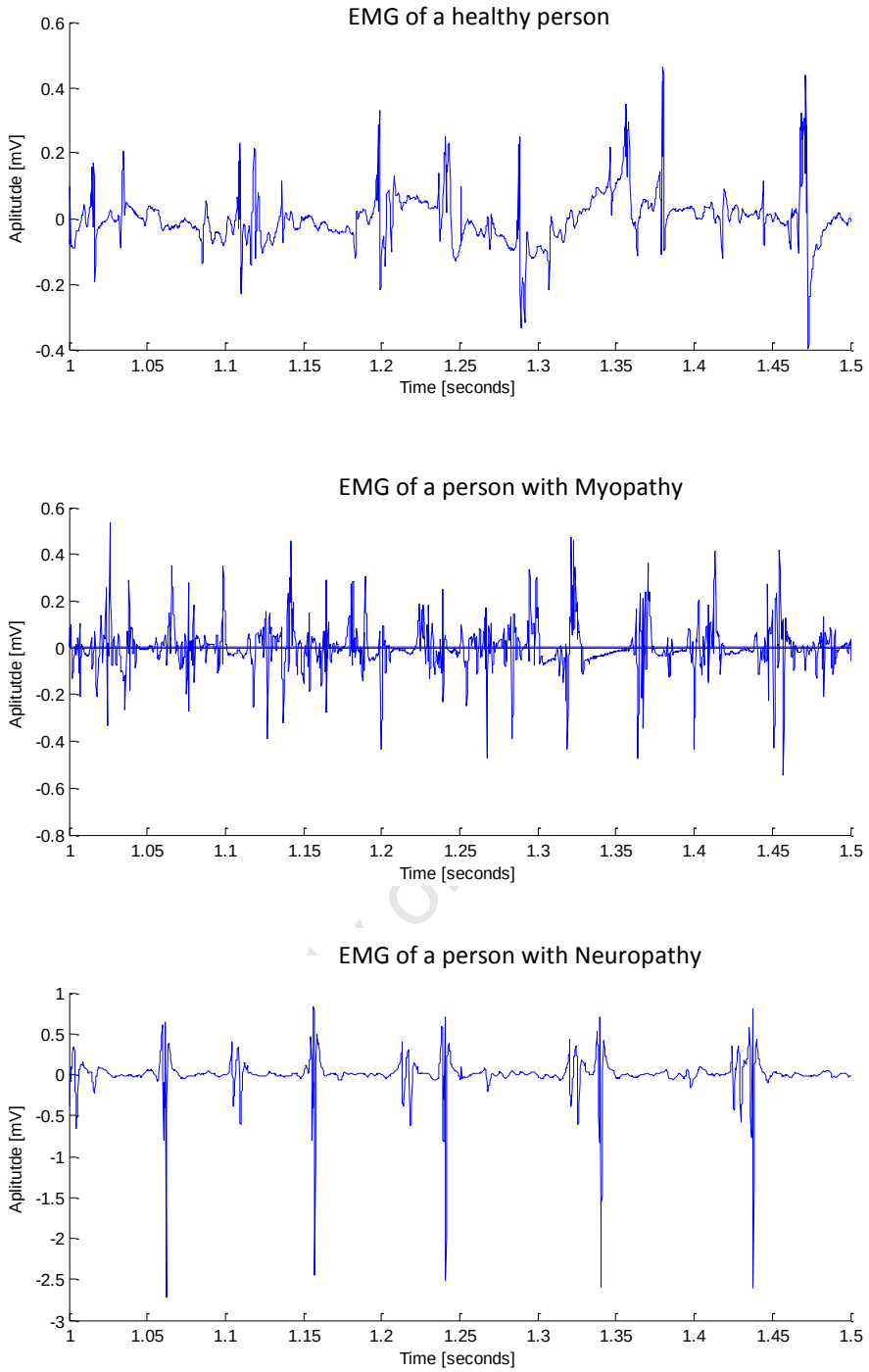

Fig 5.1 Plots of a sample 0.5 s of EMG output showing a healthy person, a person with a history of myopathy and a person with neuropathy.

5.1. Methodology

EMG is the recording and analysis of the electric potential $x(t)$ which is generated by skeletal muscle fluctuations. Here, the main focus (using probability methods), is the potential difference increment, $v(t)$, at two times t and $t + kd$,

$$v(t) \equiv \Delta x(t) = x(t + kd) - x(t). \tag{5.1}$$

$\Delta x(t)$ is a potential difference fluctuation, d the temporal resolution of the time series data and k is the discreet number of d separations between two positions t. The potential difference increment, $v(t)$ is the time scale-dependent measure. The use of probability methods, to investigate complex fluctuating systems, requires the construction of different sizes of nested scales. While the study of wind turbulence in chapter 4 involved the behaviour of velocity increments across nested length scales, here the hierarchical system is defined on time scales, $t_n < t_{n-1} < \cdots < t_0$. Similarly to the analysis of wind turbulence this method requires the testing of several assumptions.

The first assumption to be tested is whether there is correlation between potential difference increments, $v(t_i)$ across different time scales t_i. Suppose the value of $v(t)$ at some initial position (scale) t_0 is fixed and that $v(t_i)$ for any $t_i < t_0$ can be predicted only probabilistically, then a stochastic system is defined by the investigation of the state of the system at successive instants $t_n < t_{n-1} < \cdots < t_0$. The joint density function for n random variables $v(t_n), v(t_{n-1}), \dots,$ and $v(t_0)$ is then defined as

$$P\big(v(t_n); v(t_{n-1}); \dots; v(t_1); v(t_0)\big) = P\big(v(t_0)\big)P\big(v(t_n); v(t_{n-1}); \dots; v(t_1)\big|v(t_0)\big). \tag{5.2}$$

Equation (5.2) describes a dependency of $v(t_i)$ for any $t_i < t_0$. If potential difference increments, $v(t_i)$ were independent for any $t_i < t_0$ then equation (5.2) factorises into

$$P\big(v(t_n); v(t_{n-1}); \dots; v(t_1); v(t_0)\big) = P\big(v(t_0)\big)P\big(v(t_{n-1})\big)P\big(v(t_n)\big) \dots P\big(v(t_1)\big), \tag{5.3}$$

a random process. The second assumption that should be tested, is whether the stochastic process described by equation (5.2), can be reduced to a binary-scale transition function, as represented by the right-hand side of equation (5.4)

$$P_1^{(n)}\big(v(t_n)\big|v(t_{n-1});\dots;v(t_1);\mathrm{v}(t_0)\big) = P_1^{(n)}\big(v(t_n)\big|v(t_{n-1})\big) \equiv P\big(v(t_n)\big|v(t_{n-1})\big), \tag{5.4}$$

for all $n \geq 2$ and $t_{n-1} \leq t_n$. As in the previous chapter the Chapman-Kolmogorov equation

$$P\big(v(t_1)\big|v(t_0)\big) = \int_{-\infty}^{\infty} P\big(v(t_1)\big|v(t_i)\big)P\big(v(t_i)\big|v(t_0)\big)\,\mathrm{d}v_i, \qquad \text{for } (t_1 \leq t_i \leq t_0), \tag{5.5}$$

is used to test the Markov property. However, in this chapter it is shown that the Markov property is a subset of the binary-scale transition function $P\big(v(t_n)\big|v(t_{n-1})\big)$, which can characterise both Markov and non-Markov properties of a stochastic process. This suggest that the Kramers-Moyal expansion, and hence the Fokker-Planck equation, includes expressions on the non-Markov nature of that system.

The third assumption to be tested, is whether any even Kramers-Moyal moment greater than the second order equals zero. If $D_k = 0$, where k is an even number, then Pawula's theorem applies and the Kramers-Moyal expansion may be truncated at the second order. The Kramers-Moyal moments are estimated directly from the measured time series as the limiting moments M_k of the transition probability distributions

$$D_k(v(t_i),\tau_i) = \frac{1}{k!}\lim_{\tau\to\tau_i} M_k(v(t_i),\tau_i), \tag{5.6a}$$

where

$$M_k(v(t_i),\tau_i) = \frac{1}{\tau-\tau_i}\int (v(t)-v(t_i))^k P(v(t),\tau|v(t_i),\tau_i)\mathrm{d}v \tag{5.6b}$$

and $\tau = \ln(t_0/t_1)$ for $t_1 < t_0$.

If the above assumptions are satisfied then the first two Kramers-Moyal coefficients form the Fokker-Planck equation,

$$\frac{\partial P(v(t),\tau)}{\partial \tau} = -\frac{\partial}{\partial v}[D_1(v(t),\tau)P(v(t),\tau)] + \frac{1}{2}\frac{\partial^2}{\partial v^2}[D_2(v(t),\tau)P(v(t),\tau)]. \tag{5.7}$$

Equation (5.7) describes how the statistics of the potential difference increments $v(t)$ behave across time scales for EMG data of people having the three medical conditions exhibited in Fig 5.1. The data analysed can be obtained from [120]. Each time-series was tested for stationarity using the Augmented Dicky-Fuller test [121,122] included in the Econometrics Toolbox of MATLAB®. The data was corrected for stationarity using a 5-point moving average and was standardised by dividing $x(t)$ by its standard deviation, σ. The sample sizes of each medical condition are 148 858 observations.

5.2. Testing of the Assumptions

To test the assumption that there is a dependence of $v(t_i)$ for any $t_i < t_0$ the joint probability density function

$$P\big(v(t_1); v(t_0)\big), \tag{5.8}$$

and the conditional probability density function

$$P\big(v(t_1)\big|v(t_0)\big) = \frac{P\big(v(t_1); v(t_0)\big)}{P\big(v(t_0)\big)}, \tag{5.9}$$

are calculated for potential difference increments $v(t_1)$ and $v(t_0)$, for scales t_1 and t_0 for position t and for all t for $t_1 < t_0$ from the data. $P\big(v(t_1)\big|v(t_0)\big)$ denotes the usual meaning discussed in chapters 2 and 4. Equations (5.8) and (5.9) are plotted as contour plots for the data of persons having the three medical conditions in Fig 5.2. The time scales are arbitrarily chosen for $t_1 = 5d$ and $t_0 = 10d$, where $d = 1/50$ kHz represents the temporal resolution or period. The contour lines correspond to $\log_{10} P = -1, -1.5, .., -3.5$. Contour lines outside these intervals have been deleted for presentation purposes. Fig 5.2 shows the contour lines are aligned at a 45 degree angle to the axis of the plots which is evidence of a correlation function across these two time scales and that the potential difference increments $v(t)$ are a stochastic variable in t. The contour plots of persons with neuropathy show a less tilted form.

To test the Markov assumption the Chapman-Kolmogorov equation (5.5) is rewritten as

$$S = P\big(v(t_1)\big|v(t_0)\big) - \int_{-\infty}^{\infty} P\big(v(t_1)\big|v(t_i)\big)P\big(v(t_i)\big|v(t_0)\big)\,\mathrm{d}t_i, \qquad \text{for } (t_1 \le t_i \le t_0). \tag{5.10}$$

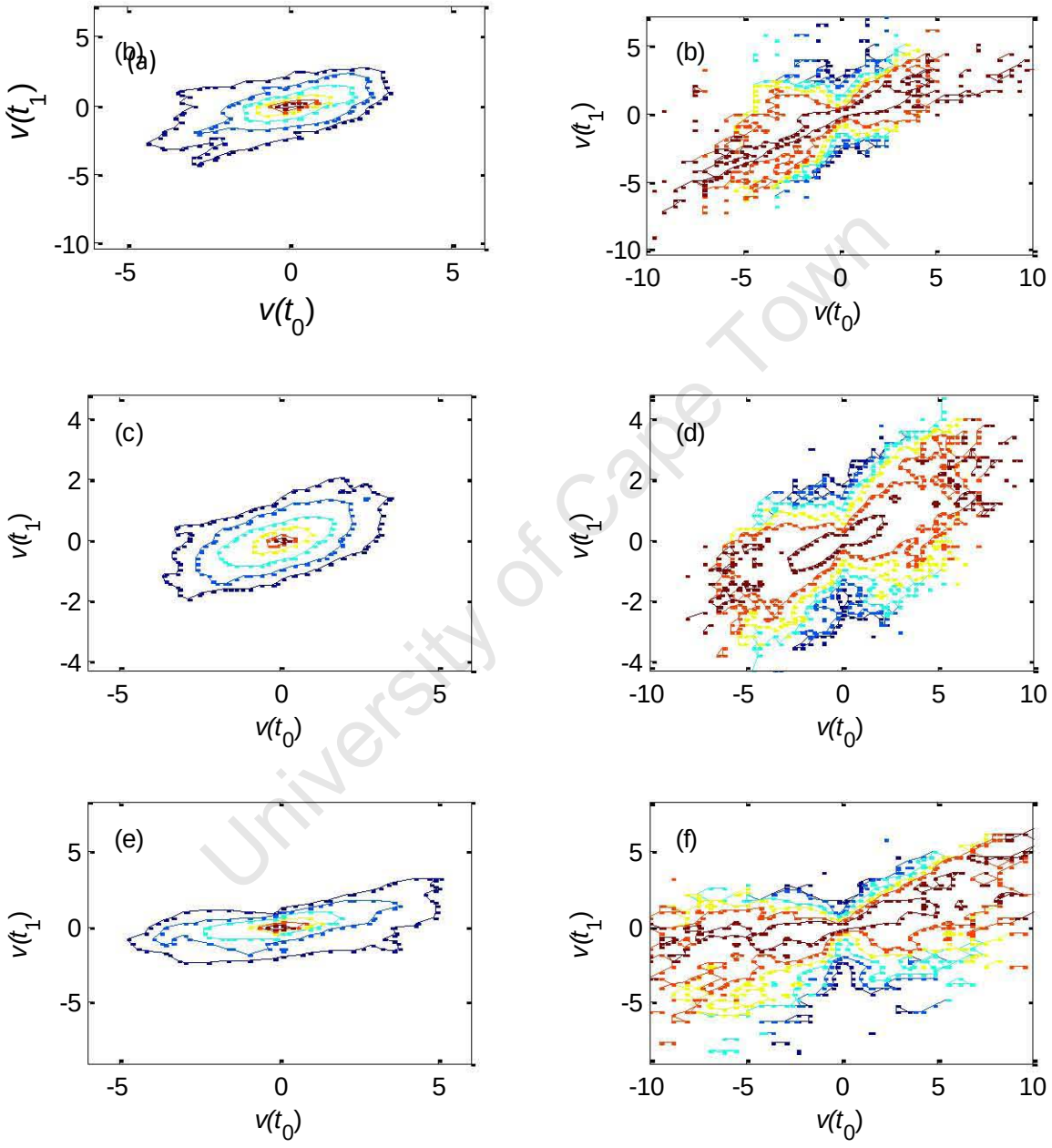

Fig 5.2 (a) and (b) are contour plots of the joint probability density and conditional probability density of healthy persons. (c) and (d) are for persons with myopathy and (e) and (f) for persons with neuropathy. The contour lines correspond to $\log_{10}P = -1, -1.5, .., -3.5$.

The Chapman-Kolmogorov equation is valid where the function S achieves values of zero. Equation (5.10) is plotted as line and mesh plots for arbitrarily chosen values of $t_1 = 50d$, $t_i = 100d$ and $t_0 = 150d$ in Fig 5.3. The rows are plots exhibiting the medical conditions of persons with healthy muscles, persons with myopathy and persons with neuropathy, from top to bottom.

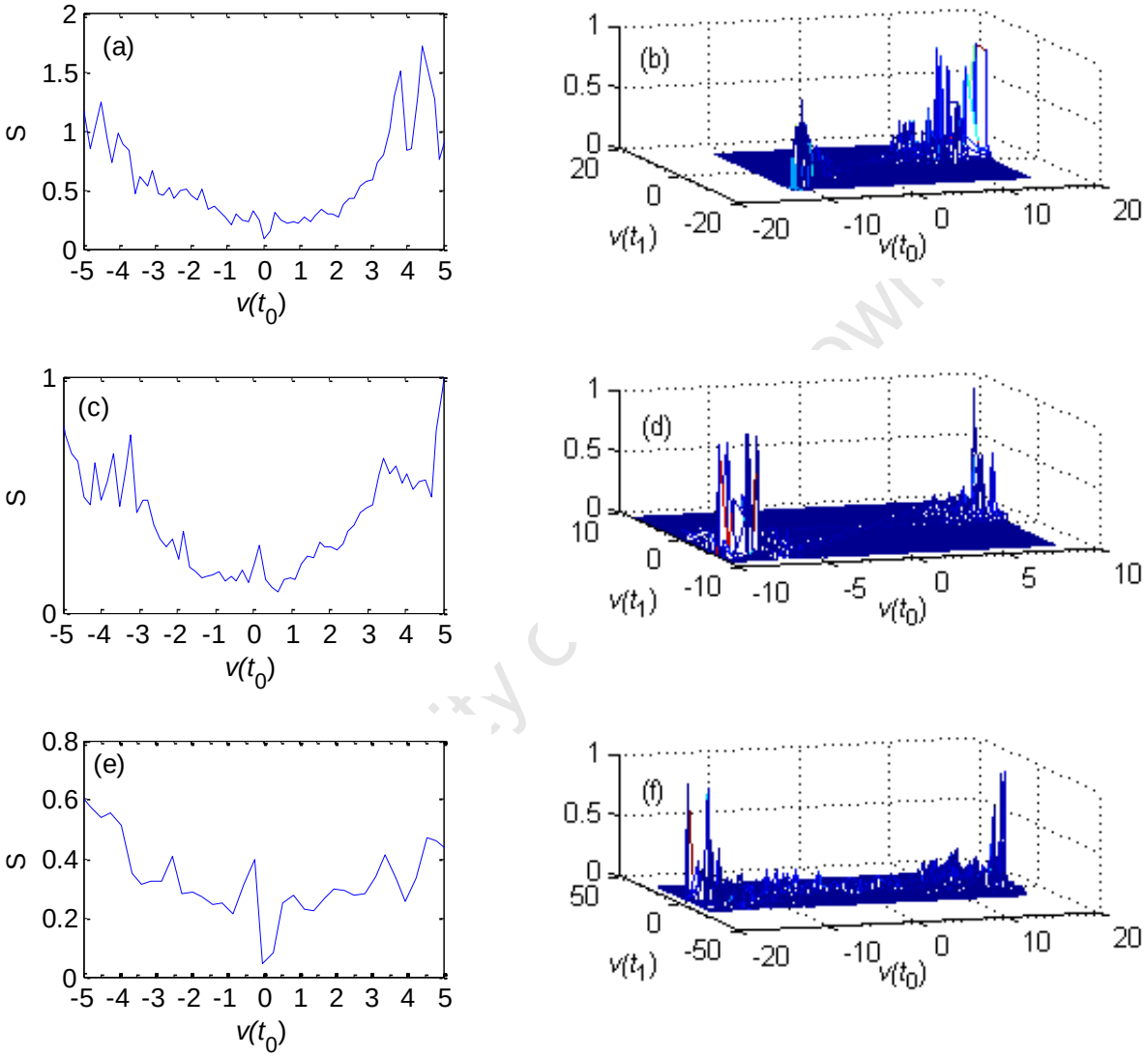

Fig 5.3 (a) and (b) are line and mesh plots of the S function, equation (5.10), of a healthy person. (c) and (d) are of persons with myopathy and (e) and (f) of persons with neuropathy. $t_1 = 50d$, $t_i = 100d$ and $t_0 = 150d$.

Fig 5.3 shows that the necessary conditions for the Markov property, exist in the range of approximately -2σ mV and +2σ mV, while the non-Markov property of this stochastic process is found outside of this interval for the time scales chosen.

The Markov property is now investigated using the Chapman-Kolmogorov equation, given by equation (5.5) for velocity increments of $S\big(v(t_0)\big) \approx 0$ *i.e*. approximately between -2σ mV and +2σ mV. The integral on the right-hand side of equation (5.5) is plotted as dashes while the solid line represents the left-hand side in Fig 5.4. Three cross-sections are made in plot (a), at $v(r_0) = -2\sigma$ mV to give plot (b), $v(r_0) = 0$ mV to produce plot (c) and $v(r_0) = 2\sigma$ mV to produce plot (d). The solid circles represent the integral on the right-hand side. Where the points overlap the Chapman-Kolmogorov equation (5.5) is valid. The two-sample Kolmogorov-Smirnov test confirms that the Chapman-Kolmogorov equation (5.5) is satisfied for $t_1 = 50d$, $t_i = 100d$ and $t_0 = 150d$ for increments between -2 σ mV and 2σ mV and therefore the necessary condition exists for the Markov property to be valid for this range of potential difference increments.

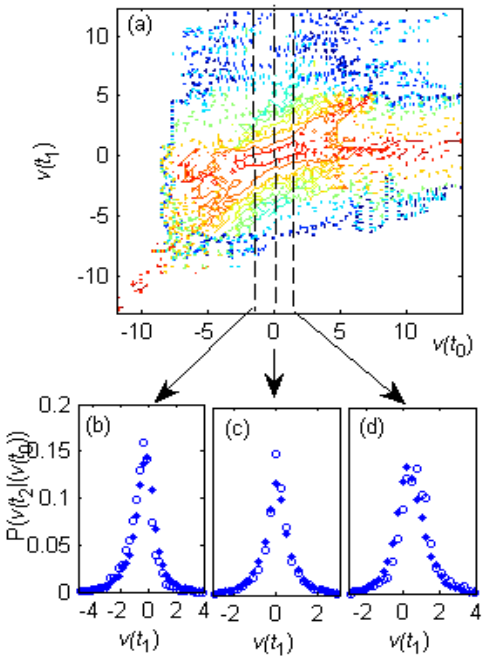

Healthy person.

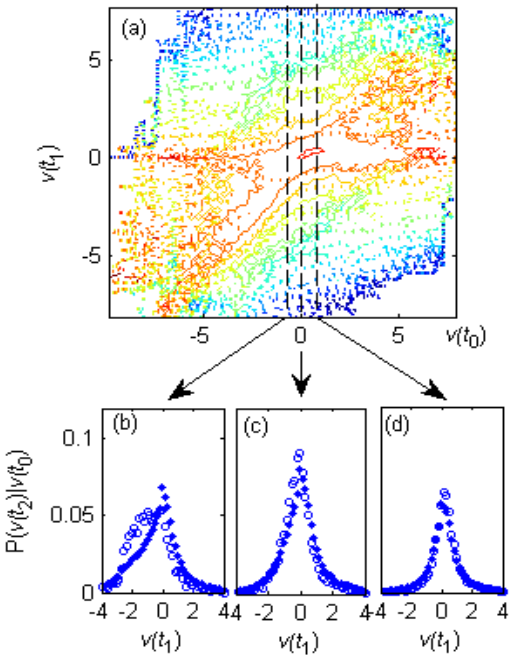

Person with Myopathy

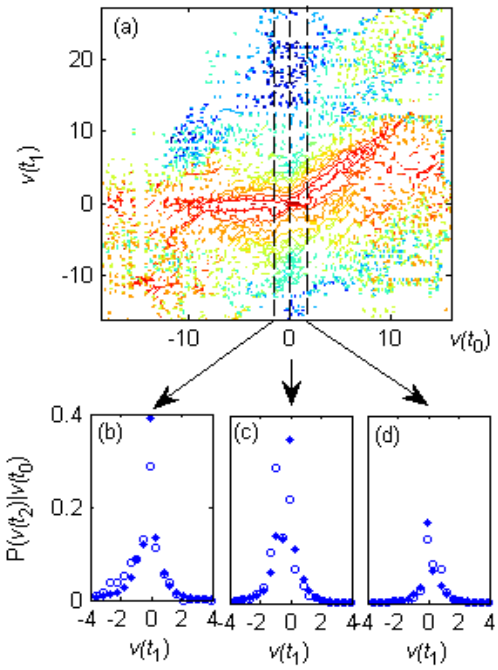

Person with Neuropathy

Fig 5.4 The integral on the right-hand side of Chapman-Kolmogorov equation (5.5) is plotted as dashes while the solid line represents the left-hand side. Three cross-sections are made in plot (a) at $v(t_0) = -2\sigma$ mV to give plot (b), $v(t_0) = 0$ mV to produce plot (c) and $v(t_0) = 2\sigma$ mV to produce plot (d). The solid circles represent the integral on the right-hand side of equation (5.5) while the crosses represent the left-hand side. The open circles are drawn larger for clarity.

The last assumption involves testing Pawula's theorem, and showing that

$$D_4(v(t),\tau) = \frac{1}{24}\lim_{\Delta\tau\to 0}\frac{1}{\Delta\tau}M_4(v(t),\tau) = 0, \tag{5.11a}$$

where

$$M_4(v(t),\tau) = \frac{1}{\Delta\tau}\int (v'-v)^4 P(v',\tau+\Delta\tau|v,\tau)\mathrm{d}v'. \tag{5.11b}$$

The fourth moment $M_4(v(t),\tau)$ is plotted in Fig 5.5.

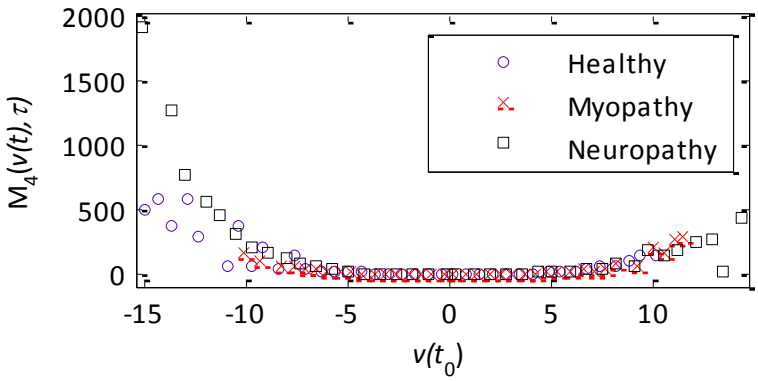

Fig 5.5 The fourth moment $M_4(v(t),\tau)$ for $t_1 = 50d$, and $t_0 = 150d$.

Fig 5.5 shows that $\lim(\Delta\tau\to 0)(1/\Delta\tau)M_4(v(t),\tau) = 0$ not only for the interval of increments having the Markov property, *i.e.* between -2σ mV and +2σ mV but also for non-Markov increments, approximately -8σ mV and +8σ mV. The Kramers-Moyal expansion is truncated at the second moment to produce the Fokker-Planck equation (5.7).

5.3. The Diagnostic Tool

Having concluded the testing of the assumptions, the coefficients of the Fokker-Planck equation can be directly calculated from the time series data. The first Kramers-Moyal coefficient is given by

$$D_1(v(t),\tau) = \lim_{\Delta\tau\to 0}\frac{1}{\Delta\tau}M_1(v(t),\tau), \tag{5.12a}$$

where

$$M_1(v(t),\tau) = \frac{1}{\Delta\tau}\int (v'-v)P(v',\tau+\Delta\tau|v,\tau)\mathrm{d}v'. \tag{5.12b}$$

The first moment $M_1(v(t),\tau)$ is calculated and plotted in Figs. 5.6. The plots indicate a linear relationship between the velocity fluctuation $v(t)$ and $M_1(v(t),\tau)$. In fact the linear trend is of a significant range for all three conditions. Such a linear dependence is characteristic of an oscillatory process [123]. The drift coefficient is calculated as a linear function of $v(t_0)$ using

$$D_1(v(t),\tau) = a_1 v + a_2, \tag{5.13}$$

but only for the interval in which the Markov property is valid, *i.e.* -2σ mV and +2σ mV.

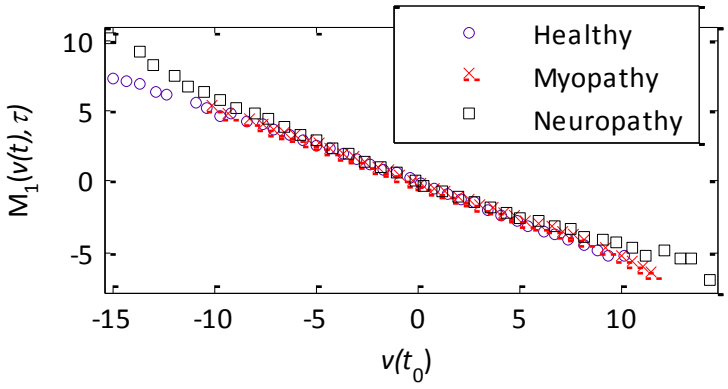

Fig 5.6 The first moment $M_1(v(t),\tau)$ for the three medical conditions. $t_1 = 50d$, and $t_0 = 150d$.

The striking feature about Fig 5.6 is that a linear fit to the Markov increments (approximately between -2σ mV and +2σ mV) would produce a drift coefficient equivalent to one obtained by a linear fit of the non-Markov range of increments (outside the interval -2σ mV and +2σ mV) but in the range where $\lim(\Delta\tau\to 0)(1/\Delta\tau)M_4(v(t),\tau) = 0$, *i.e.* approximately between -8σ mV and +8σ mV, as is shown in Fig 5.5. This result suggests that a binary-scale transition function, can contain Markov and non-Markov expressions of a stochastic system, in the range of $\lim(\Delta\tau\to 0)(1/\Delta\tau)M_4(v(t),\tau) = 0$. The first and second coefficients can only be estimated in the interval in which Pawula's theorem is satisfied. All three medical conditions have the same drift coefficient.

The second Kramers-Moyal coefficient is given by

$$D_2(v(t),\tau) = \lim_{\Delta\tau\to 0}\frac{1}{\Delta\tau}M_2(v(t),\tau), \tag{5.14a}$$

where

$$M_2(v(t),\tau) = \frac{1}{\Delta\tau}\int (v'-v)^2 P(v',\tau+\Delta\tau|v,\tau)\mathrm{d}v'. \tag{5.14b}$$

The second moment $M_2(v(t),\tau)$ is calculated and plotted in Fig 5.7. The diffusion coefficient is a quadratic function of $v(t_0)$ for all three medical conditions. The diffusion term has the characteristic parabolic, single minimum form with asymmetry. A quadratic fit using

$$D_2(v(t),\tau) = b_1 v^2 + b_2 v + b_3 \tag{5.15}$$

is estimated for the interval in which the Markov property is valid, *i.e.* -2σ mV and +2σ mV.

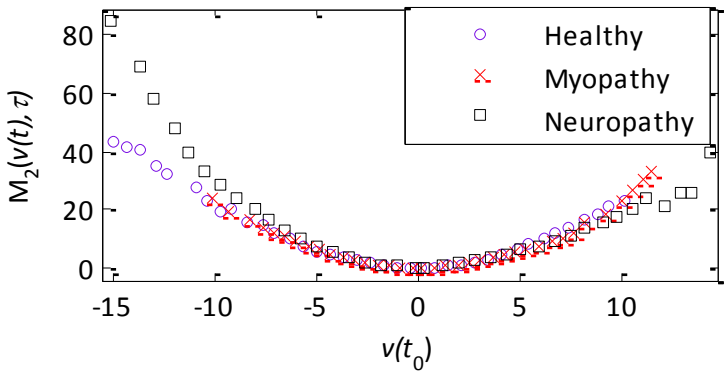

Fig 5.7 The second moment $M_2(v(t),\tau)$ for the three medical conditions. $t_1 = 50d$, and $t_0 = 150d$.

Similar to the drift coefficient, the diffusion coefficient has both a Markov and non-Markov range of increments that lie on the same parabolic curve and would thus produce the same diffusion coefficient, in the range of increments in which Pawula's theorem is satisfied.

The drift and diffusion coefficients in their present form provide no clear distinguishable characteristics of the three medical conditions. To obtain a diagnostic tool a surface plot of each

fitted coefficient, $\widehat{D}_1$ and $\widehat{D}_2$, is plotted against $v(t_0)$, obtained for arbitrary chosen scales $t_1 = 2d$ and $t_0 = 3d$ to $12d$, *i.e.* from $\tau = \ln(t_0/t_1) = 0.405$ to $\tau = 1.791$. The fitted coefficients are obtained by first estimating the parameters a_k and b_k, using equations (5.13) and (5.15) for each time scale. The resulting matrix represents a surface plot which is plotted for all three medical conditions in Fig 6.8.

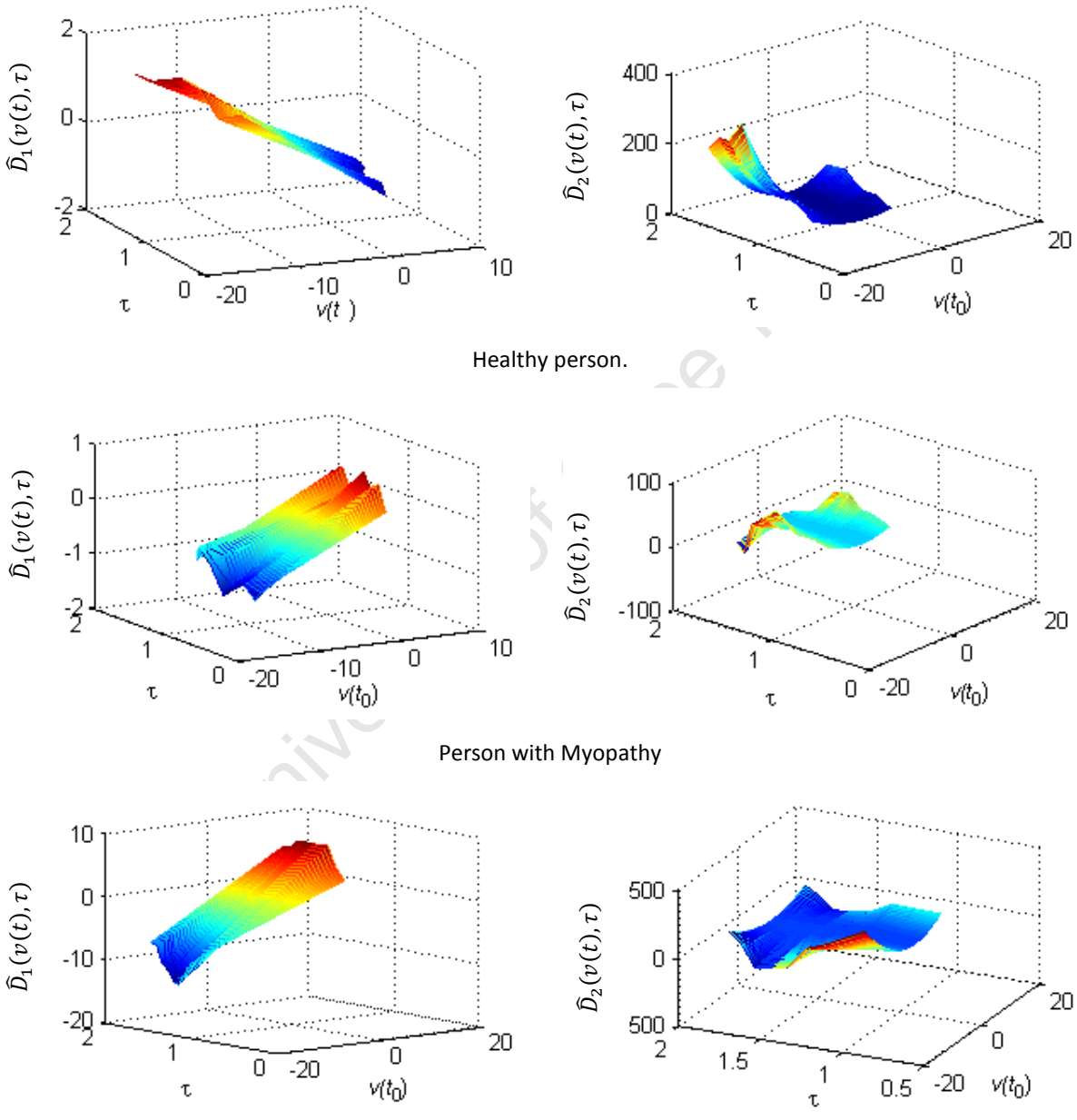

Fig 5.8 Surface plots of the fitted drift and diffusion coefficients for $\tau = 0.405$ to 1.791.

The fitted drift coefficients exhibit clearly distinguishable behaviour for the three medical conditions, for the time scales chosen.. The surface plot of $\widehat{D}_1(v(t),\tau)$ of the healthy person has a negative slope in the $\widehat{D}_1(v(t),\tau)$, $v(t_0)$ plane. The slopes of $\widehat{D}_1(v(t),\tau)$ for persons with diseased muscles are positive. The diffusion surface plots do not produce clear distinct behaviour for the three conditions. To obtain a more definitive result a cross-section is taken through an arbitrarily chosen value of $\tau = 1.252$. The cross-sections are plotted in Fig 5.9. The different gradients are clearly observable for the three medical conditions.

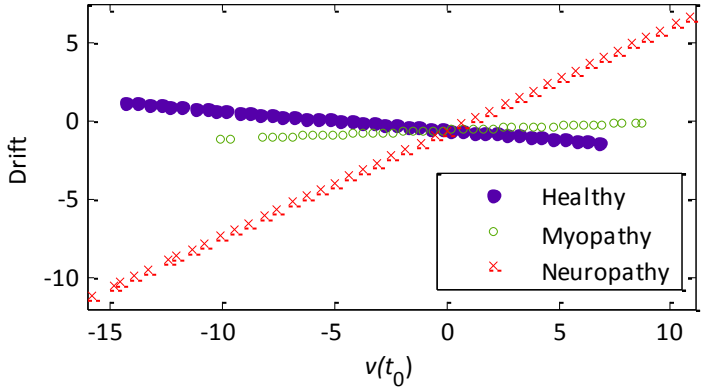

Fig 5.9 A cross-section through $\tau = 1.252$ for all three medical conditions.

The parameters of a linear fit

$$\widehat{D}_1(v(t),\tau) = c_1 v + c_2 \tag{5.16}$$

are estimated and listed in Table 5.1.

Table 5.1. Parameters of equation (5.16) for the three conditions.

Condition	c_1	c_2
Healthy	-0.1206	-0.5401
Myopathy	0.05581	-0.5675
Neuropathy	0.6681	-0.5802

5.4. Summary and Conclusions

Electrical signals due to muscle activity have been shown to behave in a complex manner. The fluctuations exhibit correlations typical of the type, by dynamical systems far from equilibrium. These electrical fluctuations found in EMG data have similar statistical properties characterised by a degree of stochasticity. The stochastic nature of the potential difference increments were tested and $v(t)$ were found to be stochastic in τ for small scales. The Markov property was tested using the Chapman-Kolmogorov equation. The Chapman-Kolmogorov equation was however, only found to be satisfied for small fluctuations around 0 mV, approximately $\pm 2\sigma$ mV. Plots of the first and second Kramers-Moyal coefficients found both the Markov and non-Markov range of increments to produce the same parameters of their fitted functions and thus the same drift and diffusion coefficients. It suggests that the Kramers-Moyal expansion is valid for any binary-scale transition function, Markov or non-Markov, while the first and second coefficients can only be estimated in the interval in which Pawula's theorem is satisfied. As a consequence, the definition of a Markovian stochastic process as is commonly given by equation (2.33), may include non-Markov fluctuations or increments. Thus, for certain types of stochastic systems, the Fokker-Planck equation does not only express the Markov nature of that process but may also include non-Markov aspects. Linear and quadratic functions were fitted to the first and second Kramers-Moyal coefficients. The functions were then plotted as surfaces using the values of $v(t_0)$ obtained for time $\tau = 0.405$ to $\tau = 1.791$. The fitted drift coefficients exhibited clearly distinguishable behaviour for the three medical conditions. The surface plot of the drift of the healthy person has a negative slope in the $\widehat{D}_1(v(t), \tau)$, $v(t_0)$ plane. The slopes of the fitted drift coefficients for the persons with diseased muscles are positive. The diffusion surface plots do not produce clear distinct behaviour for the three conditions. To obtain a more definitive result cross-sections were taken through an arbitrary point at $\tau = 1.252$ and parameters were found for the drift as a function of $v(t_0)$ for all three conditions. The gradient of $\widehat{D}_1(v(t), \tau)$, shows healthy muscles to have a negative slope while diseased muscles have positive slopes. Another cross-section through τ would of course produce different results for the gradients. These tests, combined with clinical findings, could aid the clinician for a confident diagnosis of the three medical conditions discussed.

CHAPTER 6
A PREDICTION TOOL FOR THE FINANCIAL MARKETS

In the analysis of wind turbulence in chapter 4, it was shown that the coefficients of the Fokker-Planck equation, revealed how the order of complexity depends on the scale at which a turbulent flow is observed. The analysis of the scaling of turbulent flows focused on the velocity increments for a given length separation. It revealed how a negative drift coefficient, can be interpreted as an upward pressure on the velocity increments, driving the system towards larger fluctuations of the velocity and thus greater wind turbulence. In the study of electromyography, in chapter 5, the analysis focused on the potential difference increments for given time scales. The Fokker-Planck coefficients were estimated for a range of scales, and it was found that the parameters of the fitted drift coefficients, could distinguish between healthy skeletal muscles, diseased muscles and diseased nervous systems. A diagnostic tool was developed based on the behaviour of the drift coefficient across selected time scales. In this chapter, the aim which was not relevant in the previous two chapters, is to develop a prediction tool. Here the Fokker-Planck equation describes the statistics of price changes, correlated on different time scales [47-59]. The analysis of the drift and diffusion coefficients, focus on obtaining reliable parameters, which may classify financial markets in terms of the predictability of price changes.

In 1996 Ghashgaie *et al* [124] made an analogy between hydrodynamic turbulence and an information cascade. This analogy is based on the idea that there is a correspondence between the dissipation of kinetic energy, across different length scales in a turbulent flow and the transmission of information, between different time scales in the financial markets. There is a cascade like transition in the data structure from large scales to smaller scales. It is generally assumed that this information cascade, results from a combination of the behavior of investors and the trading mechanisms [125], which allow for information possessed by long-term investors to be passed on to shorter term investors. Financial markets are complex systems consisting of many interacting components which are subject to a continuous flow of information [47]. Amongst the many market indicators are observables such as fluctuating prices which can be shown to be stochastic variables [53, 58]. The detection and description of these market indicators and their underlying patterns is important for identifying mechanisms governing market dynamics. It is also important to quantify each market in terms of how it reacts to and propagates disturbances. Examples include the dissipation of economic shocks and the efficiency of disseminating information [126-130]. Such

comparative studies have been done before using common quantities such as volatility [131-134] and Hurst exponents [131,135-141] described below, as well as other market statistical properties such as GARCH models [142,143].

Unlike the examples of electromyography and wind turbulence, an important measure in classifying the behaviour of time series data in financial markets is short term predictability, which is normally described by the Hurst exponent H [102]. The Hurst exponent is interpreted as the relative tendency of a time series to either cluster in some direction or regress to a longer term mean value. For example, if a value of H lies close to 0.5 then price changes on the financial markets would be entirely unpredictable and would indicate a random walk. A value of H between 0 and 0.5 would mean that the change in price exhibits anti-persistent or mean reversion behaviour. An increase in a price would tend to be followed by a decrease (or a decrease will be followed by an increase). A Hurst Exponent value between 0.5 and 1 indicates persistent behaviour and that the change in the price has a trend. Series of this type are the easiest of the three types of time series data to predict.

A popular approach to estimating the Hurst exponent is the rescaled range analysis (R/S analysis) method [102]. Consider a time series, $x = x_1, x_2, \dots, x_n$. The first step is to calculate the mean $\mu = 1/n \sum_{i=1}^{n} x_i$ and then to generate the mean adjusted series $y_t = x_t - \mu$, for $t = 1, 2, \dots, n$. Next generate the cumulative deviate series $z_t = \sum_{i=1}^{t} y_i$, the range series $R_t = \max(z_1, z_2, \dots, z_t) - \min(z_1, z_2, \dots, z_t)$ for $t = 1,2, \dots, n$ and the standard deviation series $S_t = \sqrt{\frac{1}{t}\sum_{i=1}^{t}(x_i - \mu)^2}$ $t = 1, 2, \dots, n$. The rescaled range series is calculated using $(R/S)_t = R_t/S_t$ $t = 1, 2, \dots, n$. Hurst found that (R/S) scales by power-law as time increases, which indicates that $(R/S)_t = ct^H$, where c is a constant. H is found by plotting (R/S) versus time t in log-log axis. The slope of the regression line is the Hurst exponent.

The prediction tool developed in this work is used to examine fifteen financial time series data sets consisting of five foreign exchange rates, six stocks, three market indexes and one commodity, Brent oil.

6.1. Methodology

Analogously to wind turbulence, there exists a cascade feature in the flow of information, in the financial markets, in an average sense from large scales to progressively smaller scales. Here, the approach is to describe the joint statistics of the change in prices on many different time scales t_i. This is achieved by the knowledge of the conditional probability distribution function, $P\big(v(t_1)\big|v(t_0)\big)$. By these probability density functions the correlations between scales are worked out, showing how the order of complexity and disorder is linked between scales. The statistics of the scale-dependent measure is shown to obey the Chapman-Kolmogorov equation evolving in t, which can be written in differential form, as the Kramers-Moyal expansion. The stochastic variable of interest is the change in price or price increment, $v(t)$ between two temporal locations t which are a time interval kd apart,

$$v(t) \equiv \Delta x(t) = x(t + kd) - x(t), \tag{6.1}$$

where $\Delta x(t)$ is a price fluctuation, d the temporal resolution of the time series data and k is the discreet number of d separations between two positions t. From the work of Peinke *et al* [144] stochastic equivalence is found for relative changes $r(t) = (x(t + kd))/(x(t))$ and logarithmic returns $l(t) = \ln\,(x(t + kd))/(x(t))$.

Following similar methods discussed for the study of wind turbulence and electromyography, several assumptions have to be tested before applying the Kramers-Moyal expansion to the time series data.

First it needs to be established that the particular financial market represents a system whose discrete changes can be described by a stochastic process. As these changes are the direct consequence of both the behaviour of the participating traders and the trading mechanisms, it is implicitly assumed that these will be the main microscopic factors determining the transport coefficients. Suppose the value of $v(t)$ at some initial position (scale) t_0 is fixed and that $v(t_i)$ for any $t_i < t_0$ can be predicted only probabilistically, then a stochastic system is defined by the investigation of the state of the system at successive instants $t_n < t_{n-1} < \cdots < t_0$. The joint distribution function for n random variables $v(t_n), v(t_{n-1}), \ldots,$ and $v(t_0)$ is then defined as

$$P\big(v(t_n); v(t_{n-1}); \dots; v(t_1); \mathrm{v}(t_0)\big) = P\big(\mathrm{v}(t_0)\big)P\big(v(t_n); v(t_{n-1}); \dots; v(t_1)\big|\mathrm{v}(t_0)\big). \tag{6.2}$$

Equation (6.2) describes the stochastic dependency of $v(t_i)$ for any $t_i < t_0$ and represents a stochastic system.

The second assumption that should be tested is whether the stochastic process described by equation (6.2) can be reduced to a binary-scale transition function, as represented by the right-hand side of equation (6.3)

$$P_1^{(n)}\big(v(t_n)\big|v(t_{n-1}); \dots; v(t_1); \mathrm{v}(t_0)\big) = P_1^{(n)}\big(v(t_n)\big|v(t_{n-1})\big) \equiv P\big(v(t_n)\big|v(t_{n-1})\big), \tag{6.3}$$

for all $n \geq 2$ and $t_{n-1} \leq t_n$.

This feature is tested by using the Chapman-Kolmogorov equation,

$$P\big(v(t_1)\big|v(t_0)\big) = \int_{-\infty}^{\infty} P\big(v(t_1)\big|v(t_i)\big)P\big(v(t_i)\big|v(t_0)\big)\,\mathrm{d}v_i, \qquad \text{for } (t_1 \leq t_i \leq t_0), \tag{6.4}$$

and compared with tests using the conditional probability distribution function,

$$P\big(v(t_2)\big|v(t_1)\big) = P\big(v(t_2)\big|v(t_1); v(t_0)\big), \tag{6.5}$$

by taking a cross-section through $v(t_0) \cong 0$. Close to 35 percent of the total fluctuations of some of the financial instruments studied in this work lie close to the mean, $v(t_0) \cong 0$.

The third assumption to be tested is whether any even Kramers-Moyal moment greater than the second order equals zero. The Kramers-Moyal moments are estimated directly from the measured time series as the limiting moments M_k of the transition probability distributions

$$D_k(v(t_i), \tau_i) = \frac{1}{k!}\lim_{\tau \to \tau_i} M_k(v(t_i), \tau_i) = \frac{1}{k!}\lim_{\tau \to \tau_i}\frac{1}{\tau - \tau_i}\int (v(t) - v(t_i))^k P(v(t), \tau | v(t_i), \tau_i)\mathrm{d}v, \tag{6.6}$$

where $\tau = \ln(t_0/t_1)$ for $t_1 < t_0$. If the above assumptions prove to be true then the first two Kramers-Moyal coefficients form the Fokker-Planck equation

$$\frac{\partial P(v(t),\tau)}{\partial \tau} = -\frac{\partial}{\partial v}[D_1(v(t),\tau)P(v(t),\tau)] + \frac{1}{2}\frac{\partial^2}{\partial v^2}[D_2(v(t),\tau)P(v(t),\tau)], \tag{6.7}$$

which describes how the statistics of price increments $v(t)$ are correlated across time scales.

To estimate the drift coefficient a linear fit is made to $M_1(v(t),\tau)$ using

$$D_1(v(t),\tau) = a_1 v + a_2, \tag{6.8}$$

while for the diffusion coefficient a quadrat fit is made to $M_2(v(t),\tau)$ using

$$D_2(v(t),\tau) = b_1 v^2 + b_2 v + b_3. \tag{6.9}$$

To construct a prediction tool the parameters a_k and b_k are plotted for several arbitrary chosen time scales $t_1 = 3d$ and $t_0 = 60d$ to $6d$, *i.e.* from $\tau = \ln(t_0/t_1) = 2.996$ to $\tau = 0.693$. The choice of time scales depends on the time horizon of interest. In the analyses of these plotted parameters there are several important features. Firstly, which parameters behave in a spurious manner with no discernable pattern, thus suggesting no good predictive value? Secondly, is there a convergence of the parameters a_k and b_k? Convergence in τ may be a possible measure of market efficiency. An efficient market would reflect all the available information in the prices. Lastly, which parameters show steady behaviour across time scales? These are the parameters which could indicate if there are different trends for the different financial markets. After these parameters have been identified they are plotted and a suitable fit is obtained. The parameters of this new analysis are then compared against the Hurst exponents, estimated using three different methods, included in the Wavelet Toolbox of MATLAB® [102]. The first method of estimating the Hurst exponent is based on the discrete second-order derivative [145]. The second one has similar properties but is estimated using a wavelet-based adaptation [145]. The third method, estimates H using the slope of the log-log plot of the detail variance versus the level [146].

6.2. The Data

Fifteen sets of financial time series data were studied consisting of five foreign exchange rates, six stocks, three market indexes and one commodity, Brent oil. The foreign exchange rates are the British Pound/US Dollar (£/US$), Euro/US Dollar (€/US$), Japanese Yen/ US Dollar (¥/US$), US Dollar/Swiss Franc (US$/CHF) and the US Dollar/South Africa Rand (US$/ZAR). The stocks are Allianz AG, Google, BP, Nokia, Walmart and Freddie Mac. The stock indexes are COMPQ, FTSE-100 and DAX. The choice of data was limited to the availability of the data sets on Dukascopy [147], one of only a few websites offering limited free financial datasets. The time series were sampled from 16th January 2006 to 16th October 2009 for all instruments, except for Freddie-Mac which ranged from 11th May 2007 to 1st August 2008. The sample sizes and codes of the financial instruments are listed in table 6.1.

Table 6.1. The fifteen sets of financial time series data are opening retail prices with a temporal resolution of $d = 10$ minutes. The difference in sample sizes is due to holidays, trading hours of the different markets and some missing observations.

Code	Instrument	Type	Sample size
1	£/US$	Foreign Exchange	195848
2	€/US$	Foreign Exchange	195848
3	¥/US$	Foreign Exchange	191255
4	US$/CHF	Foreign Exchange	141310
5	US$/ZAR	Foreign Exchange	141415
6	Allianz AG	Stock	60090
7	Google	Stock	37522
8	BP	Stock	46696
9	Nokia	Stock	32475
10	Walmart	Stock	38040
11	Freddie Mac	Stock	11875
12	COMPQ	Stock Index	32755
13	FTSE-100	Stock Index	39951
14	DAX	Stock Index	42714
15	Brent	Commodity	117452

Plots of six selected time series are shown in Fig. 6.1. All fifteen time series data have a temporal resolution of $d = 10$ minutes. Previous works have also shown that daily averages may be used [148]. Each financial time series was standardised by dividing the original observation, $x(t)$, by its standard deviation, σ, and was tested for stationarity using the Augmented Dicky-Fuller [121-122] test included in the Econometrics Toolbox of MATLAB®.

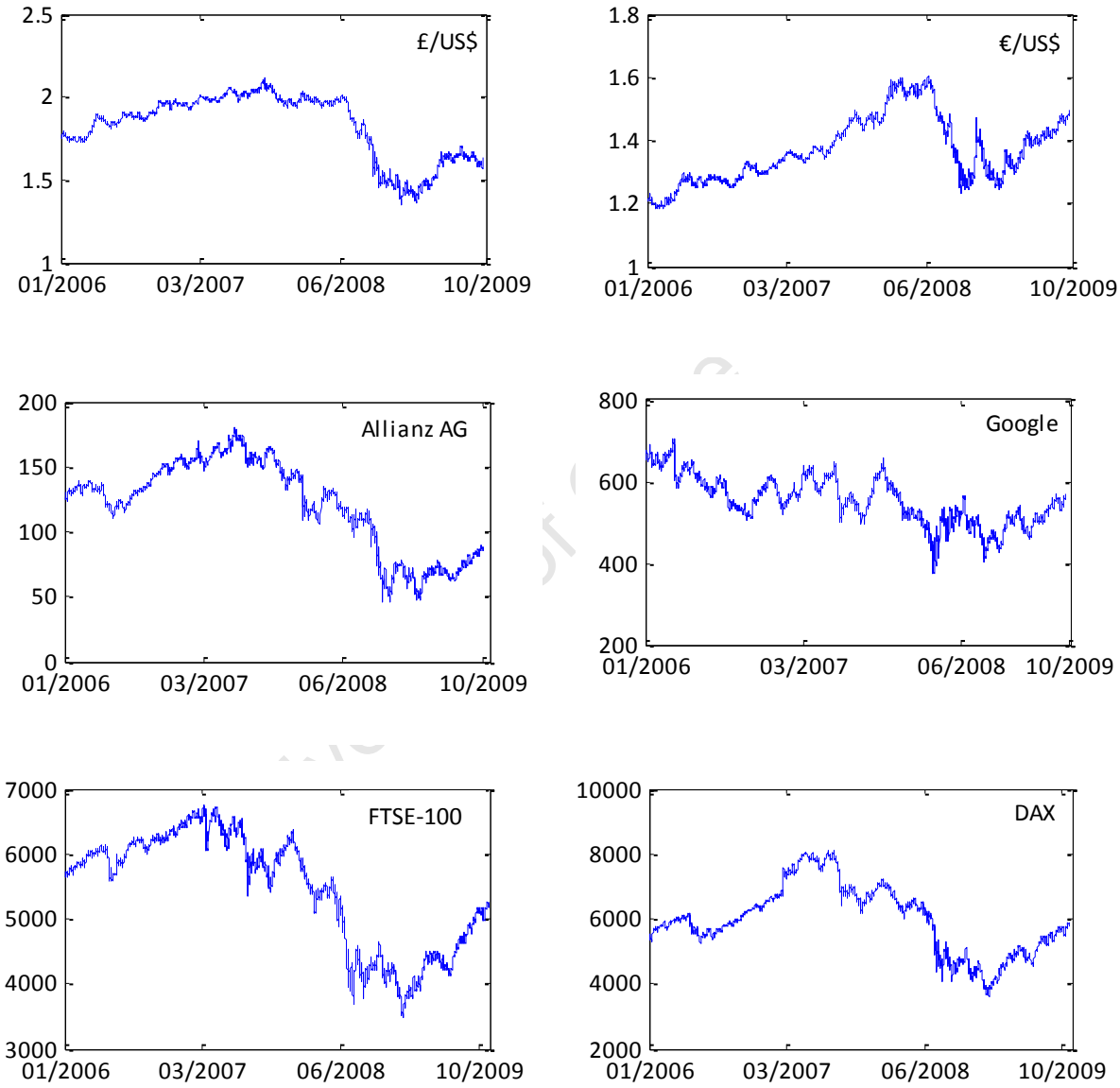

Fig 6.1 Six of the fifteen time series plots. Data sampled from trading days, 16 January 2006 to 16 October 2009 with a resolution of 10 minutes.

6.3. Testing of the Assumptions

The first assumption to be tested is whether price increments $v(t)$ are correlated across the time scales of interest. To test this assumption, the joint probability distribution function

$$P\big(v(t_1); v(t_0)\big), \tag{6.10}$$

and the corresponding conditional probability distribution function

$$P\big(v(t_1)\big|v(t_0)\big) = \frac{P\big(v(t_1); v(t_0)\big)}{P\big(v(t_0)\big)}, \tag{6.11}$$

are computed for arbitrary chosen time scales, $t_1 = 20d$ and $t_0 = 40d$ and bin number of 150 for both scales, for all fifteen time series data. A sample of six of the fifteen contour plots of the joint and conditional probability distribution functions are shown in Fig 6.2 and Fig 6.3, respectively.

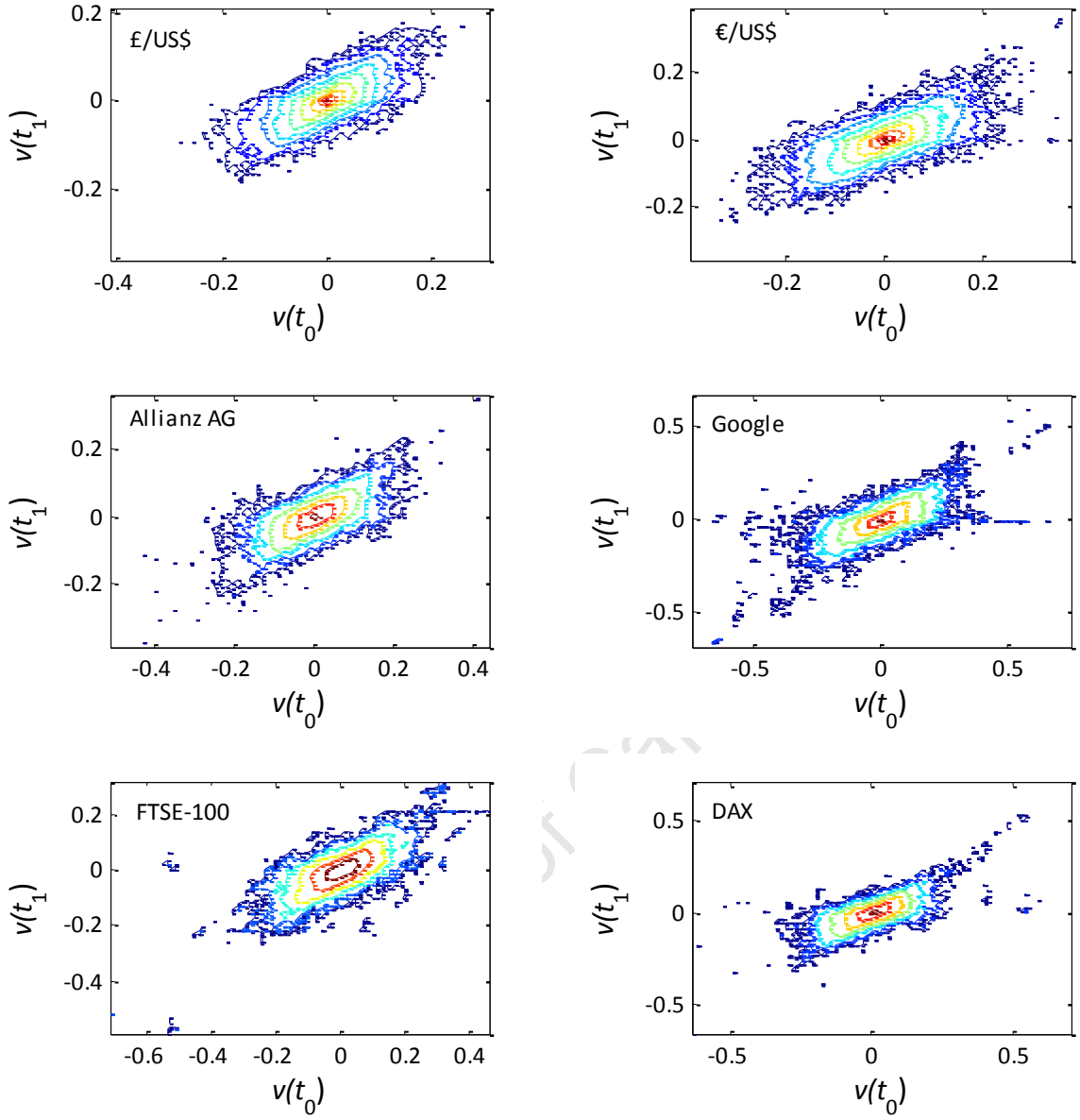

Fig 6.2 Contour plots of the joint probability density functions $P\big(v(t_1); v(t_0)\big)$ for the time scales are $t_1 = 20d$ and $t_0 = 40d$, where $d = 10$ minutes. The contour lines correspond to $\log_{10}P = -1.5, -2.0, 2.5, \ldots, -5.0$.

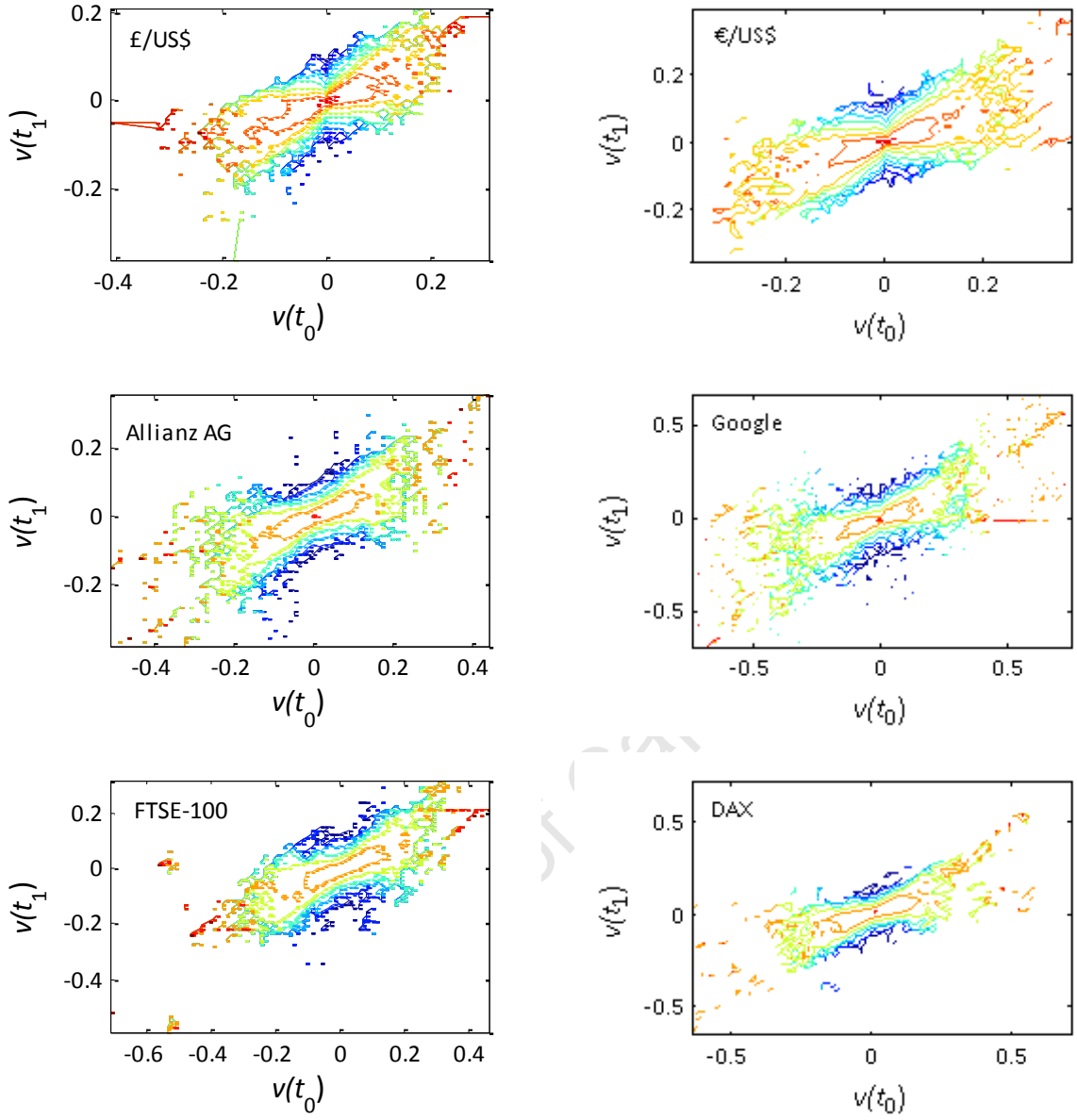

Fig 6.3 Contour plots of the conditional probability density functions $P(v(t_1)|v(t_0)) = P(v(t_1); v(t_0))/P(v(t_0))$ for the time scales are $t_1 = 20d$ and $t_0 = 40d$, where $d = 10$ minutes. The contour lines correspond to $\log_{10}P = -0.5, -1.0, 1.5, \ldots, -4.5$.

Fig 6.2 and Fig 6.3 show the contour lines to be aligned at a 45 degree angle to the axis of the plots for both the joint and conditional probability density functions. This indicates that price increments are correlated across these time scales, and that the price increment $v(t)$ is a stochastic variable in t. This was found to be true for all fifteen time series with significant price fluctuations between $\pm 0.2\sigma$.

The second assumption that should be tested is whether the stochastic process, described by equation (6.2), can be reduced to a binary-scale transition function, for computational convenience. This is tested using the Chapman-Kolmogorov equation (6.4) and the conditional probability distribution function (equation (6.5)). The validity of equation (6.4) is evaluated by comparing the left-hand and right-hand side of the equation in a contour plot for $(t_1 \leq t_i \leq t_0)$. Six of the fifteen plots are plotted in Fig 6.4. The right-hand side of the Chapman-Kolmogorov equation (6.4) is plotted as broken lines. Where the lines overlap the equation is valid.

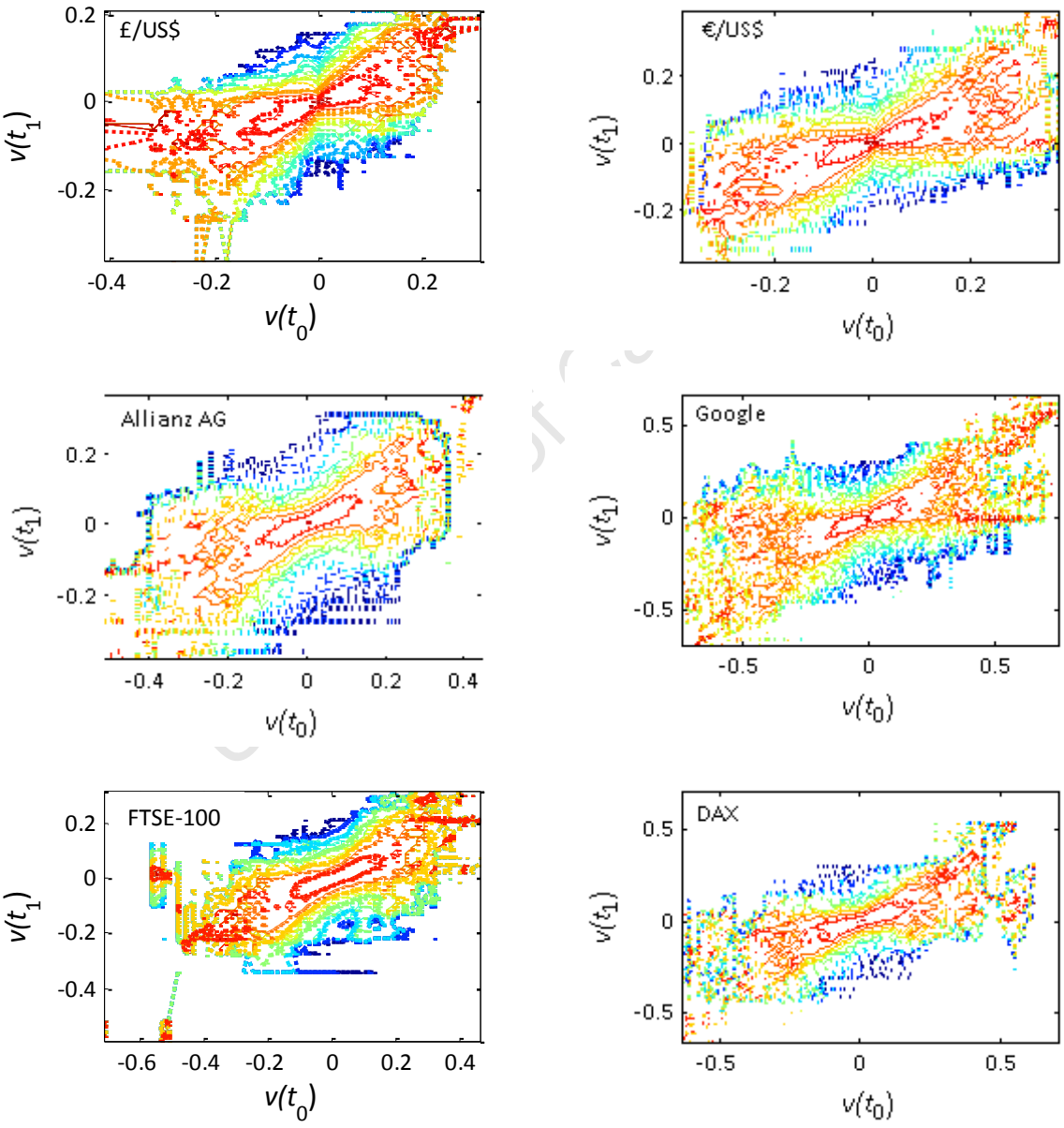

Fig 6.4 Contour plots of the Chapman-Kolmogorov equation (6.4). The integral on the right-hand side is plotted in broken lines.

The contour lines show that the Chapman-Kolmogorov equation is approximately valid for small fluctuations. To obtain more exact values the Chapman-Kolmogorov equation (6.4) is rewritten as

$$CK = P\big(v(t_1)\big|v(t_0)\big) - \int_{-\infty}^{\infty} P\big(v(t_1)\big|v(t_i)\big)P\big(v(t_i)\big|v(t_0)\big)\,\mathrm{d}t_i. \tag{6.12}$$

The binary-scale transition function, as represented by the right-hand side of equation (6.3), is thus at best only valid for price increments when $CK = 0$. The function CK is plotted in Fig 6.5 and has minimum values of approximately between $v(t_0) = -0.2\sigma$ and 0.2σ.

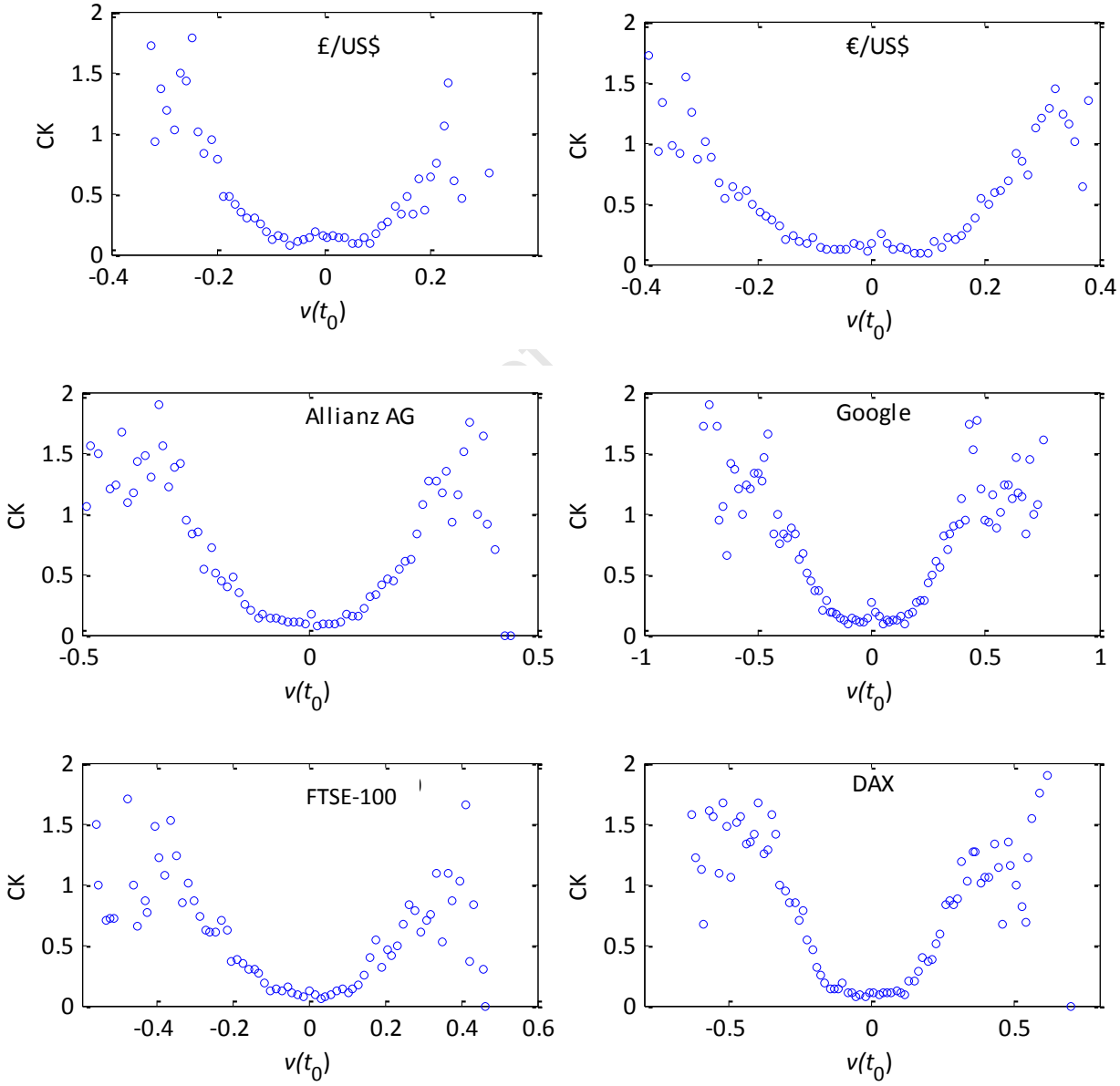

Fig 6.5 Plots of the Chapman-Kolmogorov equation in the form of equation (6.12).

An alternative approach to testing equation (6.3), is to use the triple scale conditional probability distribution function

$$P\big(v(t_2)\big|v(t_1)\big) = P\big(v(t_2)\big|v(t_1); v(t_0)\big). \tag{6.13}$$

The difficulty of using equation (6.13) is that it involves evaluating a 3 dimensional matrix which expresses the joint probability densities of the price increments. It is this difficulty which makes the Chapman-Kolmogorov equation more appealing to most authors when testing the Markov property [87] as it involves only evaluating a 2 dimensional matrix. However, one can get around this difficulty by stipulating some prior parameterisation of the conditional moments, as was done for the wind turbulence case. For example, equation (6.13) can be rewritten as

$$P\big(v(t_2)\big|v(t_1)\big) = P(v(t_2)|v(t_1); v(t_0) = k), \tag{6.14}$$

for a triplet time scale, where $v(t_0) = k$ represents a cross-section through the mean of the distribution, typically at $k \cong 0$ effectively reducing the matrix to two dimensions. The two methods of testing the reduction to a binary-scale transition function, represented by equations (6.4) and (6.14) are now compared using the Euro/US Dollar exchange rate data. Equations (6.4) and (6.14) are plotted as contour plots in Fig 6.6 (a) and Fig 6.6 (b), respectively. In this particular example 31.11% of the fluctuations occur at $v(t_0) = -0.0016\sigma$, the mean fluctuation.

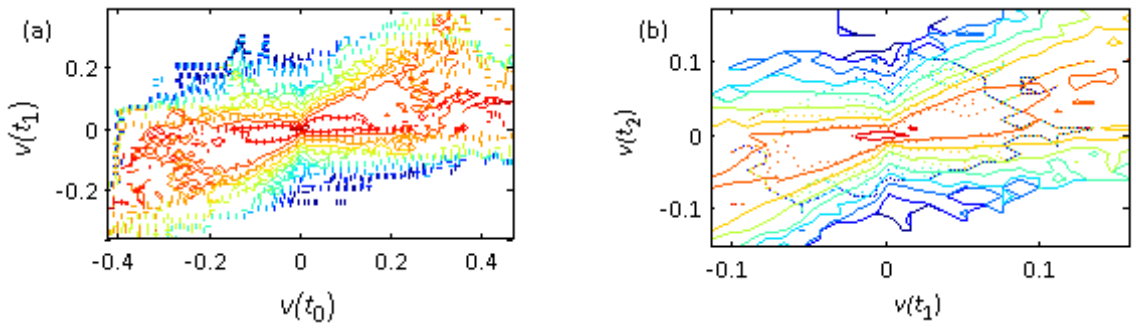

Fig 6.6 (a) A contour plot of equation (6.14) with $v(t_0) = -0.0016$. (b) A contour plot of the Chapman-Kolmogorov equation (6.4). The right-hand side of these two equations is plotted as broken lines. Here $t_2 = 20d$, $t_1 = 40d$ and $t_0 = 60d$. The number of bins is 150 for all time scales.

The right-hand side of equations (6.14) and (6.4) are plotted as broken lines while the solid lines represent the left-hand side. Where the lines overlap the binary-scale transition function is valid, as

represented by the right-hand side of equation (6.3). It has been argued that a test based on the whole transition distribution is preferable to tests based on the specific conditional moments [87] which is another reason why many authors have used the Chapman-Kolmogorov equation to test the Markov property. However, for large time scales, there is a discrepancy between the results of using the Chapman-Kolmogorov equation and the conditional probability density function using the triplet scale given by equation (6.14). These two methods are now compared using the method discussed in section 4.3 for wind turbulence. First, equation (6.14) is rewritten as

$$MP = P\big(v(t_2)\big|v(t_1)\big) - P(v(t_2)|v(t_1); v(t_0) = k). \tag{6.15}$$

Equations (6.12) and (6.15) are then computed for increasing time scales, $t_2 = 20d$, $t_1 = (40 + c10)d$ and $t_0 = (60 + c20)d$, where $c = 1$ to 50. The method involves taking cross-sections at $v(t_0) \cong 0$ in equation (6.15) for each of the 50 cases produced by c. Next, cross-sections are made for each of the fifty distribution function at $v(t_0) \cong 0$ and $v(t_1) \cong 0$ for the Chapman-Kolmogorov case, equation (6.12) and the conditional probability function, equation (6.15), respectively. An example of one of the 50 distribution functions using the Euro/US Dollar exchange rate data, is plotted in Fig 6.7 for $t_2 = 20d$, $t_1 = 40d$ and $t_0 = 60d$. The solid circles are the distributions of the second terms on the right-hand side of equations (6.12) and (6.15). Where the circles overlap the Chapman-Kolmogorov, equation (6.12) and the conditional probability function, equation (6.15), are valid for those increments. The open circles are drawn larger for clarity. Thus, the stochastic process, described by equation (6.2), can be reduced to a binary-scale transition function. The two-sample Kolmogorov-Smirnov test used in chapter 4 rejects the null hypothesis and the two distributions are the same at a 5 percent level of significance.

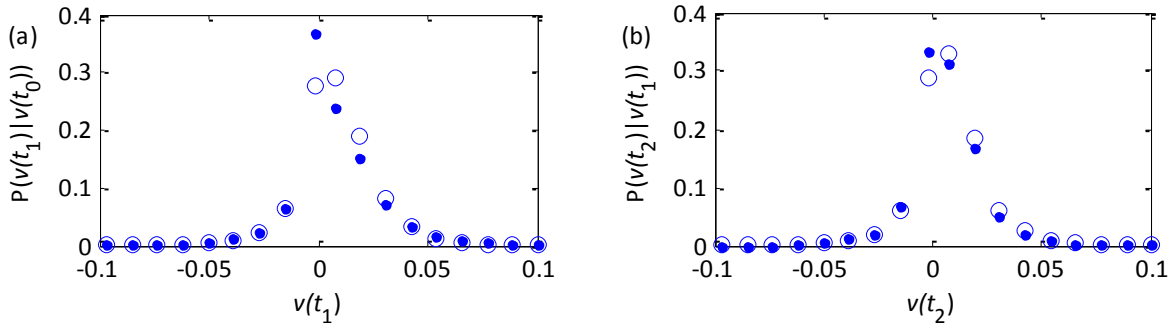

Fig 6.7 (a) Distributions of the Chapman-Kolmogorov equation for a cross-section at $v(t_0) \cong 0$ and (b) equation (6.15) with a cross-section at $v(t_1) \cong 0$. The solid circles are the distributions of the second terms on the right-hand side of equations (6.12) and (6.15). The open circle gives the distributions of the first term. Both plots were obtained for a fixed time intervals $t_2 = 20d$, $t_1 = 40d$ and $t_0 = 60d$.

These cross-sections allow for a goodness of fit test between the two distributions, represented by the solid and open circles, for each time scale, by minimising equations (6.12) and (6.15). Once again, the open circles are drawn larger for clarity. The results are plotted Fig 6.8.

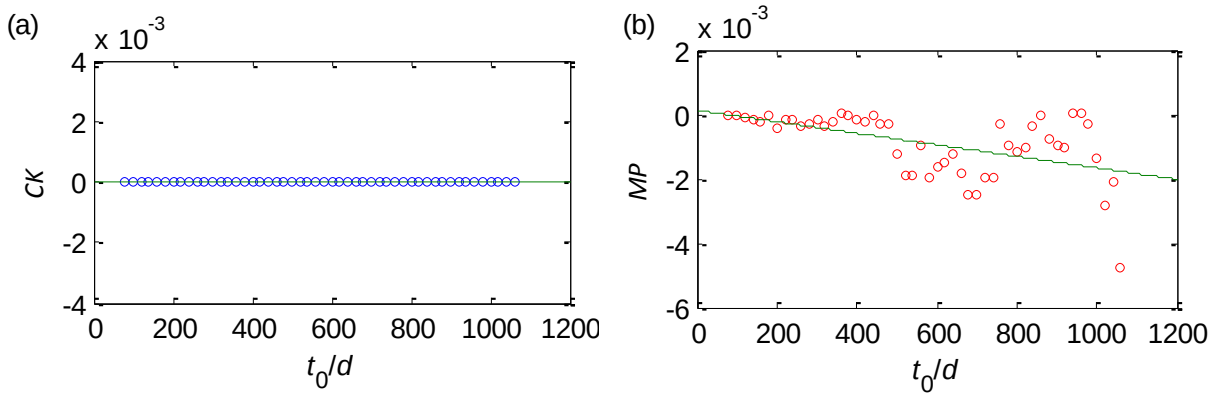

Fig 6.8 (a) Plot of the Chapman-Kolmogorov equation (6.12) for a cross-section at $v(t_0) \cong 0$. (b) Plot of the conditional probability distribution function, equation (6.15), for a cross-section at $v(t_1) \cong 0$. Both plots were obtained for time intervals $t_2 = 20d$, $t_1 = (40 + c10)d$ and $t_0 = (60 + c20)d$, where $c = 1$ to 50.

The Chapman-Kolmogorov equation test (equation (6.12)) suggests, in Fig 6.8 (a), that the binary-scale transition function is sufficient at describing the stochastic system for all scales tested. However, test using the conditional probability distribution function (equation (6.15)) shows, in Fig 6.8 (b), that for the same large scales, the binary-scale transition function is not able to account for all possible paths and permutations that price changes could take. This discrepancy between the two tests was found to be true for all fifteen financial time series data.

The last assumption involves testing Pawula's theorem, and showing that

$$D_4(v(t),\tau) = \frac{1}{24}\lim_{\Delta\tau\to 0} M_4(v(t),\tau) = 0, \tag{6.16a}$$

$$M_4(v(t),\tau) = \frac{1}{\Delta\tau}\int (v'-v)^4 P(v',\tau+\Delta\tau|v,\tau)\mathrm{d}v'. \tag{6.16b}$$

The fourth moment $M_4(v(t),\tau)$ is plotted in Fig 6.9 for six of the financial time series discussed earlier.

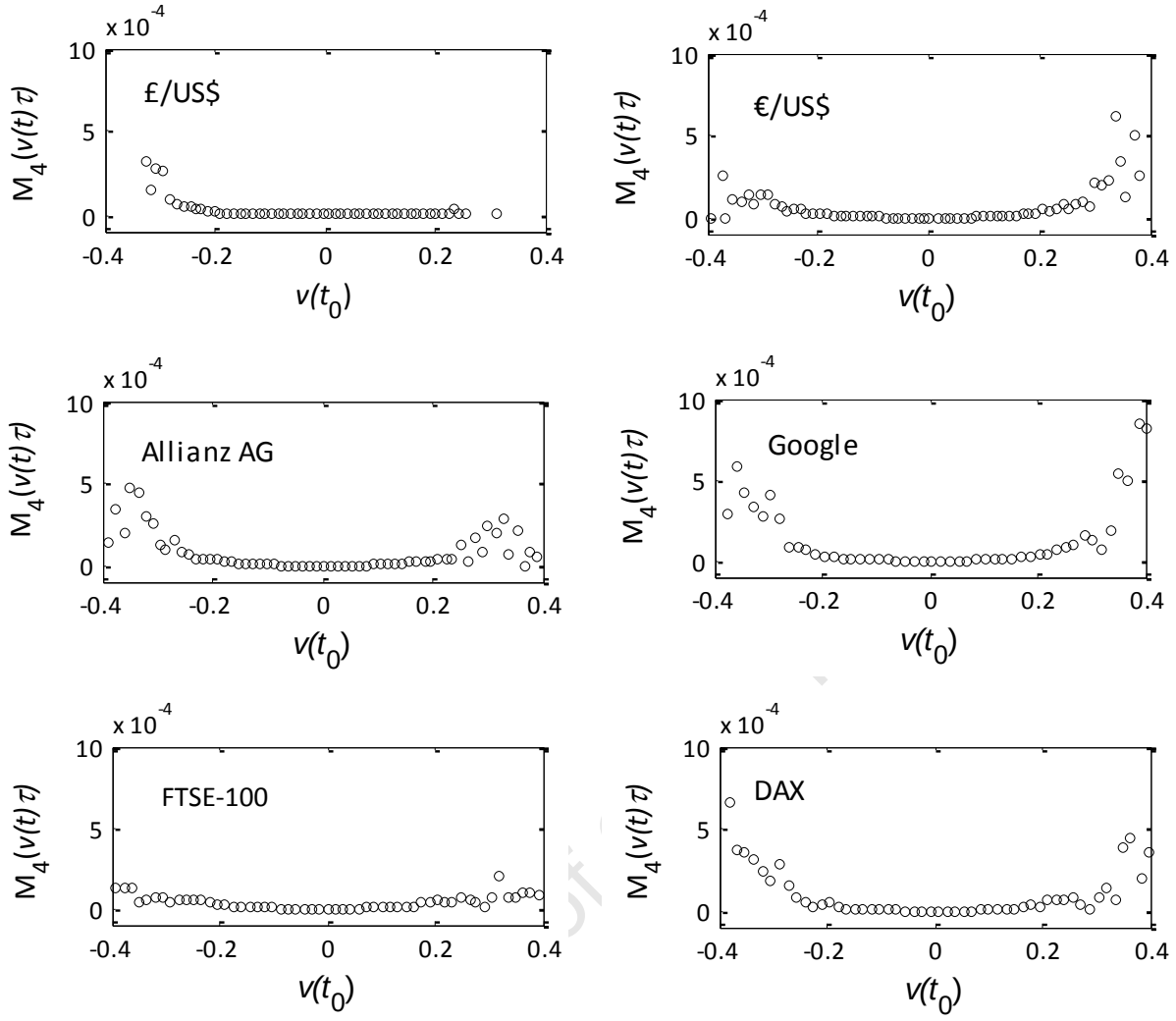

Fig 6.9 Plots of $M_4(v(t),\tau)$ for six of the fifteen time series.

Fig 6.9 shows that $\lim_{\Delta\tau\to 0}\frac{1}{\Delta\tau}M_4(v(t),\tau)=0$ in the interval $v(t_0)=-0.2\sigma$ and 0.2σ for the six time series is same interval of price increments in which the Chapman-Kolmogorov equation is satisfied, as shown in Fig 6.4 and Fig 6.5. This was found to be approximately true for all fifteen financial instruments. The Kramers-Moyal expansion can now be truncated at the second term to produce the Fokker-Planck equation, equation (6.7).

6.4. The Prediction Tool

Having concluded the testing of the assumptions, the coefficients of the Fokker-Planck equation can be directly calculated from the time series data using the Kramers-Moyal expansion,

$$D_1(v(t),\tau) = \lim_{\Delta\tau\to 0}\frac{1}{\Delta\tau}M_1(v(t),\tau), \tag{6.17a}$$

$$M_1(v(t),\tau) = \frac{1}{\Delta\tau}\int (v'-v)P(v',\tau+\Delta\tau|v,\tau)\mathrm{d}v' \tag{6.17b}$$

and

$$D_2(v(t),\tau) = \lim_{\Delta\tau\to 0}\frac{1}{\Delta\tau}M_2(v(t),\tau), \tag{6.18a}$$

$$M_2(v(t),\tau) = \frac{1}{\Delta\tau}\int (v'-v)^2P(v',\tau+\Delta\tau|v,\tau)\,\mathrm{d}v'. \tag{6.18b}$$

The first moment M_1 is shown in Fig 6.10 for the six selected time series, and show the now characteristic linear function of $v(t_0)$.

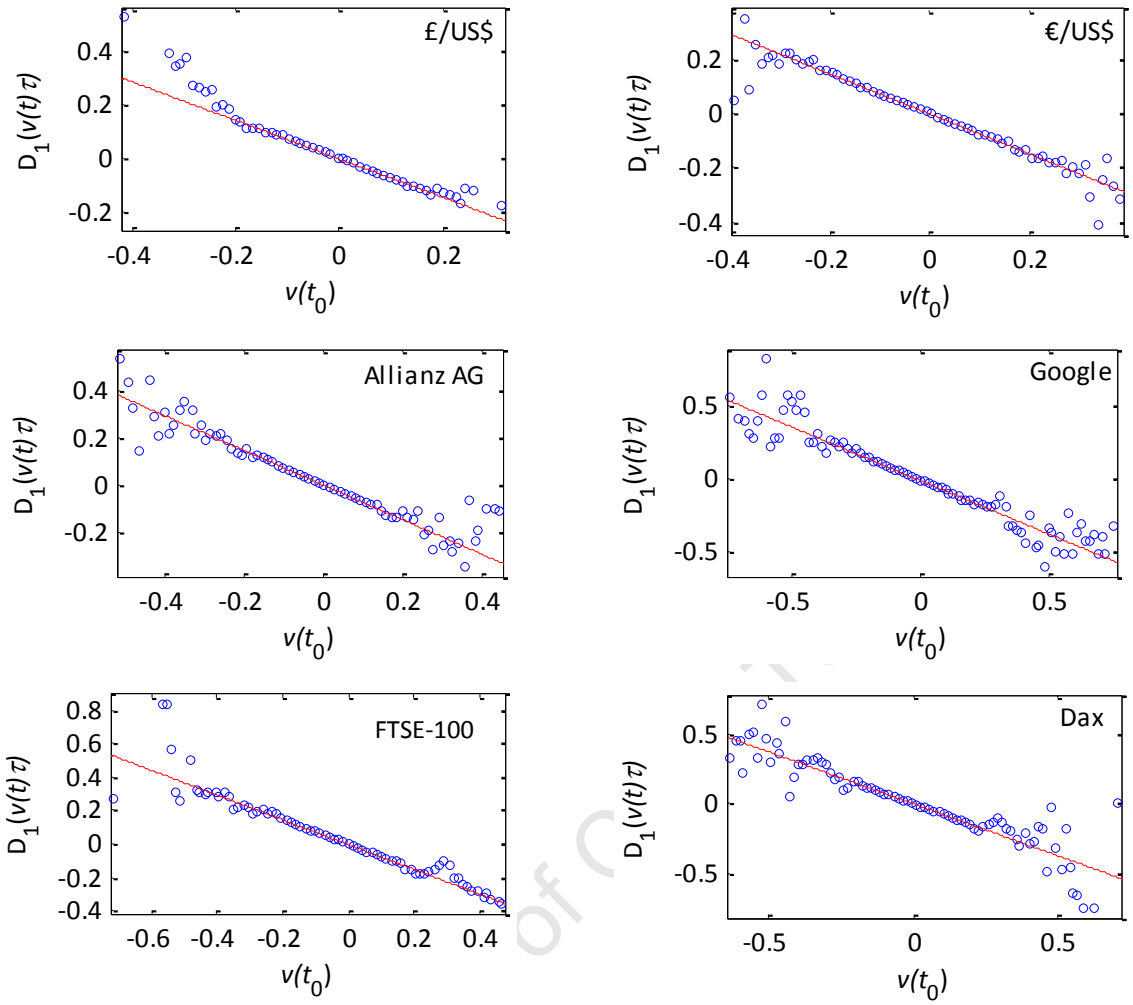

Fig 6.10 Plots of the drift term, $D_1(v(t),\tau)$. The fitted line was obtained by fitting a linear polynomial to the points in the $v(t_0) = -0.2\sigma$ and 0.2σ interval. The time scales are $t_1 = 20d$ and $t_0 = 40d$. The number of bins are 150 for both scales.

The drift term, $D_1(v(t),\tau)$, is obtained by fitting a linear polynomial

$$D_1(v(t),\tau) = a_1 v + a_2, \tag{6.19}$$

to the data in the interval for which the assumptions are valid, *i.e.* $v(t_0) = -0.2\sigma$ and 0.2σ. Using £/US$ as an example the equation for the linear fit is

$$D_1(v(t),\tau) = -0.716v + 0.002475 \tag{6.20}$$

with 95% confidence bounds coefficients on

$$\begin{aligned} a_2 &= (-0.004062, -0.0008886) \\ a_1 &= (-0.7305, -0.7015). \end{aligned} \tag{6.21}$$

It is interesting to note that only this interval, $v(t_0) = -0.2\sigma$ to 0.2σ, satisfy the linear polynomial, equation 6.19, Pawula's theorem and the Chapman-Kolmogorov equation. This is true for all fifteen financial time series data sets. This is in contrast to the electromyography data sets where both the Markov and non Markov fluctuations satisfied the linear polynomial and Pawula's theorem, see Fig 5.5 and 5.6.

The second moment M_2 is now plotted as open circles in Fig 6.11 for the same six selected time series, and show the same characteristic quadratic function of $v(t_0)$. The fourth moment M_4 is also shown as crosses.

The diffusion term, $D_2(v(t), \tau)$ is obtained as a quadratic function

$$D_2(v(t), \tau) = b_1 v^2 + b_2 v + b_3 \tag{6.22}$$

in the interval for which equation (6.3) is valid, *i.e.* $v(t_0) = -0.2\sigma \text{ and } 0.2\sigma$. Using £/US$ as an example the equation for the fit is

$$D_2(v(t), \tau) = 0.239\, v^2 + 0.003409 v + 0.0002924 \tag{6.23}$$

with 95% confidence bounds coefficients on

$$\begin{aligned} b_3 &= (0.0001402, 0.0004446) \\ b_2 &= (0.002471, 0.004347) \\ b_1 &= (0.2295, 0.2485). \end{aligned} \tag{6.24}$$

The linear and quadratic forms of the fitted first and second Kramers-Moyal coefficients, were found for all fifteen financial time series.

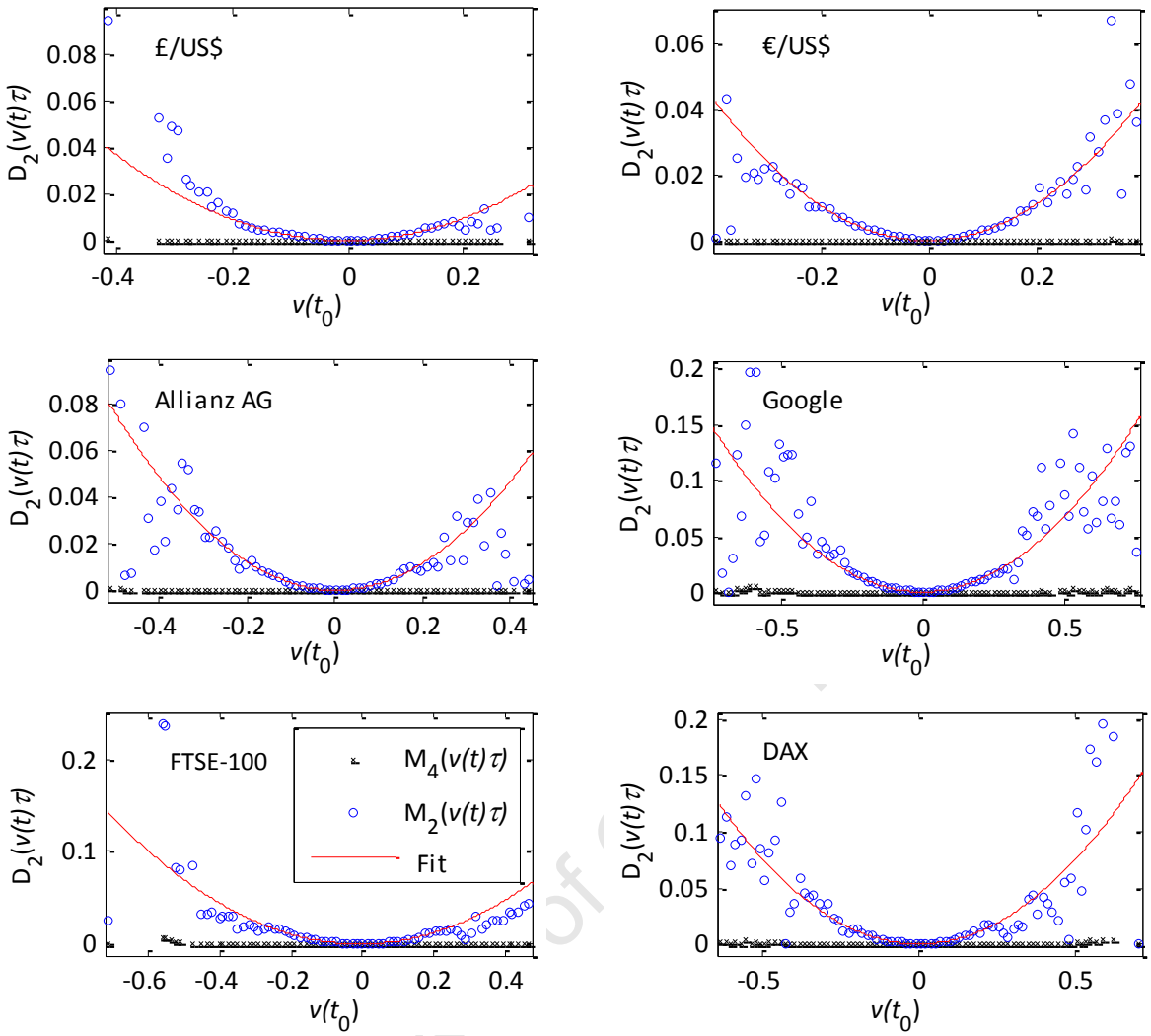

Fig 6.11 Plots of the diffusion term, $D_2(v(t),\tau)$, (open circles). The fitted line was obtained by fitting a linear polynomial of the 2nd order to the data in the CK-interval $v(t_0) = -0.2\sigma$ and 0.2σ. $M_4(v(t),\tau)$ is shown as crosses. The time scales are $t_1 = 20d$ and $t_0 = 40d$. The number of bins is 150 for both scales.

The drift and diffusion coefficients are now interpreted using the reciprocal of the change in time scales, as discussed for the case of the length scale in wind turbulence. A negative drift coefficient can be interpreted as an upward pressure on the price increments, driving the market towards larger fluctuations of positive changes in price. The greater the diffusion term, the greater the fluctuations of the change in price around the mean, which is interpreted as greater volatility in the price.

The construction of a prediction tool for times series data involves identifying the parameters a_k and b_k, in equations (6.19) and (6.22) respectively, which show steady behaviour across time scales. An inspection of the confidence bounds coefficients in equations (6.21) and (6.24) for the £/US$ example, suggest that the parameters a_2, b_2 and b_3, being so close to zero, may be statistically insignificant in characterising the distributions of price fluctuations and/or having any predictive value. To obtain a clearer understanding of the evolution of the these parameters across time scales they are plotted for time scales $t_1 = 3d$ and $t_0 = 60d$ to $6d$, *i.e.* from $\tau = \ln(t_0/t_1) = 2.996$ to $\tau = 0.693$. The parameters for these time scales are shown in Fig 6.12 with several features being noteworthy. There does not seem to be a significant difference between the six types of financial instruments. Parameters a_2, b_2 and b_3 behave in a spurious manner around zero with no discernable pattern and thus offer no good predictive value. Parameters a_1 and b_1 are the only two parameters that show steady behaviour across time scales and could thus potentially govern the significant asymmetries in the distribution of price changes. There is also a convergence of the parameters a and b at approximately $\tau = 2$ *i.e.* about $t_0 = 22d$ or 220 minutes. This convergence in τ may be a possible measure of market efficiency.

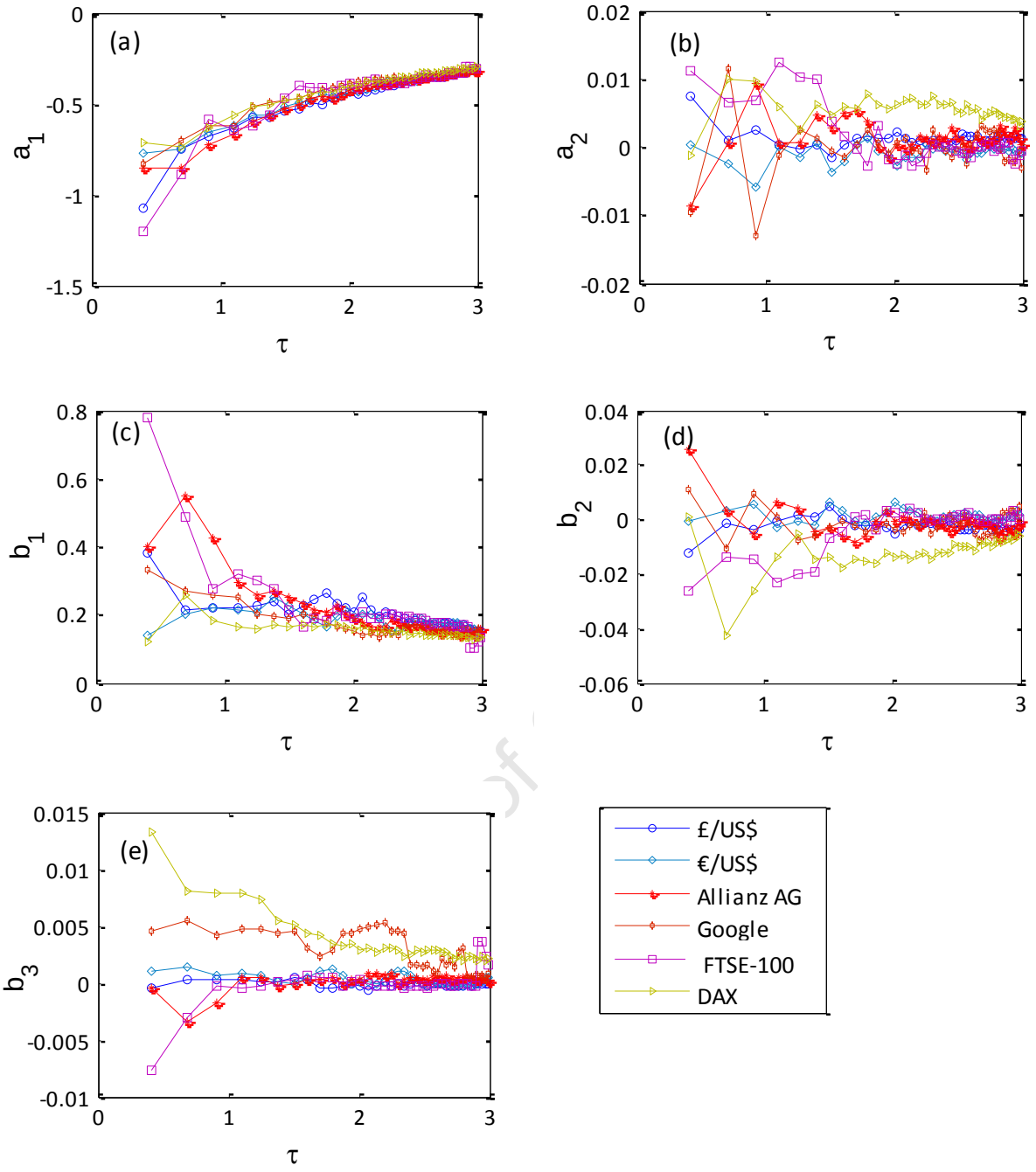

Fig 6.12 Plots of the parameters a_k and b_k for time scales $t_1 = 3d$ and $t_0 = 60d$ to $6d$.

The focus is now on parameters a_1 and b_1, which are shown in Fig 6.13 for all fifteen financial instruments.

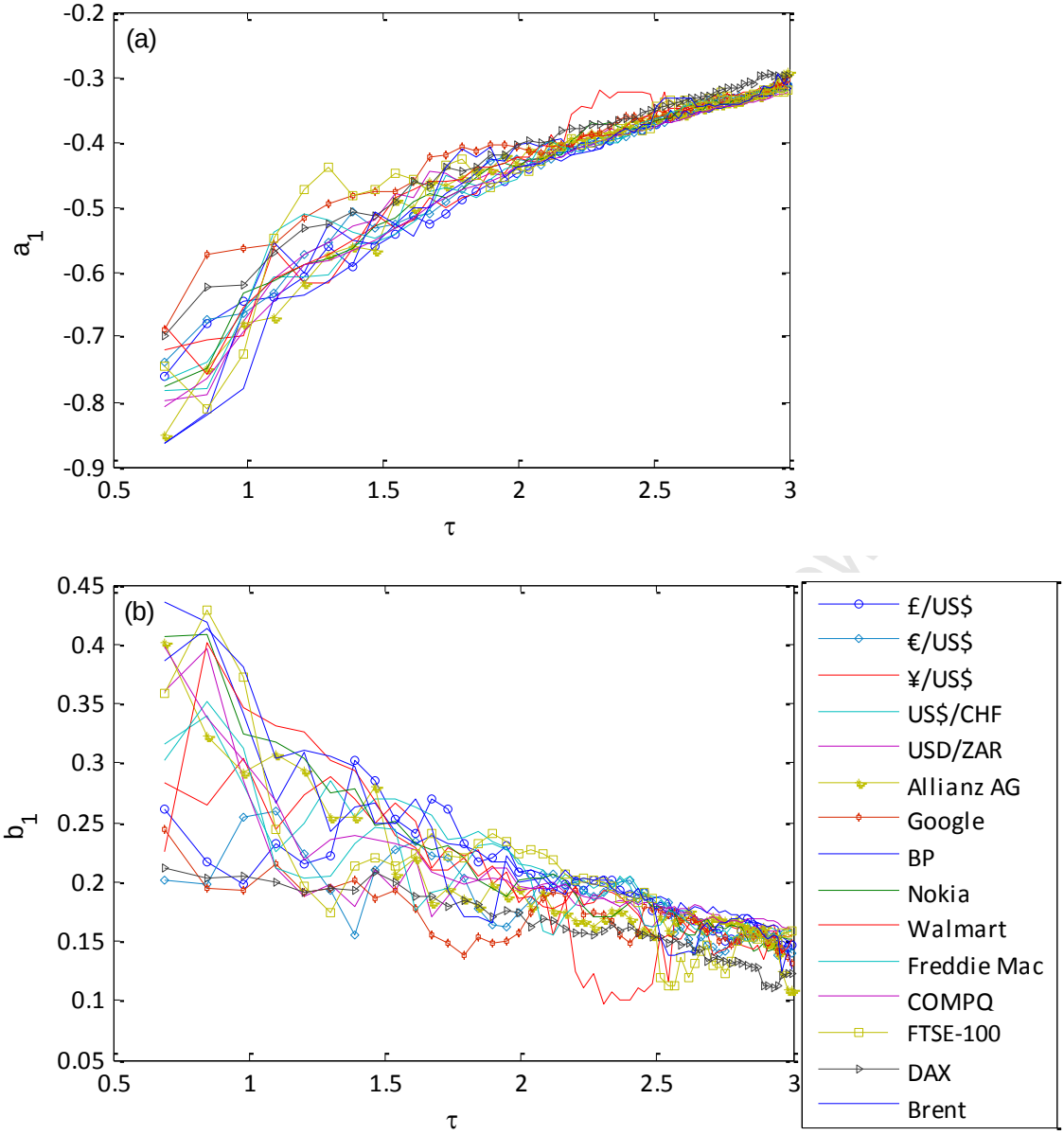

Fig 6.13 The plots of parameters a_1 and b_1 for all fifteen times series.

The plots of a_1 and b_1 suggest that a linear or exponential fit may be appropriate. In Fig 6.14, £/US$ is used as an example to fit a linear polynomial and exponential function to both a_1 and b_1. The linear polynomial for a_1 is

$$a_1 = c_1\tau + c_2 \tag{6.25}$$

and for b_1

$$b_1 = \mathrm{d}_1\tau + \mathrm{d}_2. \tag{6.26}$$

The exponential function fitted to a_1 is

$$a_1 = k_1 \exp(k_2\tau) \tag{6.27}$$

and to b_1

$$b_1 = l_1 \exp(l_2\tau). \tag{6.28}$$

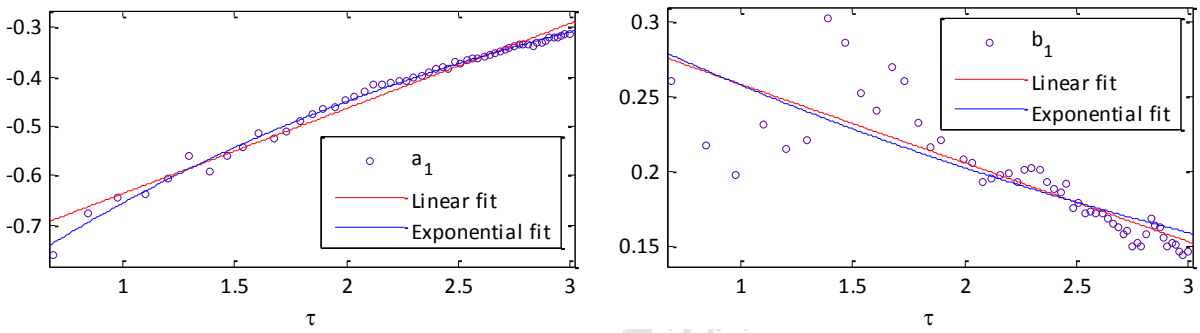

Fig 6.14 An exponential and linear function fit to the parameters of a_1 and b_1 for £/US$.

Exponential and linear fits are applied to the parameters a_1 and b_1 for all fifteen financial time series. These estimated parameters are tabulated in table 6.2.

A time-series is considered random if the drift term $D_1 = 0$. Recall that τ relates the ratio of the two time scales and is analogous to the Reynolds number discussed in chapter 4 where for low Reynolds numbers there is laminar flow while turbulent flow occurs at high Reynolds numbers. Thus as the length of the cascade increases, as illustrated in Fig 4.7, there is a loss of dependency across scales and the time series becomes more random and therefore it is more difficult to make predictions. The parameter c_1 in equation (6.25) can be defined as

$$\mathrm{c}_1 = \frac{\partial^2 D_1(v(t),\tau)}{\partial v \partial \tau}. \tag{6.29}$$

Table 6.2. Parameters c and d are obtained by fitting a linear function to a and b while parameters k and l are obtained by fitting an exponential function to a and b, respectively.

code	Instrument	c_1	c_2	d_1	d_2	k_1	k_2	l_1	l_2	H_1	H_2	H_3
1	£/US$	0.172	-0.810	-0.053	0.312	-0.956	-0.376	-0.053	0.312	0.475	0.471	0.505
2	€/US$	0.163	-0.780	-0.039	0.267	-0.918	-0.365	-0.039	0.267	0.473	0.469	0.428
3	¥/US$	0.171	-0.790	-0.068	0.331	-0.957	-0.395	-0.068	0.331	0.449	0.442	0.541
4	US$/CHF	0.171	-0.806	-0.070	0.360	-0.982	-0.389	-0.070	0.360	0.454	0.454	0.434
5	US$/ZAR	0.168	-0.793	-0.054	0.309	-0.991	-0.400	-0.054	0.309	0.252	0.256	0.297
6	Allianz AG	0.183	-0.827	-0.079	0.363	-1.027	-0.419	-0.079	0.363	0.466	0.467	0.554
7	Google	0.123	-0.669	-0.025	0.224	-0.754	-0.298	-0.025	0.224	0.396	0.404	0.511
8	BP	0.174	-0.809	-0.086	0.400	-0.993	-0.399	-0.086	0.400	0.442	0.447	0.506
9	Nokia	0.170	-0.795	-0.092	0.405	-0.976	-0.393	-0.092	0.405	0.484	0.480	0.580
10	Walmart	0.163	-0.773	-0.087	0.387	-0.935	-0.382	-0.087	0.387	0.468	0.454	0.499
11	Freddie Mac	0.164	-0.783	-0.059	0.320	-0.932	-0.373	-0.059	0.320	0.452	0.472	0.619
12	COMPQ	0.176	-0.823	-0.064	0.340	-0.971	-0.380	-0.064	0.340	0.535	0.529	0.560
13	FTSE-100	0.152	-0.748	-0.083	0.376	-0.888	-0.361	-0.083	0.376	0.541	0.541	0.533
14	DAX	0.150	-0.727	-0.043	0.255	-0.851	-0.358	-0.043	0.255	0.448	0.444	0.573
15	Brent	0.198	-0.867	-0.096	0.416	-1.102	-0.446	-0.096	0.416	0.488	0.492	0.628

In order to establish which parameter listed in table 7.2 is the best predictive tool they are compared to the three Hurst exponents calculated for each financial instrument. The three Hurst exponents are plotted in Fig 6.15.

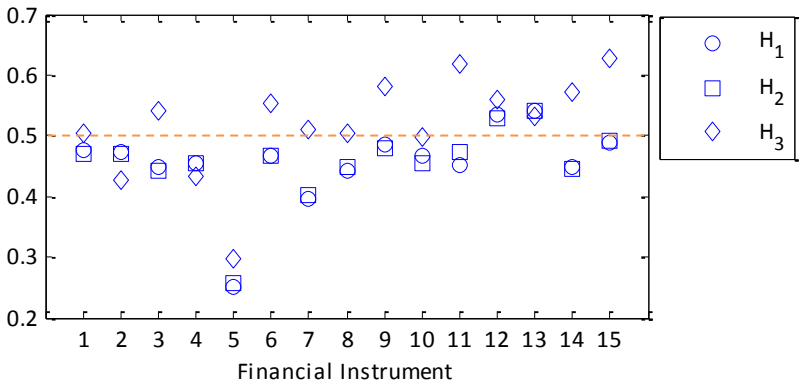

Fig 6.15 Hurst exponents calculated using three different methods for each financial time series .

The first method of estimating the Hurst exponent, H_1, is based on the discrete second-order derivative [137]. The second method estimates H_2 using a wavelet-based adaptation [145]. The third method, estimates H_3 using the slope of the log-log plot of the detail variance versus the level [146]. Fig 6.15 shows that H_1 and H_2 behave similar while H_3, which is less accurate, consistently gives higher values. The striking feature however is that the only developing market analysed, represented by the US dollar/ South African Rand (US$/ZAR), has extreme anti-persistent behaviour, *i.e*. future values will have a tendency to return to a longer term mean value. Mature markets of the developed countries often have Hurst exponents closer to 0.5 than emerging markets indicating that they are more efficient and less predictable [47,149-152]. However, recent studies have ranked the South African exchange rate with that of the more developed markets [149,153-155]. H_1 and H_2 show that COMPQ and FTSE-100 are the only two instruments having persistent behaviour. This would make them the most predictable of the time series. The other instruments exhibit mostly anti-persistent behaviour with Nokia and Brent oil the most random time series.

In order to compare these Hurst exponents with the estimated parameters in table 6.2, the parameters are rescaled with a suitable constant so that they approximate the Hurst exponents, particularly, H_1 and H_2. A suitable rescaling constant can be found by using the two-sample Kolmogorov-Smirnov test discussed in chapter 4. It was found that c_1 offers the best approximation. The results are shown in Fig 6.16. Thus the drift coefficient is the main factor in determining the predictability of the studied time series. Using c_1 as the new prediction tool it is interesting to note that contrary to the Hurst exponents US$/ZAR is ranked alongside the developed markets. This follows increasing evidence that emerging markets are becoming more efficient [149]. This is particularly true for South Africa which has a highly developed banking and financial sector comparable to most developed nations [149,153-155]. Along with the FTSE-100 these two markets are distinctly different to the Hurst exponents possibly suggesting this new method of estimating may be capturing additional information lost by the Hurst exponent methods. The c_1 parameter suggests no differences between types of markets or instruments. However, Brent oil, the only commodity analysed does show a significant difference in predictive behaviour from the other instruments. It exhibits persistent behaviour. The financial stock Google shows relatively strong anti-persistent behaviour.

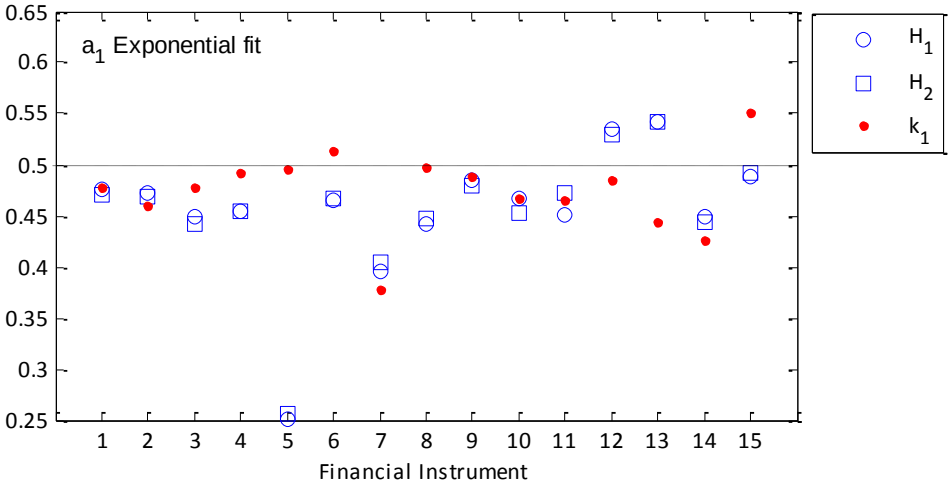

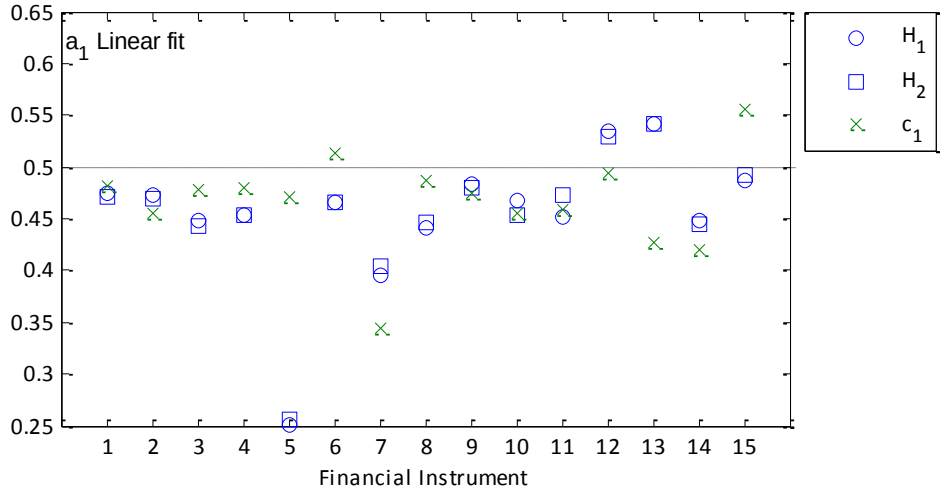

Fig 6.16 The estimated parameters in table 6.2 are rescaled with a suitable constant so that they approximate the Hurst exponents, particularly, H_1 and H_2. It was found that c_1 offers the best approximation.

It was demonstrated in [137] that the financial markets do not have the same predictability, as expressed by their Hurst exponents, for all periods. Thus c_1 is now estimated for increasing t_1 and t_0, as described in table 7.3. The results are plotted in Fig 6.17.

Table 7.3

α: $t_1 = 3d$ and $t_0 = 6d$ to $60d$
β: $t_1 = 4d$ and $t_0 = 8d$ to $80d$
γ: $t_1 = 5d$ and $t_0 = 10d$ to $100d$
δ: $t_1 = 6d$ and $t_0 = 12d$ to $120d$

Interestingly the length of the cascade which can be specified in terms of the ratio of the largest to smallest scales is a ratio that is related to the Reynolds number defined in chapter 4.

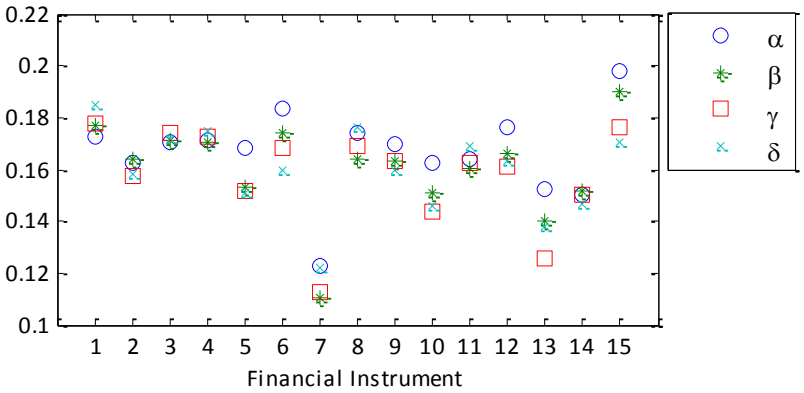

Fig 6.17 Plot of c_1 for four time scales defined in Table 6.3

Here, a difference between the types of instrument (foreign exchange, stock index, or commodity) can be observed. The values of c_1 for foreign exchange time series seem static with the exception of α for US$/ZAR. Stocks show c_1 to be slightly larger for α while even larger for indices with the exception of FTSE-100. Brent oil, the only commodity, has the greatest difference in c_1 values for the different time scales.

6.5. Summary and Conclusions

The aim of this chapter was to characterise the fifteen selected financial instruments in terms of predictability. Predictability was defined as the change in price, having either persistent behaviour or anti-persistent behaviour. Zero predictability is when the change in price represents a random walk.

Following similar methods used in the study of wind turbulence and electromyography, several assumptions had to be tested. Firstly, whether price increments are correlated across nested time scales. This was tested by plotting contour plots of the joint and conditional probability densities for various time scales. The contour lines were aligned at a 45 degree angle to the axis of the plots for both the joint and conditional functions indicating a stochastic dependence of price increments between the time scales tested. The second assumption that was tested was whether the stochastic process concluded in the first assumption could be reduced to a binary-scale transition function. This was done using two methods. The first method used the Chapman-Kolmogorov equation and the second by prior parameterisation of the conditional moments through the mean of one of the distributions of a triple scale conditional probability distribution function. The Chapman-Kolmogorov equation gave consistently positive results, while the conditional probability distribution function test failed for the same large time scales. The third assumption tested was whether any even Kramers-Moyal coefficient greater than the second order equals zero. The $\lim_{\Delta\tau\to 0} 1/\Delta\tau\, M_4(v(t),\tau) = 0$, was found in the interval for which the Chapman-Kolmogorov equation was satisfied and for all fifteen time series tested.

The first and second Kramers-Moyal coefficients were calculated directly from the time series data. The firsts moment M_1 were found to be a linear function of $v(t_0)$ while the second moments M_2 were found to be a quadratic function of $v(t_0)$. The price increments, $v(t_0) = -0.2\sigma$ to 0.2σ, satisfy equation (6.3), allowing the stochastic process to be reduced to a binary-scale transition function, Pawula's theorem and the Chapman-Kolmogorov equation.

The negative drift coefficient was interpreted, using the reciprocal nature of τ, as having an upward pressure on the price increments and driving the market towards larger fluctuations of positive changes in price, *i.e*. shifting the mean of the distribution towards greater changes in prices. The diffusion term spreads the fluctuations around the mean change in price.

To construct the prediction tool the parameters of the fitted functions of the drift and diffusion coefficients were studied for various time scales. It was found that a parameter of the drift coefficient, c_1, was the most stable across time scales and the best at approximating the Hurst exponents. The Hurst exponents ranked the only developing market analysed, represented by the US dollar/South African Rand (US$/ZAR), as having extreme anti-persistent behaviour. However, the prediction tool ranked this market with the other mature markets of the developed countries. Along with the FTSE-100 these two instruments were found to be distinctly different to the Hurst exponents, possibly suggesting the method using the Kramers-Moyal coefficients, may be adding additional information not captured by the Hurst exponent methods. To examine possible differences in the predictive characteristics of c_1, different time periods was studied. The results indicated different predictive behaviour of the price increments for foreign exchange, indeces, stock markets and commodities. The values of c_1 for foreign exchange seemed static across different periods, with the exception of US$/ZAR. Stocks showed c_1 to be slightly larger for α and even larger for indices with the exception of FTSE-100. Brent oil, the only commodity, has the greatest difference in c_1 values for the different time scales. This length in the different periods is analogous to the Reynolds number defined in chapter 4. It can be concluded that the slope of the drift coefficient is best at describing the predictive behaviour of price changes. It also reveals that similar to the Hurst exponents, exchange rates are the least predictable, but unlike the Hurst exponents, the prices of Brent oil is the best to predict and over any relative length of period.

CHAPTER 7
CONCLUSION

In this present work it was shown that the construction of a Fokker-Planck equation describing the stochastic dependency of a certain scale-dependent measure across nested scales makes no assumptions about the nature of the distribution function, the transport processes, or the specific form of the transport equation and can be applied to any fluctuating system: physical, biological and even non-physical. There are however several specific assumptions that need to be tested before the Fokker-Planck coefficients can be estimated. Firstly it had to be shown that the scale-dependent measure is a stochastic process across nested scales. Secondly, it had to be demonstrated that a binary-scale transition function describing this stochastic dependency is sufficient, and thirdly, that Pawula's theorem applies. Once these assumptions had been proven a Fokker-Planck equation could be constructed via a Kramers-Moyal expansion. In this work, a probabilistic method of analysing time series data, characterised by a degree of stochasticity, was applied to the study of three different systems: wind turbulence, a physical system; electromyography, a biological system and the financial markets, a non-physical system. The study of applying probabilistic methods to these three different systems reveals several new useful applications and theoretical outcomes.

Firstly, common to all three systems studied, and that by other authors, is the characteristic negative linear function of the estimated drift coefficient and the parabolic, single minimum form of the diffusion coefficient. In this work, the drift and diffusion coefficients are mapped onto reciprocal time or length scales. The interpretation of the drift and diffusion coefficients in such a situation is not straightforward, because of the need for two conceptual leaps required to map the coefficients, for example, from reciprocal time scales to normal time. Firstly, and probably most importantly, the transition from nested time scales to a progressive time, from past to future, needs to be taken into account. To do this, one has to consider the limiting behaviour over the longest time interval. The second conceptual difficulty is that the use of a reciprocal time interval reverses the sense of the transport coefficients, so that a distribution with high diffusion coefficient spreads less than one with a low diffusion coefficient, and the direction of drift is reversed. For example, in the case of wind turbulence it was found that a negative value of the drift term causes the mean of the distribution to shift towards a greater number of larger wind velocity fluctuations rather than acting as a restoring force to the equilibrium situation. However, with the use of a reciprocal time interval, it should be noted that the distribution function can present no information extrapolated to future times. The

analysis presented here is not explicitly predictive. However, the transport coefficients over the reference time interval can be accurately determined, and these can be used to analyse the underlying behaviour of the distribution. It is however left to the qualified observer, to interpret this behaviour and make qualitative predictions of future trends.

A second theoretical outcome of this work has shown that for certain types of stochastic systems a binary transition function is sufficient for the Kramers-Moyal expansion. It should be noted from recent discussions in the literature, that although a Markov process leads to a Fokker-Planck equation, a Fokker-Planck equation does not necessarily imply the existence of a Markov process [26, 78-80,156]. An example of such an instance was found in the study of electromyography, (in chapter 5), where the binary-scale transition function described a subclass of the stochastic process which was clearly non-Markov and did not satisfy the Chapman-Kolmogorov equation. Yet the Kramers-Moyal expansion yielded moments which fitted the linear regression line for both the Markov and non-Markov interval of fluctuations, as shown in Fig 5.6. Furthermore, it was shown for wind turbulence and the financial markets that for increasing Reynolds numbers the Chapman-Kolmogorov equation consistently produced positive results while a parametised triple-scale transition function test for the Markov property, yielded negative results for the same scales.

In chapter 4, a new idea was introduced to use a Fokker-Planck equation containing Boltzmann collision terms in the drift and diffusion coefficients to describe the stochastic dependency of velocity increments of two independent turbulent flows interacting with one another. The application of this method required the Boltzmann molecular chaos assumption and that the two velocity components remain coupled for very brief moments after the collision [14]. In addition to the above assumptions, it was necessary to assume that a Boltzmann approach to the theory of Brownian motion is, (at least on physical grounds), equivalent to using the Langevin and Fokker-Planck equations. It was found that the cross-stream velocity component acts as though it injects energy into the streamwise velocity component leading to greater turbulence. This type of Fokker-Planck equation allowed for the further quantification of the deterministic and random influences due to internal and external fluctuations.

In the study of electromyography, (chapter 5), it was found that for specific time scales the fitted drift coefficient showed asymmetrical behaviour for the three medical conditions studied while the diffusion coefficient did not produce clear distinct behaviour. EMG data exhibit similar behaviour to that found in [47] with reversals of the direction of the drift coefficients for larger differences in time

scales. This suggests an interesting study to further investigate the probability distributions of these three medical conditions. These tests, combined with clinical findings, could aid the clinician for a confident diagnosis of the three medical conditions discussed.

To construct the prediction tool for the financial markets the parameters of the fitted functions of the drift and diffusion coefficients were studied for various time scales. It was found that a parameter of the drift coefficient, c_1, was the most stable across time scales and the best at approximating the Hurst exponents. Unlike analysis based on Hurst exponents this work ranked the only developing market analysed, represented by the US dollar/South African Rand (US$/ZAR), with the other mature markets of the industrialised countries. The method using the Kramers-Moyal coefficients may therefore be including additional information not captured by the Hurst exponent methods. A possible reason [149] is that South Africa borrows in its domestic currency, Rands, unlike most of the developing countries. Furthermore, South Africa has a dual economy [150] matching other industrialised countries with a productive and industrialized economy that exhibits many characteristics associated with the developed countries.

The results of the predictive tool indicated different predictive behaviour of the price increments for foreign exchange, indeces, stock markets and commodities for increasing differences in the time scales. This length in the different time scales is analogous to the Reynolds number defined in chapter 4. It can be concluded that the slope of the drift coefficient is best at describing the predictive behaviour of price changes.

REFERENCES

[1] Kolmorogov, A.N., 1941, Dokl. Akad.Nauk, SSSR 30, 301.

[2] Kolmorogov, A.N., 1941, Dokl. Akad., SSSR 32, 16.

[3] Aoki, M., 2004, *Modeling Aggregate Behavior and Fluctuations in Economics: Stochastic Views of Interacting Agents*, Cambridge University Press, Cape Town.

[4] Bolker, B., 2008, *Ecological Models and Data in R*, Princeton University Press.

[5] McCandless, G., 2008, *The ABCs of RBCs: An Introduction to Dynamic Macroeconomic Models*, Harvard University Press.

[6] Ripley, B.D., 2006, *Stochastic Simulation*, Wiley-Interscience.

[7] MacKeown, P., 1997, *Stochastic Simulation in Physics*, Springer, Singapore.

[8] Grassmann, W., 1981, *Stochastic Systems for Management*, Arnold, London.

[9] Kottegoda, N., 1980, *Stochastic Water Resources Technology*, Macmillan, London.

[10] Taylor, S., 2007, *Asset Price Dynamics, Volatility, and Prediction*, Princeton University Press.

[11] Svetlozar, T., 2004, *Handbook of Computational and Numerical Methods in Finance*, Birkhäuser, Boston.

[12] Larson, H., 1979, *Probabilistic Models in Engineering Sciences*, Wiley, New York.

[13] Keilson, J., 1965, *Green's Function Methods in Probability Theory*, Charles Griffin, London.

[14] Kampen, N.G., 1992, *Stochastic Processes in Physics and Chemistry*, Elsevier, Amsterdam.

[15]Kampen, N.G., 1989, *Probabilistic Methods in Physics, Disordered Solids: Structures and Processes*, Di Bartolo, New York.

[16] Horsthemke, W. & Lefever, R., 1984, *Noise-Induced Transitions*, Springer, Berlin.

[17] Ma, S.K., 1976, *Modern Theory of Critical Phenomena*, Benjamin, New York.

[18] Nicholis, G. & Prigogine, I., 1977, *Self-Organisations in Nonequilibrium Systems: from Dissipative Structures to Order through Fluctuations*, Wiley, New York.

[19] Stanley, H.E., 1971, *Introduction to Phase Transitions and Critical Phenomena*, Oxford University Press, New York.

[20] Gardiner, C.W., 1985, *Handbook of Stochastic Methods*, 2nd edition, Springer.

[21] Gillespie, D.T., 1992, *Markov Processes an Introduction for Physical Scientist*, Academic press, Boston.

[22] Pardoux, E., 2008, *Markov Processes and Applications: Algorithms, Networks, Genome and Finance*, Wiley, Chichester.

[23] Ibe, O.C., 2009, *Markov Processes for Stochastic Modelling*, Academic Press, Boston.

[24] Rosenblatt, M., 1971, *Markov Processes: Structure and Asymptotic Behaviour*, Springer, Berlin.

[25] Dynkin, E.B., 1965, *Markov Processes*, Academic Press, New York.

[26] Risken, H., 1989, *The Fokker-Planck Equation*, 2nd edition, Springer.

[27] Frank, T.D., 2005, *Nonlinear Fokker-Planck equations: Fundamentals and Applications*, Springer.

[28] Soize, C., 1994, *The Fokker-Planck Equation for Stochastic Dynamical Systems and its Explicit Steady State Solutions*, World Scientific.

[29] McCauley, J.L., 2004, *Dynamics of markets: econophysics and finance*, Cambridge University Press.

[30] Schulz, M., 2003, *Statistical physics and economics: concepts, tools, and applications*, Springer.

[31] Lord Rayleigh, 1891, Phil. Mag. 32, Scientific Papers III, 424.

[32] Lord Rayleigh, 1902, Phil. Mag. 32, Scientific Papers III, 473.

[33] Einstein, A., 1905, Annalen der Physik, 17, 549-560.

[34] Einstein, A., 1906, Annalen der Physik, 19, 371.

[35] Smoluchowski von, M., 1906, Annalen der Physik, 21, 756.

[36] Smoluchowski von, M., 1916, PhysikZeits, 17, 557.

[37] Fokker, A.D., 1913, Thesis, Leiden.

[38] Fokker, A.D., 1914, Annalen der Physik , 43, 810.

[39] Planck, M., Sitzungsber, Preuss. Akad.Wissens, 324, 1917 - PhysikalischeAbhandlungen undVortra¨ge II (Vieweg, Braunschweig 1958) 435

[40] Kolmogorov, A., 1931, Mathem. Annalen, 104, 415.

[41] Friedrich, R. & Peinke, J., 1997, Physica D 102, 147.

[42] Renner, C., Peinke, J., & Friedrich, R., 2001, J. Fluid Mech, 433, 383 – 409.

[43]Peinke, J., & Friedrich, R., 1997, Phys. Rev. Lett. 78, 863.

[44] Naert, A, Friedrich, R, & Peinke, J., 1997, Phys. Rev. E 56, 6719 – 6722.

[45] Hosokawa, I., 2002, Physical Review E 65, 027301.

[46] Tutkun, M. & Mydlarski, L., 2004, New Journal of Physics 6, 49.

[47] Tang, L.H., & Huang, Z.F., 2000, Physica A 2288, 444-450.

[48] Shiller, R., 1989, *Market Volatility*, MIT Press, Boston.

[49] Arneodo, A., Muzy, J., & Sornette, D., 1998, Eur. Phy. J. B 2, 277 – 282.

[50] Sornette, D., 2001, Physica A 290, 211-217.

[51] Frank, T.D., 2007, Physics Lett. A 360, 552-562.

[52] Smirnov, A.P., Shmelev, A.B. & Sheinin, E.Y., 2004, Physica A 344, 203-206.

[53] Renner, C., Peinke, J., & Friedrich, R., 2000, Phys. Rev. Lett. 84, 5224.

[54] Lim, G., Kim, S., Scalas, E., Kim, k. & Chang, K., 2008, Physica A, 387 2823-2830.

[55] Ivanova, K. & Ausloos, M., 2003, Phys Rev E 68, 046122.

[56] Cortines, A.A.G., Riera, R. & Anteneodo, C., 2007, Eur. Phys. J. B 60, 385-389.

[57] Cortines, A.A.G., Riera, R. & Anteneodo, C., 2008, Eur. Phys. J. B 65, 289-294.

[58] Renner, C., Peinke, J., & Friedrich, R., 2001, Physica A 298, 499 – 520.

[59] Ghasemi, F., *et al*, 2007, Physical Review E 75, 060102-1.

[60] Ghasemi, F., Peinke, J., Sahimi, M. & Tabar, M.R., 2005, Eur. Phys. J. B 47, 411-415.

[61] Ghasemi, F., Peinke, J., Sahimi, M. & Tabar, M.R., 2006, Int. J. Modern Physics C 14 4, 571-580.

[62] Petelczyc, M. & Zebrowski, J.J., 2009, Acta Physica Polonica B, 40 5.

[63] Ghasemi, F., Peinke, J., Sahimi, M, & Tabar, M.R., 2006, J. Biological Physics 32, 117-128.

[64] Petelczyc, M., Zebrowski, J. J., Baranowski, R., 2009, Physical Review E 80 3, 031127.

[65] Buchner, T., Petelczyc, M., Zebrowski, J., *et al.*, 2009, CHAOS 19 2, 028504.

[66] Pawula, R.F., 1967, Phys. Rev. 162 1, 186-188.

[67] Pawula, R.F., 1967, IEEE Trans. Inform. Theory 13, 33.

[68] Montgomery, D., 1971, The Physics of Fluids 14 10, 2088-2090.

[69] Helbing, D., 1993, Physica A 196, 241-258.

[70] Helbing, D., 1992, Behavioral Science 37, 190-214.

[71] Helbing, D., 1992, Physica A 181, 29-52.

[72] Helbing, D., 1995, *Quantitative Socio dynamics – Stochastic Methods and Models of Social Interacting Process*, Kluwer academic Publishers.

[73] Kramers, H.A., 1940, Physica 7, 284.

[74] Moyal, J.E., 1949, J.R. Stat. Soc. 11, 151-210.

[75] Ivanova, K. & Ackerman T.P., 2007, Journal of Atmospheric and Solar-Terrestrial Physics 69, 2265-2278.

[76] Snell, J.L., 1997, Statistical Science Vol. 12, No. 4.

[77] Feller, W., 1959, Annals of Mathematical Statistics 30, 1252-1253.

[78] Frank, T.D., 2004, Physica A 331, 391 – 408.

[79] Frank, T.D., 2007, Physica A 38, 453 – 464.

[80] Frank, T.D., 2003, Physica A 320, 204 – 210.

[81] Cercignani, C., Illner, R., & Pulvirenti, M., 1994, *The Mathematical Theory of Dilute Gases*, Springer-Verlag, New York.

[82] Cercignani, C., 1987, *The Boltzmann Equation and its Applications*, Springer-Verlag, New York.

[83] Kang, H.S., Chester, S. & Meneveau, C., 2003, J. Fluid Mech. vol. 480, 129–160.

[84] Ibe, O.C., 2009, *Markov Processes for Stochastic Modelling*, Elsevier.

[85] Stratonovich, R.L., 1963, *Topics in the Theory of Random Noise*, Gordon and Breach, New York.

[86] Ehrenfest, P. & Ehrenfest, T., 2002, *The Conceptual Foundations of the Statistical Approach in Mechanics*, Dover Publications.

[87] Amaro de Matos, J. & Fernandes, M., 2007, Journal of Econometrics 141, 44-64.

[88] Cohen, E.G.D., 1962, *In Fundamental Problems in Statistical Mechanics*, North-Holland, Amsterdam.

[89] Nordsieck, A., Lamb, W.E.& Uhlenbeck, G.E., 1940,Physica 7, 344.

[90] Kuusel, T., 2004, Phys. Rev E69, 031916.

[91] Tabar, M.R., Ghasemi, F., & Friedrich, R., 2006, Comp. Science Engin., 8, 2.

[92] The data may be downloaded at the JHU Turbulence Database Cluster from http://turbulence.pha.jhu.edu. Last viewed on 30th September 2010. It can also be found on the DVD-ROM in folder \Data\Chapter 4.

[93] Pope, S.B., 2000, *Turbulent Flows*, Cambridge University Press.

[94] Miake-Lye & Papantoniou, 1983, Phys. Flds. 26 11, 3185 – 3192.

[95] Castaing, B., Gagne, Y. & Hopfinger, E.J., 1990, Physica D 46, 177.

[96] Atm S 547 Boundary Layer Meteorology Brtherton

[97] Marcq, P. & Naert, A., 1998, Physica D 124, 368 – 381.

[98] Waechter, M., Kouzmitchev, A. & Peinke, J., 2004, Physical Review E 70, 055103.

[99] Mantegna, R. & Stanley, H., 2001, *An Introduction to Econophysics–Correlations and Complexity in Finance*, Cambridge University Press.

[100] Avila, R. & RodrÌguez-Meza, M.A., 2004, REVISTA MEXICANA DE FíSICA 50 (2), 156–161.

[101] Sitte, R. & Sitte, J., 2002, Applied Intelligence 16, 163–171.

[102] Bardet, J.M., Lang, G., Oppenheim, G., Philippe, A., Stoev, S. & Taqqu, M.S., 2003,'*Semi-Parametric Estimation of the Long-Range Dependence Parameter: a Survey*', Theory and Applications of Long-Range Dependence, Birkhäuser, 557-577.

[103] Newland, D.E., 2005, *An Introduction to Random Vibrations, Spectral &Wavelet Analysis*, Dover Publications, New York.

[104] Yakhot, V., 1998, Phys. Rev. E 57, 1737.

[105] Waechter, M., Kouzmitchev, A. & Peinke, J., 2004, Physical Review E 70, 055103.

[106] Comte-Bellot, G., & Corrsin, S., 1966, J. Fluid Mech 25, 657–682.

[107] Comte-Bellot, G. & Corrsin, S., 1971, J. Fluid Mech48, 273–337.

[108] Masey F., 1951, Journal of the American Statistical Association, vol 46, 253, 68-78.

[109] Huang, G.Y., Chen, Y., Zhang, Y. & Wang, Y.H., 2007, Chinese Phys 16, 975 -983.

[110] Mizuno, T., Takayasu, H. & Takayasu, M., 2007, Physica A 382, 187 – 192.

[111] Torquato, S., 2002, *Random Heterogenous Materials*, Springer, New York.

[112] Sahimi, M., 2003, *Heterogenous Materials*, vol 2, Springer, New York.

[113] Peng, C.K., Mietus, J., Hausdor, J.M., Havlin, S., Stanley, H.E. & Goldberger, L.A., 1993, Phys.

Rev. Lett. 70, 1343.

[114] Bunde, A., Havlin, S., Kantelhardt, J.W., Penzel, T., Peter, J.H. & Voigt, K., 2000, Phys. Rev. Lett. 85, 3736.

[115] Bernaola-Galvan, P., Ivanov, P.C., Amaral, L.N. & Stanley, H.E., 2001, Phys. Rev. Lett. 87, 168105.

[116] Schulte-Frohlinde, V., Ashkenanzy, Y., Ivanov, P.C., Glass, L., Goldberger, A.L, & Stanley, H.E., 2001, Phys.Rev. Lett.87, 068104.

[117] Ashkennanzy, Y., Ivanov, P.C., Havlin, S., Peng, C.K., Goldberger, A.L. & Stanley, H.E., 2001, Phys. Rev. Lett.86, 1900.

[118] Kimura, J., 1983*, Electrodiagnosis in Diseases of Nerve and Muscle: Principles and Practice*, FA Davis, Philadelphia.

[119] Nelson, R.M. & Currier, D.P., 1987, *Clinical Electrotherapy*, Appleton & Lange, Los Altos.

[120] The data may be obtained from the PhysioBank Archive Index at http://www.physionet.org/physiobank/database/. It can also be found on the DVD-ROM in folder \Data\Chapter 5\

[121] Dickey, D. A., & Fuller W., 1979, Journal of the American Statistical Association. Vol. 74, 427–431.

[122] Dickey, D. A., & Fuller, W., 1981, Econometrica, Vol. 49, pp. 1057–1072.

[123] Kirchner, J., Meyer, W., Elsholz, M. & Hensel, B., 2007, Phys. Rev. E76, 021110.

[124] Ghashghaie, S., Breymann, W., Peinke, J., Talkner, P. & Dodge Y., 1996, Nature 381, 767 – 770.

[125] Corker, L.A., 2006, Drift-Diffusion of a vacancy in inhomogeneous media and its material constants. A Fokker-Planck equation approach with an application to foreign exchange data. (MSc-thesis)

[126] Anderson, T., 1985, Economics Letters Vol 18, Issues 2-3, 121-124.

[127] Singh, A. & Weisse, b., 1998, World Development Vol. 26, No. 4, 607-622.

[128] Khan, M. & Zahler, R., 1985, *Trade and Financial Liberalization Given External Shocks and Inconsistent Domestic Policies*, IMF Staff Papers, v. 32, n. 1.

[129] Lim, L., 1999, Journal of Asian Business, Vol.15, No.1, 79-81.

[130] Wu, Y., 2001, Journal of Asian Economics, 12, 445-458.

[131] Coronel-Brizio, H.F., Hernandez-Montoya, A.R., Heurta-Quintanilla, R. & Rodríguez-Achach, M., 2007, Physica A 380, 391.

[132] Ferreira, N.B., Menezes, R. & Mendes, D.A., 2007, Physica A 382, 73.

[133] Park, J.H., Nam, S.K.& Eom, K.S., 2007, Asia-Pacific Journal of Financial Studies 36, 533.

[134] Edwards, S. & Samuel, R., 2003, Review of Economics and Statistics 85, 328.

[135] Di Matteo, T., Aste, T. & Dacorogna, M.M., 2003, Physica A 324, 183.

[136] Di Matteo, T., Aste, T. & Dacorogna, M.M., 2005, J. Banking and Finance 29, 827.

[137] Cajueiro, D.O., & Tabak, B.M., 2004, Physica A 336, 521.

[138] Zunino, L., Tabak, B.M., Pérez D.G., Garavaglia, M. & Rosso, O.A., 2007, Eur. Phy. J. B 60, 111.

[139] May, C.T., 1999, *Nonlinear Pricing: Theory & Applications*, Wiley, New York.

[140] Corazza, M. & Malliaris, A.G., 2002, Multinational Finance Journal 6(2), 65-98.

[141] Grech, D. & Mazur, Z., 2004, Physica A 336, 133-145.

[142] Davidson, R. & Mackinnon J., 2004, *Econometric theory and methods*, Oxford University Press, New York.

[143] Kleiber, C. & Zeileis, A., 2008, *Applied Econometrics,* Springer, New York.

[144] Karth M, Peinke J, von Ossietzky C, 2002, Complexity, Volume 8, Issue 2, 34-42.

[145] Istas, J. & Lang, G., 1994, Ann. Inst. Poincaré, 33, 407-436.

[146] Flandrin, P., 1992, IEEE Trans. on Inf. Th. 38, 910-917.

[147] The data may be obtained from Dukascopy at http://www.dukascopy.com/freeApplets/exp/ It can also be found on the DVD-ROM in folder \Data\Chapter 6\

[148] Ivanova K., Ausloos, 2003, Phys. Rev. E 68, 4, 046122.

[149] Frankel, J., 2007, South African Journal of Economics, Economic Society of South Africa, vol. 75(3), 425-441, 09.

[150] Wickham, P., 2002, IMF Working Paper No. 02/82

[151] Lawrence, E., Hinkle, P., Montiel, J. & Montiel, P., 1999, *Exchange rate misalignment: concepts and measurement for developing countries*, Oxford University Press.

[152] Hausmann, R., Panizza, U. & Rigobon, R., 2006, Journal of International Money and Finance, v25, 93-124.

[153] Aron, J, Elbadawi, I. & Kahn, B, 2000, *Real and Monetary Determinants of the Real Exchange Rate in South Africa*, in Development Issues in South Africa, edited by Elbadawi, I. & Hartzenberg, T., MacMillan, London.

[154] MacDonald, Ronald, and Luca Ricci, 2004, IMF Working Paper /03/44. South African Journal of Economics, 2004 vol.72:2; p.282.

[155] Bank for International Settlements -- 67th Annual Report, V. *Exchange rates and capital flows in industrial countries*

[156] McCauley, J.L., 2007, Physica A 382, 445 – 452.

APPENDIX A – DETAILS OF DATA USED IN THESIS

CHAPTER 4

The data may be obtained from the JHU turbulence database cluster at http://turbulence.pha.jhu.edu. It can also be found on the DVD-ROM in folder \Data\Chapter 4\ m20h1-01.dat

Description of the data

```
c  Reads one of the active grid data files.
c  Measurements were performed at a sampling rate of 40kHz
c  nxm: measurement location, 20,30,40,50
c  nh: filter scale, nh=1 for 5mm, nh=2 for 10mm,
c      nh=3 for 20mm, nh=4 for 40mm
c  nfile: file number from 1 to 30
c  ndim=1: streamwise velocity
c  ndim=2: cross-stream velocity
c  nprobe=1: probe #1
c  nprobe=2: probe #2
c  nprobe=3: probe #3
c  nprobe=4: probe #4
c  ndata: time series from 1 to 1200000
c  realu: velocity data [m/s]
c  First four columns: streamwise velocities from probe #1 to probe #4
c  Next four columns: cross-stream velocities from probe #1 to probe #4
c  After reading, to save space we recommend you store the data into
c  binary format of your choosing.

      implicit none
      integer, parameter :: ndim=2,nprobe=4,ndata=1200000
      integer, parameter :: nxm=20,nh=1,nfile=1
      real,    dimension(ndim,nprobe,ndata) :: realu
      integer, dimension(0:9) :: NASCII
      character(len=2)  :: dir
      character(len=15) :: fname
      character(len=1)  :: c1,c2,c3,c4,c5
      integer :: k,k1,k2,k4,k5

      NASCII(0)=ICHAR('0')
      NASCII(1)=ICHAR('1')
```

CHAPTER 5

The data may be obtained from the *PhysioBank* Archive Index *at* http://www.physionet.org/physiobank/database/ . It can also be found on the DVD-ROM in folder \Data\Chapter 5\

Description of the data
Healthy person
emg_healthy 1 4000 50860
emg_healthy.dat 16 10000/mV 16 0 -333 -29438 0 EMG
<age>: 44 <sex>: M <diagnoses> no history of neuromuscular disease
EMG from 25mm concentric needle electrode placed in tibialis anterior muscle
patient dorsiflexed the foot gently against resistance, then relaxed

Myopathy
emg_myopathy 1 4000 110337
emg_myopathy.dat 16 10000/mv 16 0 -50 -6380 0 EMG
<age>: 57 <sex>: M
<diagnoses>: myopathy due to long history of polymostis
<medications>: steroids, low-dose methotrexate
EMG from 25mm concentric needle electrode placed in tibialis anterior muscle
patient dorsiflexed the foot gently against resistance, then relaxed

Neuropathy
emg_neuropathy 1 4000 147858
emg_neuropathy.dat 16 10000/mV 16 0 900 16686 0 EMG
<age>: 62 <sex>: M
<diagnoses>: chronic low back pain and neuropathy due to a
right L5 radiculopathy
EMG from 25mm concentric needle electrode placed in tibialis anterior muscle
patient dorsiflexed the foot gently against resistance, then relaxed

CHAPTER 6

The data may be obtained from Dukascopy at http://www.dukascopy.com/freeApplets/exp/. It can also be found on the DVD-ROM in folder \Data\Chapter 6\

#	Instrument	Type	Sample size
1	£/US$	Foreign Exchange	195848
2	€/US$	Foreign Exchange	195848
3	¥/US$	Foreign Exchange	191255
4	US$/CHF	Foreign Exchange	141310
5	US$/ZAR	Foreign Exchange	141415
6	Allianz AG	Stock	60090
7	Google	Stock	37522
8	BP	Stock	46696
9	Nokia	Stock	32475
10	Walmart	Stock	38040
11	Freddie Mac	Stock	11875
12	COMPQ	Stock Index	32755
13	FTSE-100	Stock Index	39951
14	DAX	Stock Index	42714
15	Brent	Commodity	117452

The programs listed below may be found on the DVD ROM.

#	Matlab Program Name	Description
B1	Kramers_Moyal_Turb.m	Calculates the moments of the first four Kramers-Moyal coefficients and producers contour plots of the joint and conditional probability density functions. $P(v(r_1); v(r_0))$ and $P(v(r_1)\|v(r_0)) = \frac{P(v(r_1);v(r_0))}{P(v(r_0))}$
B2	Markov_Turb.m	Test the Markov property. Plots a contour plot of $P(v(r_2)\|v(r_1)) = P(v(r_2)\|v(r_1); v(r_0) = 0)$. Cross-sections can be plotted from the output.
B3	Chapman_kolgrov_Turb.m	Test Chapman-Kolmogorov equation. Cross-sections can be plotted from the output.
B4	Mol_Chaos_Turb.m	Test the molecular chaos assumption. Producers a contour plot of $P(u_\alpha(x); u_\beta(x)) = P(u_\alpha(x))P(u_\beta(x))$
B5	Random_JPDF.m	This program demonstrates the independence between two time series by considering contour plots of the joint and conditional probability functions. The data is randomly generated.
B6	FPE_Sol.m	Solves the Fokker-Planck equation.

B1

```
% Kramers_Moyal_Turb.m
%
% Finds the moments of the first four Kramers-Moyal coefficients for wind
% turbulence dataset,'m20h1-01.dat'. Plots the joint and conditional
% probability as contour plots.
%
% Matlab 7.4.0 (R2007a)
%
%
% Lloyd A Corker
% University of Cape Town
% Department of Physics
% PhD Thesis
% lcorker@uwc.ac.za
% 2010 February
%
%
%------------------------------------------------------------------------
% Reset memory and clear the screen
clear; clc
%------------------------------------------------------------------------
t=cputime;
% load data
Data(1) = fopen('m20h1-01.dat');
% Read the first column
    Col_1 = textscan(Data(1), '%f %*f %*f %*f %*f %*f %*f %*f');
    % Close the file
    fclose(Data(1));
    % Transform your cell array into an ordinary matrix
M20h1 = Col_1{1};
```

```
% First four columns: streamwise velocities from probe #1 to probe #4
% Next four columns: cross-stream velocities from probe #1 to probe #4
%-------------------------------------------------------------------------
% Choose length scales: Scale1 < Scale0
r1 = 100; %Scale1
r0 = 300; %Scale0
% Choose number of bins for each scale.
numBins_r0 = 100;
numBins_r1 = 100;
% Preallocate memory
binMean_r0 = zeros(1,numBins_r0);
binMean_r1 = zeros(1,numBins_r1);
%-------------------------------------------------------------------------
%Construct length scales by taking velocity increments v_r1 and v_r0
v_r1= M20h1(r1 + 1:end) - M20h1(1:end - r1);
v_r0 = M20h1(r0 + 1:end) - M20h1(1:end - r0);
%-------------------------------------------------------------------------
% Ensure the two time series have have equal number of observations.
v_r1(end + r1 - r0 + 1:end) = [];
%-------------------------------------------------------------------------
% bin the time series into the number of bins
%Bins for Scale1
lowLimit_r1 = min(v_r1);
upLimit_r1 = max(v_r1)+ 1;
binLimits_r1 = linspace(lowLimit_r1, upLimit_r1, numBins_r1 +1);
[not_needed,whichBin_r1] = histc(v_r1,binLimits_r1);
%Bins for Scale0
lowLimit_r0 = min(v_r0);
upLimit_r0 = max(v_r0)+ 1;
binLimits_r0 = linspace(lowLimit_r0, upLimit_r0, numBins_r0 +1);
[not_needed,whichBin_r0] = histc(v_r0,binLimits_r0);
for i=1:numBins_r0
    r0_flagBinMembers = (whichBin_r0==i);
    binMembers_r0 = v_r0(r0_flagBinMembers);
    binMean_r0(i) = mean(binMembers_r0);
end
for i=1:numBins_r1
   r1_flagBinMembers = (whichBin_r1==i);
    binMembers_r1 = v_r1(r1_flagBinMembers);
    binMean_r1(i) = mean(binMembers_r1);
end
% the below is our binned data we shall use to calculate the K-M moments
v_r1_Binned = binMean_r1(whichBin_r1)';
v_r0_Binned = binMean_r0(whichBin_r0)';
%-------------------------------------------------------------------------
% Evaluate: P(v_r1_Binned|v_r0_Binned), Scale1 < Scale0
Table_r0 = tabulate(v_r0_Binned);
%P(v_r0_Binned)
 Prob_v_r0 = Table_r0(:,3)/100;
  %Joint Probability: P(v_r1_Binned;v_r0_Binned)
 [MassPDF_r1_r0] = crosstab(v_r1_Binned,v_r0_Binned);
 JointPDF_r1_r0 = MassPDF_r1_r0/length(v_r0_Binned);
 %Conditional Probability: P(v_r1_Binned|v_r0_Binned)
 CondPDF_r1_r0 = JointPDF_r1_r0/diag(Prob_v_r0);
%-------------------------------------------------------------------------
% Finds the Kramers-Moyal Moments

            Mx = unique(v_r0_Binned);
            My = unique(v_r1_Binned);
```

```
      % The first Kramers-Moyal coefficient, KM1
        [nrows,ncol]=size(JointPDF_r1_r0);
        Dx = zeros(nrows,ncol);
            for row=1:nrows;
                for col=1:ncol;
                    Dx(row,col)=(My(row)-Mx(col))*CondPDF_r1_r0(row,col);
                end
            end
         KM1 =-(r1/r1-r0)*sum(Dx);

          % The second Kramers-Moyal coefficient, KM2
            for row=1:nrows;
                for col=1:ncol;
                    Dx(row,col)=(My(row)-Mx(col))^2*CondPDF_r1_r0(row,col);
                end
            end
          KM2 =-(1/2)*(r1/r1-r0)*sum(Dx);

        % The fourth Kramers-Moyal coefficient, KM4
            for row=1:nrows;
                for col=1:ncol;
                    Dx(row,col)=(((My(row)-
Mx(col)))^4)*CondPDF_r1_r0(row,col);
                end
            end
          KM4 =-(1/24)*(r0/r1-r0)*sum(Dx);
%-----------------------------------------------------------------------
% Plots the contour plots of the joint and conditional probability
functions
hold on;
% Create contour
[C2,h] =contour(Mx,My,log10(JointPDF_r1_r0));
clabel(C2,h,'LabelSpacing',150,'FontSize',10);
% Create xlabel
xlabel({'\itv(\itr\rm_0)'},'FontSize',12);
% Create ylabel
ylabel({'\itv(\itr\rm_1)'},'FontSize',12);
p1 = figure;
[C2,h] =contour(Mx,My,log10(CondPDF_r1_r0));
 clabel(C2,h,'LabelSpacing',150,'FontSize',10)
% Create xlabel
xlabel({'\itv(\itr\rm_0)'},'FontSize',12);
% Create ylabel
ylabel({'\itv(\itr\rm_1)'},'FontSize',12);
disp(cputime -t);
```

B2

```
% Markov_Turb.m
%
% Test the Markov assumption.
%
% Written using Matlab 7.4.0 (R2007a)
%
%
% Lloyd A Corker
% University of Cape Town
% Department of Physics
% PhD Thesis
% lcorker@uwc.ac.za
% 2010 February
%
%
%-------------------------------------------------------------------------
% Reset memory and clear the screen
clear; clc
%-------------------------------------------------------------------------
% load data
Data(1) = fopen('m20h1-01.dat');
% Read the first column
    Col_1 = textscan(Data(1), '%f %*f %*f %*f %*f %*f %*f %*f');
    % Close the file
    fclose(Data(1));
    % Transform your cell array into an ordinary matrix
M20h1 = Col_1{1};
% First four columns: streamwise velocities from probe #1 to probe #4
% Next four columns: cross-stream velocities from probe #1 to probe #4
%-------------------------------------------------------------------------
%Choose length scales: Scale2 < Scale1 < Scale0
r2 = 50;
r1 = 1000;
r0 = 3000;
%Choose bin width.
numBins_r0 = 100;
numBins_r1 = 100;
%-------------------------------------------------------------------------
%Construct length scales by taking velocity increments v_r2, v_r1 and v_r0
v_r1= M20h1(r1 + 1:end) - M20h1(1:end - r1);
v_r0 = M20h1(r0 + 1:end) - M20h1(1:end - r0);
v_r2 = M20h1(r2 + 1:end) - M20h1(1:end - r2);
%-------------------------------------------------------------------------
% Ensure the three time series have have equal number of observations.
v_r2(end + r2 - r0 + 1:end) = [];
v_r1(end + r1 - r0 + 1:end) = [];
%-------------------------------------------------------------------------
% bin the time series into the number of bins
%Bins for v_r2
lowLimit_r2 = min(v_r2);
upLimit_r2 = max(v_r2) + 1;
binLimits_r2 = linspace(lowLimit_r2, upLimit_r2, numBins_r1 +1);
[not_needed,whichBin_r2] = histc(v_r2,binLimits_r2);
%Bins for v_r1
lowLimit_r1 = min(v_r1);
upLimit_r1 = max(v_r1)+ 1;
binLimits_r1 = linspace(lowLimit_r1, upLimit_r1, numBins_r1 +1);
```

```
[not_needed,whichBin_r1] = histc(v_r1,binLimits_r1);
%Bins for v_r0
lowLimit_r0 = min(v_r0);
upLimit_r0 = max(v_r0)+ 1;
binLimits_r0 = linspace(lowLimit_r0, upLimit_r0, numBins_r0 +1);
[not_needed,whichBin_r0] = histc(v_r0,binLimits_r0);
for i=1:numBins_r0
    r0_flagBinMembers = (whichBin_r0==i);
    binMembers_r0 = v_r0(r0_flagBinMembers);
    binMean_r0(i) = mean(binMembers_r0);
end
for i=1:numBins_r1
    r2_flagBinMembers = (whichBin_r2==i);
    binMembers_r2 = v_r2(r2_flagBinMembers);
    binMean_r2(i) = mean(binMembers_r2);

    r1_flagBinMembers = (whichBin_r1==i);
    binMembers_r1 = v_r1(r1_flagBinMembers);
    binMean_r1(i) = mean(binMembers_r1);
end
v_r2_Binned = binMean_r2(whichBin_r2)';
v_r1_Binned = binMean_r1(whichBin_r1)';
v_r0_Binned = binMean_r0(whichBin_r0)';
%-------------------------------------------------------------------
Tab_vr0 = tabulate(v_r0_Binned);
[maxFreq,MaxPos] = max(Tab_vr0(:,2));
Max_Freq_vr0 = Tab_vr0(MaxPos,1);
v_r0_Pos = find(Max_Freq_vr0<v_r0_Binned &
v_r0_Binned<Max_Freq_vr0+0.0001);
Mv_r1_Binned=v_r1_Binned(v_r0_Pos);
Mv_r2_Binned=v_r2_Binned(v_r0_Pos);
%-------------------------------------------------------------------
% % Evaluate: P(X_Scale1_Binned|X_Scale0_Binned), Scale1 < Scale0
            Markx = unique(Mv_r1_Binned);
            Marky = unique(Mv_r2_Binned);
            Mx = unique(v_r1_Binned);
% [MassPDF_Mr2_Mr1] = crosstab(Mv_r2_Binned,Mv_r1_Binned);
Table_Mr1 = tabulate(Mv_r1_Binned);
%P(X_Scale0_Binned)
 Prob_Mv_r1 = Table_Mr1(:,3)/100;
%Joint Probability: P(X_Scale1_Binned;X_Scale0_Binned)
 [MassPDF_Mr2_Mr1] = crosstab(Mv_r2_Binned,Mv_r1_Binned);
 JointPDF_Mr2_Mr1 = MassPDF_Mr2_Mr1/length(Mv_r1_Binned);
 %Conditional Probability: P(X_Scale1_Binned|X_Scale0_Binned)
CondPDF_Mr2_Mr1 = JointPDF_Mr2_Mr1/diag(Prob_Mv_r1);
Log_JointPDF_Mr2_Mr1 = log10(JointPDF_Mr2_Mr1);
Log_CondPDF_Mr2_Mr1 = log10(CondPDF_Mr2_Mr1);

contour(Markx,Marky,Log_CondPDF_Mr2_Mr1,'LineStyle',':','LineWidth',2);
%-------------------------------------------------------------------
% Evaluate: P(X_Scale1_Binned|X_Scale0_Binned), Scale1 < Scale0
             Mx = unique(v_r1_Binned);
            My = unique(v_r2_Binned);
Table_r1 = tabulate(v_r1_Binned);
 %P(X_Scale0_Binned)
 Prob_v_r1 = Table_r1(:,3)/100;
 %Joint Probability: P(X_Scale1_Binned;X_Scale0_Binned)
 [MassPDF_r2_r1] = crosstab(v_r2_Binned,v_r1_Binned);
  JointPDF_r2_r1 = MassPDF_r2_r1/length(v_r1);
```

```
  %Conditional Probability: P(X_Scale1_Binned|X_Scale0_Binned)
 CondPDF_r2_r1 = JointPDF_r2_r1/diag(Prob_v_r1);
Log_JointPDF_r2_r1 = log10(JointPDF_r2_r1);
Log_CondPDF_r2_r1 = log10(CondPDF_r2_r1);
hold on;
contour(Mx,My,Log_CondPDF_r2_r1);
[dd,gg,ee] = intersect(Marky',My');
```

B3

```
% Chapman_kolgrov_Turb.m
%
% Test the validity of the Chapman-Kolmogorov equation.
%
% Written using Matlab 7.4.0 (R2007a)
%
%
% Lloyd A Corker
% University of Cape Town
% Department of Physics
% PhD Thesis
% lcorker@uwc.ac.za
% 2010 February
%
%
%-----------------------------------------------------------------
% Reset memory and clear the screen
clear; clc
%-----------------------------------------------------------------
% load data
Data(1) = fopen('m20h1-01.dat');
% Read the first column
    Col_1 = textscan(Data(1), '%f %*f %*f %*f %*f %*f %*f %*f');
    % Close the file
    fclose(Data(1));
    % Transform your cell array into an ordinary matrix
M20h1 = Col_1{1};
% First four columns: streamwise velocities from probe #1 to probe #4
% Next four columns: cross-stream velocities from probe #1 to probe #4
%-----------------------------------------------------------------
%Choose length scales: Scale2 < Scale1 < Scale0
r2 = 50;
r1 = 1000;
r0 = 3000;
%Choose bin width.
numBins_r0 = 100;
numBins_r1 = 100;
%-----------------------------------------------------------------
%Construct length scales by taking velocity increments v_r2, v_r1 and v_r0
v_r1= M20h1(r1 + 1:end) - M20h1(1:end - r1);
v_r0 = M20h1(r0 + 1:end) - M20h1(1:end - r0);
v_r2 = M20h1(r2 + 1:end) - M20h1(1:end - r2);
%-----------------------------------------------------------------
% Ensure the three time series have have equal number of observations.
v_r2(end + r2 - r0 + 1:end) = [];
v_r1(end + r1 - r0 + 1:end) = [];
%-----------------------------------------------------------------
% bin the time series into the number of bins
```

```
%Bins for v_r2
lowLimit_r2 = min(v_r2);
upLimit_r2 = max(v_r2) + 1;
binLimits_r2 = linspace(lowLimit_r2, upLimit_r2, numBins_r1 +1);
[not_needed,whichBin_r2] = histc(v_r2,binLimits_r2);
%Bins for v_r1
lowLimit_r1 = min(v_r1);
upLimit_r1 = max(v_r1)+ 1;
binLimits_r1 = linspace(lowLimit_r1, upLimit_r1, numBins_r1 +1);
[not_needed,whichBin_r1] = histc(v_r1,binLimits_r1);
%Bins for v_r0
lowLimit_r0 = min(v_r0);
upLimit_r0 = max(v_r0)+ 1;
binLimits_r0 = linspace(lowLimit_r0, upLimit_r0, numBins_r0 +1);
[not_needed,whichBin_r0] = histc(v_r0,binLimits_r0);
for i=1:numBins_r0
    r0_flagBinMembers = (whichBin_r0==i);
    binMembers_r0 = v_r0(r0_flagBinMembers);
    binMean_r0(i) = mean(binMembers_r0);
end
for i=1:numBins_r1
    r2_flagBinMembers = (whichBin_r2==i);
    binMembers_r2 = v_r2(r2_flagBinMembers);
    binMean_r2(i) = mean(binMembers_r2);
    r1_flagBinMembers = (whichBin_r1==i);
    binMembers_r1 = v_r1(r1_flagBinMembers);
    binMean_r1(i) = mean(binMembers_r1);
end
v_r2_Binned = binMean_r2(whichBin_r2)';
v_r1_Binned = binMean_r1(whichBin_r1)';
v_r0_Binned = binMean_r0(whichBin_r0)';
%-------------------------------------------------------------------
% Evaluate: P(v_r2_Binned|v_r0_Binned), r2 < r0
 Table_r0 = tabulate(v_r0_Binned);
 %P(v_r0_Binned)
 Prob_v_r0 = Table_r0(:,3)/100;
  %Joint Probability: P(v_r2_Binned;v_r0_Binned)
 [MassPDF_r2_r0] = crosstab(v_r2_Binned,v_r0_Binned);
 JointPDF_r2_r0 = MassPDF_r2_r0/(length(v_r2));
 %Conditional Probability: P(v_r2_Binned|v_r0_Binned)
 CondPDF_r2_r0 = JointPDF_r2_r0/diag(Prob_v_r0);
%-------------------------------------------------------------------
% Evaluate: P(v_r2_Binned|v_r1_Binned), r2 < r1
Table_r1 = tabulate(v_r1_Binned);
 %P(v_r1_Binned)
 Prob_v_r1 = Table_r1(:,3)/100;
  %Joint Probability: P(v_r2_Binned;v_r1_Binned)
 [MassPDF_r2_r1] = crosstab(v_r2_Binned,v_r1_Binned);
 JointPDF_r2_r1 = MassPDF_r2_r1/(length(v_r2));
  %Conditional Probability: P(v_r2_Binned|v_r1_Binned)
 CondPDF_r2_r1 = JointPDF_r2_r1/diag(Prob_v_r1);
 %-------------------------------------------------------------------
% Evaluate: P(v_r1_Binned|v_r0_Binned), r1 < r0
Table_r0 = tabulate(v_r0_Binned);
 %P(v_r0_Binned)
 Prob_v_r0 = Table_r0(:,3)/100;
 %Joint Probability: P(v_r1_Binned;v_r0_Binned)
 [MassPDF_r1_r0] = crosstab(v_r1_Binned,v_r0_Binned);
 JointPDF_r1_r0 = MassPDF_r1_r0/(length(v_r1));
 %Conditional Probability: P(v_r1_Binned|v_r0_Binned)
```

```
 CondPDF_r1_r0 = JointPDF_r1_r0/diag(Prob_v_r0);
%-------------------------------------------------------------------------
% Evaluate: P(v_r2_Binned|v_r1_Binned) =
%Sum[P(v_r2_Binned|v_r1_Binned)*P(v_r1_Binned|v_r0_Binned)]dv2, T0>T2>T1
Chapman_Kolgrv = (CondPDF_r2_r1)*(CondPDF_r1_r0);
 %-------------------------------------------------------------------------
% Finds cross-sections
            Mv0 = unique(v_r0_Binned);
            My1 = unique(v_r2_Binned);
            length_Mv0 = length(Mv0);
            Medn = round((length_Mv0)/2);
            length_My1 = length(My1);
            Med_2_0 = CondPDF_r2_r0(1:length_My1,Medn);
            MedN_2_0 = CondPDF_r2_r0(1:length_My1,Medn-15);
            MedP_2_0 = CondPDF_r2_r0(1:length_My1,Medn+10);
            Med_ChapK = Chapman_Kolgrv(1:length_My1,Medn);
            MedN_ChapK = Chapman_Kolgrv(1:length_My1,Medn-15);
            MedP_ChapK = Chapman_Kolgrv(1:length_My1,Medn+10);
%-------------------------------------------------------------------
% Plots contour plot
Log_Cond20 = log10(CondPDF_r2_r0);
Log_ChapKol = log10(Chapman_Kolgrv);
contour(Mv0,My1,Log_Cond20);
hold on;
contour(Mv0,My1,Log_ChapKol,'LineStyle',':','LineWidth',2);
% Create xlabel
xlabel({'\itv(\itr\rm_0)'},'FontSize',12);
% Create ylabel
ylabel({'\itv(\itr\rm_1)'},'FontSize',12);
%-------------------------------------------------------------
% Plots cross-sections
p1 = figure;
hold on;
plot(My1,Med_2_0,'LineStyle','none','Marker','o');
hold on;
plot(My1,Med_ChapK,'LineStyle','none','MarkerSize',20,'Marker','.');
% Create xlabel
xlabel({'\itv(\itr\rm_1)'},'FontSize',12);
% Create ylabel
ylabel({'P(\itv(\itr\rm_1)|\itv(\itr\rm_0))'},'FontSize',12);
hold off;
p1 = figure;
plot(My1,MedN_2_0,'LineStyle','none','Marker','o');
hold on;
plot(My1,MedN_ChapK,'LineStyle','none','MarkerSize',20,'Marker','.');
% Create xlabel
xlabel({'\itv(\itr\rm_1)'},'FontSize',12);
% Create ylabel
ylabel({'P(\itv(\itr\rm_1)|\itv(\itr\rm_0))'},'FontSize',12);
hold off;
p1 = figure;
plot(My1,MedP_2_0,'LineStyle','none','Marker','o');
hold on;
plot(My1,MedP_ChapK,'LineStyle','none','MarkerSize',20,'Marker','.');
% Create xlabel
xlabel({'\itv(\itr\rm_1)'},'FontSize',12);
% Create ylabel
ylabel({'P(\itv(\itr\rm_1)|\itv(\itr\rm_0))'},'FontSize',12);
```

B4

```
% Mol_Chaos_Turb.m
%
% This program demonstrates the molecular chaos assumption given by the
% independence of the cross-stream and streamwise wind velocity
% streams. It plots the joint and conditional probability functions as
% contour plots.
%
% Written using Matlab 7.4.0 (R2007a)
%
%
% Lloyd A Corker
% University of Cape Town
% Department of Physics
% PhD Thesis
% lcorker@uwc.ac.za
% 2010 February
%
%
%-----------------------------------------------------------------------
% Reset memory and clear the screen
clear; clc
% load data.
%-----------------------------------------------------------------------
% open file for reading
Data(1) = fopen('m20h1-01.dat');
% Reads the 1rst of 8 columns only
Col_1 = textscan(Data(1), '%f %*f %*f %*f %*f %*f %*f %*f');
% Transform cell array into an ordinary matrix
v_r0 = Col_1{1}; % v_r0 contains the streamwise velocity measuremnts
% opens file for reading
Data(2) = fopen('m20h1-01.dat');
% Reads the 5th of 8 columns only
Col_2 = textscan(Data(2), '%*f %*f %*f %*f %f %*f %*f %f');
% Transform cell array into an ordinary matrix
v_r1 = Col_2{1};  % v_r1 contains the cross-stream velocity measuremnts
from
% filter of 10 mm.
% Close the file
fclose(Data(1));
% First four columns: streamwise velocities from probe #1 to probe #4
% Last four columns: cross-stream velocities from probe #1 to probe #4
%-----------------------------------------------------------------------
% Choose length scales: Scale1 < Scale0
r1 = 100; %Scale1
r0 = 300; %Scale0
% Choose number of bins for each scale.
numBins_r0 = 100;
numBins_r1 = 100;
%-----------------------------------------------------------------------
%Construct length scales by taking velocity increments v_r1 and v_r0
v_r1= v_r1(r1 + 1:end) - v_r1(1:end - r1);
v_r0 = v_r0(r0 + 1:end) - v_r0(1:end - r0);
%-----------------------------------------------------------------------
% Ensure the two time series have have equal number of observations.
v_r1(end + r1 - r0 + 1:end) = [];
%-----------------------------------------------------------------------
% bin the time series into the number of bins
```

```
%Bins for Scale1
lowLimit_r1 = min(v_r1);
upLimit_r1 = max(v_r1)+ 1;
binLimits_r1 = linspace(lowLimit_r1, upLimit_r1, numBins_r1 +1);
[not_needed,whichBin_r1] = histc(v_r1,binLimits_r1);
%Bins for Scale0
lowLimit_r0 = min(v_r0);
upLimit_r0 = max(v_r0)+ 1;
binLimits_r0 = linspace(lowLimit_r0, upLimit_r0, numBins_r0 +1);
[not_needed,whichBin_r0] = histc(v_r0,binLimits_r0);
for i=1:numBins_r0
    r0_flagBinMembers = (whichBin_r0==i);
    binMembers_r0 = v_r0(r0_flagBinMembers);
    binMean_r0(i) = mean(binMembers_r0);
end
for i=1:numBins_r1
   r1_flagBinMembers = (whichBin_r1==i);
    binMembers_r1 = v_r1(r1_flagBinMembers);
    binMean_r1(i) = mean(binMembers_r1);
end
% The below reprsents the binned data used to calculate the K-M moments
v_r1_Binned = binMean_r1(whichBin_r1)';
v_r0_Binned = binMean_r0(whichBin_r0)';
%-------------------------------------------------------------------
% Evaluate: P(v_r1_Binned|v_r0_Binned), Scale1 < Scale0
 Table_r0 = tabulate(v_r0_Binned);
%P(v_r0_Binned)
 Prob_v_r0 = Table_r0(:,3)/100;
 %Joint Probability: P(v_r1_Binned;v_r0_Binned)
 [MassPDF_r1_r0] = crosstab(v_r1_Binned,v_r0_Binned);
 JointPDF_r1_r0 = MassPDF_r1_r0/length(v_r0_Binned);
 %Conditional Probability: P(v_r1_Binned|v_r0_Binned)
 CondPDF_r1_r0 = JointPDF_r1_r0/diag(Prob_v_r0);
%-------------------------------------------------------------------
% Plots the contout plots of the joint and conditional probability
functions
            Mx = unique(v_r0_Binned);
            My = unique(v_r1_Binned);
hold on;
% Create contour
contour(Mx,My,log10(JointPDF_r1_r0));
% Create xlabel
xlabel({'\mu\rm_\alpha(X)'},'FontSize',12);
% Create ylabel
ylabel({'\mu\rm_\beta(X)'},'FontSize',12);
p1 = figure;
contour(Mx,My,log10(CondPDF_r1_r0));
% Create xlabel
xlabel({'\mu\rm_\alpha(X)'},'FontSize',12);
% Create ylabel
ylabel({'\mu\rm_\beta(X)'},'FontSize',12);
```

B5

```
% Random_JPDF.m
%
% This program demonstrates the independence between two time series
% by considering contout plots of the joint and conditional probability
% functions. The data is randomly generated.
%
% Written using Matlab 7.4.0 (R2007a)
%
%
% Lloyd A Corker
% University of Cape Town
% Department of Physics
% PhD Thesis
% lcorker@uwc.ac.za
% 2010 February
%
%
%-----------------------------------------------------------------------
% Reset memory and clear the screen
clear; clc
%-----------------------------------------------------------------------
% Generate Random data.
n = 75;
f = ceil(n.*rand(100000,1));
v_r1=f(1:100000);
n = 50;
f = ceil(n.*rand(100000,1));
v_r0=f(1:100000);
%-----------------------------------------------------------------------
% Choose length scales: Scale1 < Scale0
r1 = 100; %Scale1
r0 = 300; %Scale0
% Choose number of bins for each scale.
numBins_r0 = 50;
numBins_r1 = 50;
%-----------------------------------------------------------------------
%Construct length scales by taking velocity increments v_r1 and v_r0
v_r1= v_r1(r1 + 1:end) - v_r1(1:end - r1);
v_r0 = v_r0(r0 + 1:end) - v_r0(1:end - r0);
%-----------------------------------------------------------------------
% Ensure the two time series have have equal number of observations.
v_r1(end + r1 - r0 + 1:end) = [];
%-----------------------------------------------------------------------
% bin the time series into the number of bins
%Bins for Scale1
lowLimit_r1 = min(v_r1);
upLimit_r1 = max(v_r1)+ 1;
binLimits_r1 = linspace(lowLimit_r1, upLimit_r1, numBins_r1 +1);
[not_needed,whichBin_r1] = histc(v_r1,binLimits_r1);
%Bins for Scale0
lowLimit_r0 = min(v_r0);
upLimit_r0 = max(v_r0)+ 1;
binLimits_r0 = linspace(lowLimit_r0, upLimit_r0, numBins_r0 +1);
[not_needed,whichBin_r0] = histc(v_r0,binLimits_r0);


for i=1:numBins_r0
```

```
    r0_flagBinMembers = (whichBin_r0==i);
    binMembers_r0 = v_r0(r0_flagBinMembers);
    binMean_r0(i) = mean(binMembers_r0);
end

for i=1:numBins_r1
   r1_flagBinMembers = (whichBin_r1==i);
    binMembers_r1 = v_r1(r1_flagBinMembers);
    binMean_r1(i) = mean(binMembers_r1);
end

% The below reprsents the binned data used to calculate the K-M moments
v_r1_Binned = binMean_r1(whichBin_r1)';
v_r0_Binned = binMean_r0(whichBin_r0)';

%-------------------------------------------------------------------
% Evaluate: P(v_r1_Binned|v_r0_Binned), Scale1 < Scale0
 Table_r0 = tabulate(v_r0_Binned);
 %P(v_r0_Binned)
 Prob_v_r0 = Table_r0(:,3)/100;
  %Joint Probability: P(v_r1_Binned;v_r0_Binned)
 [MassPDF_r1_r0] = crosstab(v_r1_Binned,v_r0_Binned);
 JointPDF_r1_r0 = MassPDF_r1_r0/length(v_r0_Binned);
%Conditional Probability: P(v_r1_Binned|v_r0_Binned)
 CondPDF_r1_r0 = JointPDF_r1_r0/diag(Prob_v_r0);
%-------------------------------------------------------------------
% Plots the contout plots of the joint and conditional probability
functions
            Mx = unique(v_r0_Binned);
            My = unique(v_r1_Binned);
hold on;
% Create contour
contour(Mx,My,log10(JointPDF_r1_r0));
% Create xlabel
xlabel({'\itv(\itr\rm_0)'},'FontSize',12);
% Create ylabel
ylabel({'\itv(\itr\rm_1)'},'FontSize',12);
p1 = figure;
contour(Mx,My,log10(CondPDF_r1_r0));
 % Create xlabel
xlabel({'\itv(\itr\rm_0)'},'FontSize',12);
% Create ylabel
ylabel({'\itv(\itr\rm_1)'},'FontSize',12);
```

B6

```
% FPE_Sol.m
%
% This program solves the one-dimensional Fokker-Planck equation
% using pdepe toolbox.
%
%
% Written using Matlab 7.4.0 (R2007a)
%
% Lloyd A Corker
% University of Cape Town
% Department of Physics
% PhD
% lcorker@uwc.ac.za
% 2010 February
%
%
%--------------------------------------------------------------------
function [P] = fpe(x,t,Drift)

% sets the geometry to linear
m = 0;
 % This solves the Fokker-Planck equation on the interval 0=<x>=150
% from time t = 0 to t = 1. For values of change in t and change
% in x there will be 100 values of t ranging from 0 to 1 and 401
% values of x ranging from 0 to 100.
x = linspace(0,150,401);
t = linspace(0,1,100);
sol = pdepe(m,@fpex,@fpeicx,@fpebcx,x,t,[]);

%the first solution in P:
P = sol(:,:,1);
%--------------------------------------------------------------------
%Plots the solution as a 3D mesh:
p1 = figure;
mesh(x,t,P);
xlabel('distance x','FontSize',12);
ylabel('time t','FontSize',12);
zlabel('P(x,t)','FontSize',12);
%Plots the solution profile:
p1 = figure;
hold on;
plot(x,P(1,:),'Color',[1 0 0],...
  'LineStyle',':',...
  'Marker','.',...
  'MarkerSize',3);
plot(x,P(50,:),'K--');
plot(x,P(end,:));
xlabel('distance x','FontSize',12);
ylabel('P(x,t)','FontSize',12);
legend('t=1 of 100','t=50 of 100','t=100 of 100');
%--------------------------------------------------------------------
% subfunctions:
function [Diff,f,s] = fpex(x,t,P,DPDx)
Drift = 1;
Diff = 3;
f = DPDx;
s = -Drift*x*DPDx-Drift*P;
```

```
%--------------------------------------------------------------------
% ic - initial cond. at t=0
function P0 = fpeicx(x)
P0 = ((1/30)*(2*pi)^1/2) * exp(-(1/2)*((x-30) /30)^(2));
%--------------------------------------------------------------------
% bc - boundary cond.
function [pa,qa,pb,qb] = fpebcx(xa,Pa,xb,Pb,t)
pa = Pa;
qa = 0;
pb = Pb;
qb = 0;
%////////////////////////////////////\\\\\\\\\\\\\\\\\\\\\\\\\\\\\\\\\\\\
```

Biographical Sketch

Lloyd A Corker was born and raised in Cape Town. After working as a telephone technician for several years Lloyd enrolled for a BSc degree at the University of the Western Cape with majors in Physics and Applied Mathematics. In 2003 he graduated with a MCom degree in Economics and International Finance. Lloyd has been teaching Statistics at the University of the Western Cape since 2003. In 2006 he graduated with a MSc degree in theoretical Physics at the University of Cape Town. He began reading for a PhD in theoretical Physics in 2007.